An investigation of rock cutting: towards a novel design of cutting bits

Author:
Yao, Qingyu

Publication Date:
2012

DOI:
https://doi.org/10.26190/unsworks/15522

AN INVESTIGATION OF ROCK CUTTING: TOWARDS A NOVEL DESIGN OF CUTTING BITS

BY

QINGYU YAO

A thesis submitted in fulfilment of the requirements for the degree of **Doctor of Philosophy** (PhD) in 2012

School of Mechanical and Manufacturing Engineering

The University of New South Wales

Sydney Australia

Originality Statement

'I hereby declare that this submission is my own work and to the best of my knowledge it contains no materials previously published or written by another person, or substantial proportions of material which have been accepted for the award of any other degree or diploma at UNSW or any other educational institution, except where due acknowledgement is made in the thesis. Any contribution made to the research by others, with whom I have worked at UNSW or elsewhere, is explicitly acknowledged in the thesis. I also declare that the intellectual content of this thesis is the product of my own work, except to the extent that assistance from others in the project's design and conception or in style, presentation and linguistic expression is acknowledged.'

Signed: ____________________

Date: ____________________

(a) Copyright Statement

Signed: ________________

Date: ________________

(b) Authenticity Statement

'I certify that the library deposit digital copy is a direct equivalent of the final officially approved version of my thesis. No emendation of content has occurred and if there are any minor variations in formatting, they are the result of the conversion to digital format.'

Signed: ________________

Date: ________________

Abstract

Mechanical excavation by the point attack bit of the long-wall shearers is of key importance in modern mining sites. However, serious wear, heavy airborne dust and excessive power consumption are three major problems in rock cutting using current conical bits. Regarding the above defects and enlightened by the Vicker's indentation tests on brittle materials, a pyramidal bit was put forward in order to replace the cone. Then, two stages of practical work, edge chipping and linear cutting, were set up to investigate the availability and further improvement of the pyramidal bit.

An edge chipping test can be used to simulate the rock cutting process due to the similarity of crack systems. Such experiments were then carried out to comparatively explore the cutting performances based on different crack mechanism, fine grain generations, chip sizes, cutting forces and total energy consumption. Results demonstrated that the pyramidal bit generates less radiated cracks, larger size chips and less energy consumption. Moreover, it was also found that the 2D crack trajectory of the chip from the side view is close to a straight line. The straight trajectory is angled with the force axis and this angle was found to be linearly correlated with the attack angle. In addition, the chipping force curves were found to be well quadratically fitted. The minimum peak force induced by the pyramidal bit was noted to exist at the orientation of diagonals with 45° and 135° to the free surface. Besides, the best-fit power relationship between the peak force and depth of cut was close to 1.3 and the power values of the total chipping energy and depth of cut were found to be in a range from 1.85 to 2.29.

Then, a model describing edge chipping in relation to the peak chipping force, material properties, attack angle and depth of cut was derived in line with the assumptions from

the observations in the edge chipping tests. It was discussed that the trajectory of maximum shear stress can be the most likely explanation of the straight crack path observed in chipping experiments. The derivation of toughness based on this derivation provides a convenient way of predicting the rock toughness. Specifically, the power relationship between peak chipping force, total energy and depth of cut are theoretically explained.

Linear cutting tests were carried out on Helidon sandstone and Harcourt granite for comparing the cutting and wear performances of all bit configurations. The initial pyramidal bit profile was improved by modifying the top and bottom cutting angles, side surface and setting the optimum cutting orientation, in terms of the result analyses in the cutting tests. Then, cutting performances were investigated and compared in relation to fracture mechanism, crush zone size, fragment size distribution, excavated rock mass, cutting force and specific energy. Results show the higher cutting efficiency of the improved bit configuration is dependent on the larger fraction of big fragments, much lower mean cutting force and specific energy. Fractal analysis quantitatively validates the cutting efficiency by dealing with the larger fracture surface area and 3D multivariate analyses provide a comprehensive view of the double factor effect. A power relationship was also found between the mean cutting force and depth of cut although the force amplitude is different from that in edge chipping, which further derived the power relationship between specific energy and depth of cut. Besides, PCD bits possessed much higher wear resistance than that of WC bits, which further demonstrates the availability of the potential application of pure PCD material in hard rock cutting.

Acknowledgement

No pain no gain. Having struggled and been persistent, I went through four years hard work on my PhD project, from knowing nothing about mining to identifying an improvement of a cutting bit. I would like to show my great appreciation to my supervisor, Scientia Professor, Liangchi Zhang and my co-supervisors Dr. Ronghao Bao and Dr. Haihui Ruan, who really gave me a lot of helpful advice during my study.

I would also like to thank Dr. Xingsheng Li, and Mr. Peter Clark in Mining and Exploration CSIRO Brisbane, who contributed a big effort conducting the linear tests. Also, great gratitude is due to Robert Miles and Trevor Shearing in Sydney University, who gave me a lot of help on the perpendicular edge chipping tests there. Thank Jason Nhieu for his big help setting up the experimental platform for the inclined edge chipping tests in the solid mechanics lab and Bruce Oliver who really helped me fabricate the necessary parts for the experiments in UNSW.

Furthermore, the financial support from our industrial partner Bradken and Australian Research Council (ARC) is of key importance to obtain the final achievement. I would further like to thank Jason Lunn and Craig Melmeth in Bradken who really dedicated a lot to cooperating with us in this project. The help from Steven and Peter in Hardmetals Hornsby also deserves mention.

Without their continuous help and support, the project would not have been finished so smoothly. Finally, I would like to thank my family for their encouragement and support during my PhD process.

Table of Contents

List of Figures

List of Tables

Nomenclature

a_c: half length of the initial crack

c: crack length

c_F: crack length at the peak chipping point

C: fitting coefficient

d: penetration depth

dc: differential element of crack length

d_{pp}: perpendicular penetration depth at peak chipping point

D: fractal exponent

E: Young's modulus

E_t: total energy consumed in one edge chipping process

f_c: dimensionless function for describing crack evolution

$f(\alpha)$: triangular function

$f(x,z)$: crack path function in $x-z$ plane

F: force

F_c: peak cutting force in rock cutting

F_{mc}: mean cutting force in linear cutting

F_n: normal point load

F_{pp}: perpendicular edge chipping force

F_p : general peak chipping force

F_t : tangential point load

G : energy release rate

h : depth of cut

h' : vertical distance of an inclined rock block

H : indentation hardness

K_I : Mode I stress intensity factor

K_{II} : Mode II stress intensity factor

K_c : material toughness

l : distance from the critical point of the crack to the free side

L : chip length

L' : horizontal distance of an inclined rock block

L_D : cutting distance

N : number of chips sized larger than r_d

r : radial direction in Polar Coordinates

r_d : dimension of the specific aperture of a sieve

R_a : roughness

S : fracture surface area

SE : specific energy

S_c : cross sectional area of the groove

V : volume of rock mass

W : chip width

W_t : total external work done by the bit

α : attack angle

α_0 : rake angle

α_t : angle for the direction of maximum shear stress

β : dimensionless constant independent of material

β_0 : dimensionless constant independent of material

β_c : clearance angle

γ : fracture surface energy of the material

δ : perpendicular component of the inclined penetration depth

η : coefficient related to material properties and bit geometry

θ : circumferential direction in Polar Coordinates

θ_0 : crack inclination angle from the initial crack path

θ_s : angle between sidewall and vertical line

κ : ratio of c_F and h

κ' : a coefficient related to the material properties in dynamic mode

κ^* : a coefficient related to the rock properties

λ: geometrical coefficient

μ: ratio of fracture surface energy and total energy by external work

ν: Poisson's ratio

ρ: the distance between an arbitrary point in the stress field to the origin

σ: external stress

σ_1: maximum normal stress component

σ_3: minimum normal stress component

σ_c: unconfined compressive strength of rock

σ_r: radial stress component in Polar Coordinates

σ_t: tensile strength of rock

σ_{xx}: normal stress component along x axis with normal and tangential loads

σ_{zz}: normal stress component along z axis with normal and tangential loads

σ_{xx}^n: normal stress component along x axis with normal load

σ_{zz}^n: normal stress component along z axis with normal load

σ_{xx}^t: normal stress component along x axis with tangential load

σ_{zz}^t: normal stress component along z axis with tangential load

σ_θ: circumferential stress component in Polar Coordinates

$\sigma_{\theta I}$: Mode I circumferential stress component in Polar Coordinates

$\sigma_{\theta II}$: Mode II circumferential stress component in Polar Coordinates

τ_{xz}: shear stress component with normal and tangential loads

τ_{xz}^{n}: shear stress component with normal load

τ_{xz}^{t}: shear stress component with tangential load

$\tau_{r\theta}$: shear stress component in Polar Coordinates

φ: crack deviation angle from force axis

ϕ_{C1}: breaking angle with C1 configuration

ϕ_{P1}: breaking angle with P1 configuration

ϕ_{P3}: breaking angle with P3 configuration

ϕ_{P7}: breaking angle with P7 configuration

χ: dimensionless constant in sharp indentation

$\chi^{'}$: a geometrical factor related to fracture energy

$\chi^{''}$: a geometrical factor related to fracture energy in perpendicular chipping

χ^{*}: a geometrical factor in relation to the shape of the chip

ψ: smaller angle between the directions of the initial crack and the stress

ψ_{0}: half included angle of the point-attack bit

ψ_{f}: friction angle

Chapter 1

Introduction

1.1 Background

1.1.1 Overview of rock cutting

Mechanical excavation is widely applied in many aspects of the mining field, such as tunnelling, open pit and underground coal explorations. The engineering excavation machines use power to execute effective operations and material cutting [1-19]. Specifically, a mechanical cutting machine, such as a longwall shearer (Fig. 1.1), cuts rock/coal with an array of picks (each with a bit on the pick body) installed at certain intervals (spacing) and attack angles on a rotating and moving drum [5].

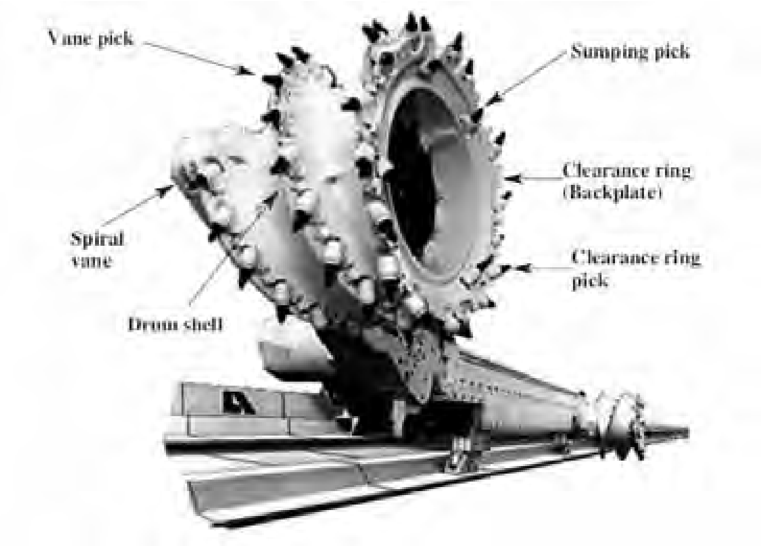

Fig. 1.1 Longwall shearer [20]

The cutting bit, which is usually sintered from powders of cemented tungsten carbide, is brazed into the pick body. Depending on its cutting actions [5], the bit can be classified as the drag bit, which hits the rock along a direction paralelling to the rock surface, and the indenter, which generates the rock breakage by perpendicularly pressing into the surface. These are the two main categories, as shown in Figs. 1.2 (a) and (b). Shape difference leads to another two categories: the radial and point-attack bits, as shown in Figs. 1.3 (a) and (b). The radial profile resembles a chisel or wedge with the pick axis perpendicular to the cutting direction. The point attack bit possesses a conical shape with its axis collinear with the pick body and angled with the cutting direction.

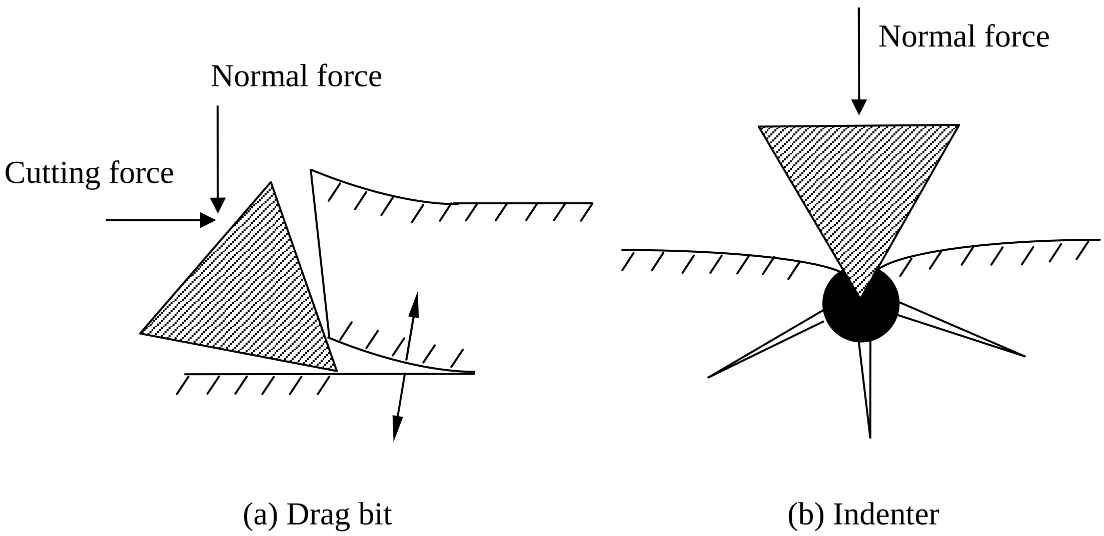

Fig. 1.2 (a) Drag bit; (b) Indenter

We specifically focus on radial and point attack bits in dragged action to understand their different wear performances in relation to cutting efficiency and tool life. Radial bits in a wedge shape were found to be suitable for cutting soft and medium-soft rocks, due to the severe wear on the front edge when cutting hard rocks [20-21]. Point attack bits with a cylindrical bottom are inserted into the circular cross-sectioned pick body, which leads to uniform bit wear, due to free rotation in pick bodies. This wear format relates to the prolongation of the tool life as the force dramatically drops after a certain degree of wear on cutting both soft and hard rocks, although the force at the beginning is higher than in others [22]. Hence, point attack bits have been widely employed for cutting rocks ranging from soft to hard rocks on roadheaders and longwall shearers.

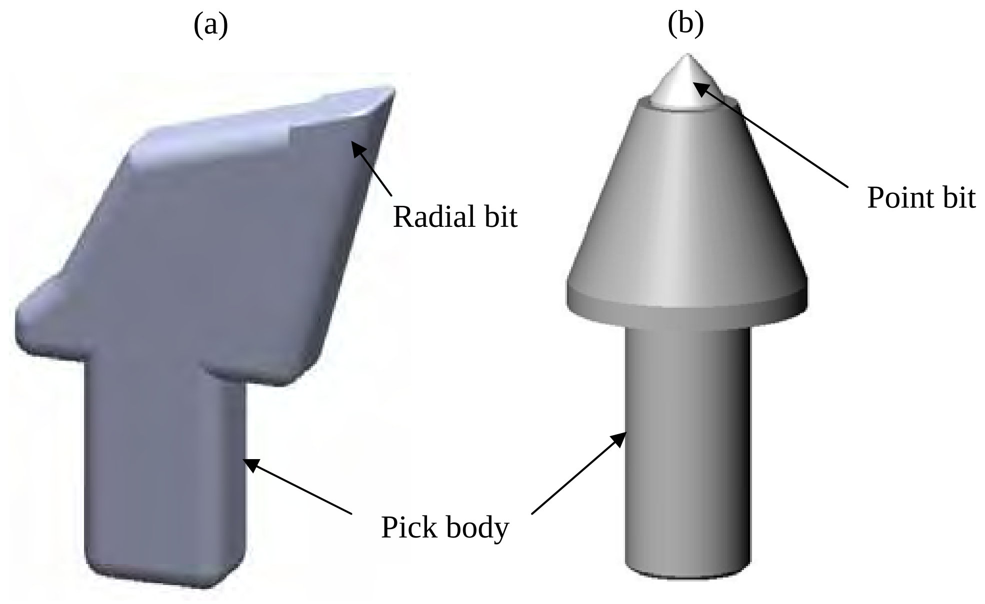

Fig. 1.3 (a) Radial pick; (b) Point-attack pick

1.1.2 Existing problems

However, several hazardous defects still exist using the current conical bit, such as the airborne dust, serious bit wear and huge consumption of energy: (1) Dust is produced during cutting, at the machine face, at conveyors, at transfer points, and by the normal movement of workers and machines. Most particles settle down rapidly. However, the airborne particles stay in the air much longer, which leads to fine dust being transferred over long distances before settling and being absorbed by the miners. Dust is hazardous due to the possibility of explosion [23-28] and methane ignition [29-31]. Moreover, it results in threats to the miners' health [32]. (2) Another factor affecting cutting performance is tool wear, which is largely reported in [33-37]. Different wear extents derive from different cutting processes. Fig. 1.4 shows some wear examples of point attack picks. From the left hand side, the first one is the original pick before any cutting action, followed by the light, medium and heavy wear of the bit and shank shoulder.

The final one shows an un-rotary cutting action with a huge wear flat surface. Serious wear on the pick leads to the delay in the cutting process, which certainly brings about increased costs on handling the labour and parts. (3) High cost results from large consumption of energy [38] and lower amount of excavated rock mass. This causes an increase of the specific energy, which governs the assessment of rock cutting efficiency. Specific energy determines the rate at which rock breaking can be carried out and also determines the power selection of the machines, a calculation which is crucial for the application on the rock and the hardness of the manufactured components of the machine. A process that demands substantial energy will result in a slow rock breaking rate.

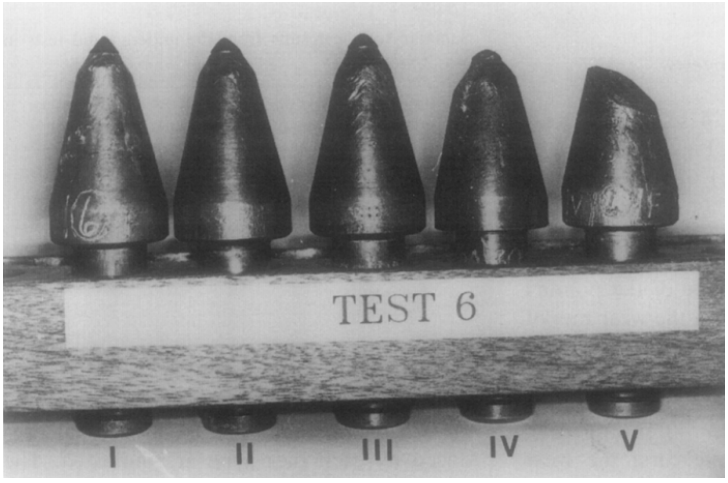

Fig. 1.4 Different worn picks [33]

1.2 Motivations and aims

In view of the defects mentioned in Section 1.2 such as heavy airborne dust generation, huge energy consumption, and serious asymmetric wear flats [5, 8-9, 15], a hypothesis related to improved bit geometry to solve the above problems is brought forward based on a series of researches focused on the bit geometrical effect on cutting efficiency [39-45]. Achanti and Hurt [39-40] conducted a number of experimental studies and found that there are several factors affecting cutting efficiency, including bit geometry, cutting head design, depth of cut and speed of cut. Further, Achanti [41] found that optimum bit geometry could result in efficient fragmentation of rock. Addala [42] reported that increase of bit angle results in the increment of dust generation. Khair [43, 45] practically investigated the cutting performances of several conical bits with different included angles and pointed out that cutting efficiency can be optimized with a certain bit angle after fixing the depth of cut and spacing. Qayyum [44] found that a bit with a larger angle causes more little cracks in the rock and therefore results in a larger amount of energy consumption and fine grains. In conclusion, bit profile is a crucial concern dominating rock cutting efficiency in relation to rock fracture, specific energy and dust generation. However, previous researches have only concentrated on the angle change of the cone without making any further investigations on the bit profile change. Hence, this thesis aims at practically finding an optimum bit geometry with a better wear-resistant material to reduce the energy consumption, dust generation and wear.

1.3 Outline of thesis

This thesis contains 6 chapters, which are listed as follows:

Chapter 1 is an overview of the background of rock cutting. It also states the current problems and the aim of this research.

Chapter 2 broadly views previous research in rock cutting in relation to the point attack bit and describes the edge chipping method exploited in this research. Then, it also critically analyses the relevant research and points out potential work that is worth doing.

Chapter 3 presents a comparison of rock chipping performances by edge chipping tests with both conical and pyramidal bits. Results show the pyramidal bit induced the bigger fragments, fewer fine grains and less total energy consumption. Detailed observations include: Chips possess geometrical similarity, which is represented by a constant ratio of chip length and chip width. Crack trajectory almost follows a linear path when watched from the side view of the chip. A plot of chipping force in relation to penetration depth exhibits a strong quadratic fitting, which infers the edge chipping force should be regarded as part of the force-depth curve in indentation. Peak force values at two extreme orientations of pyramidal bit demonstrate an approximate 10% drop of the value when diagonals are with 45° and 135° to the free side. Linear regression of the peak cutting force functioned as depth of cut shows the best power fit of 1.3. All observations are the preparations for the modelling of edge chipping in Chapter 4 and the improvement of the pyramidal bit in Chapter 5.

Chapter 4 derives an inclined peak force model in relation to the depth of cut and attack angle. Assumptions related to the crack deviation angle, extension of chip geometrical similarity and constant fraction of fracture surface energy were based on the experimental observations in Chapter 3 and the literature. The crack trajectory was predicted along the maximum shear path in the Boussinesq stress field. A simple way of measuring the toughness of rock materials was set up by applying edge chipping tests. Besides, the power relation in the literature between the perpendicular peak chipping force and depth of cut was analytically explained through further deriving this formulation.

Chapter 5 handles the linear cutting tests on sandstone and granite. Based on the experimental results and analyses, an improved profile from the pyramidal shape was designed. The cutting performances related to cutting force, specific energy, chip size and chip mass were at optimum using this improved cutting bit, compared with the original pyramidal bit and conical bit. The comparable test on granite focusing on wear resistance shows superior performances for the PCD materials relative to the WC materials. The statistical analyses on total fracture surface of chips and multi-variate effect demonstrate the superiority of the improved cutting bit on levitating the efficiency.

Chapter 6 summarises the major contributions of this thesis and future research work.

Flow chart of the thesis

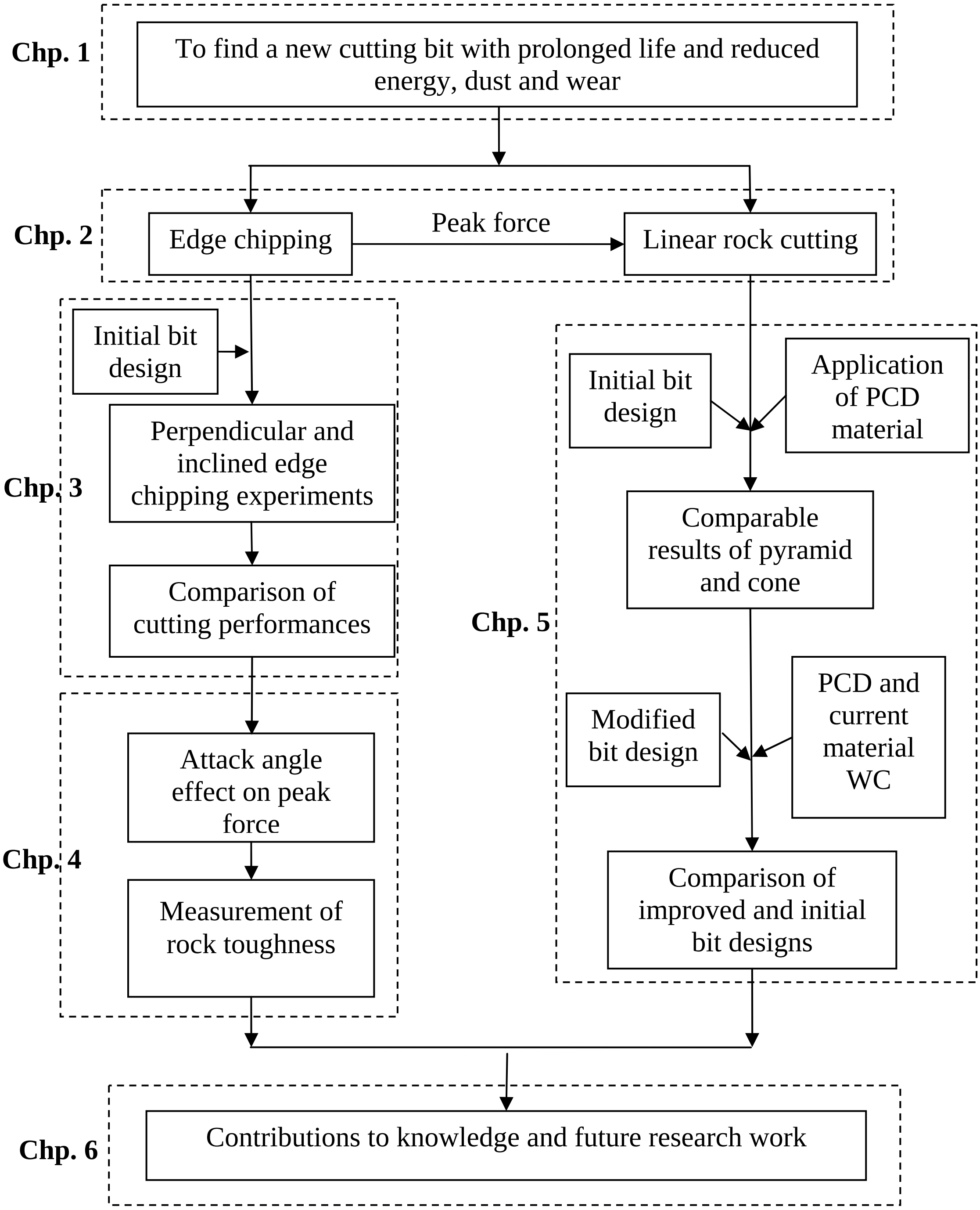

Chapter 2

Literature review

2.1 Introduction

Mechanical excavation with a point attack bit is productive, cost-effective, reliable and safe. Hence, machinery, such as roadheaders, tunnel boring machines and longwall shearers, has been used extensively in mining and underground excavation engineering [1-5]. Significant efforts have been made to understand the mechanism of rock cutting, to enhance cutting efficiency and tool life, to improve work environment and safety, and to extend the capacity of such excavation machines for high strength rocks [6-17].

However, there are several problems during cutting as discussed in Chapter 1, such as great airborne dust generation, large energy consumption and serious asymmetric wear [5, 8-9, 15, 42-45], which have attracted many researchers to resolve these problems and to improve cutting efficiency. Achanti and Khair [39] comprehensively studied the cutting efficiency of a continuous miner, indicating that the mining community should pay attention to achieving two goals: minimising energy consumptions and decreasing the dust and tool wear generated during the cutting process. These two goals were realized by making investigations focusing on the factors which affect cutting efficiency, such as bit type, cutting head design, and speed of cut [40]. Further investigations [39, 41-44] pointed out that bit geometry strongly influences the cutting force, energy consumption and also the efficient fragmentation of rock. Then the configuration of the bit was considered as the dominating factor [46-50] affecting rock cutting efficiency in comparison with other parameters, such as depth of cut and attack angle [39]. However, previous improvements of rock cutting mainly focused on different cutting conditions, e.g. different combinations of depths of cut and spacings [40, 42, 45, 50]. Although the effect of the bit included angle was studied in [39, 41, 43-44], a comprehensive study based on full-scale experiments with different bit geometries and different rocks is still in demand.

Therefore, the present progress on rock cutting and the benchmark experiments are reviewed, in order to deeply investigate the mechanism of rock cutting and then investigate the shape effect of the cutting bit. Relevant theories that can be applied in rock cutting in the following sections are also discussed.

2.2 Review of rock cutting

2.2.1 Cutting mechanism

The rock cutting mechanism was initially investigated in the early 1950s to obtain a deep understanding of the mechanical behaviour of the rock. As reported in [51-53], rock fracture under point bit indentation generally experiences three stages: the building up of the stress field, formation of the crush zone, cracking and chipping of the subsurface materials. The following sections specifically focus on the details on the processes mentioned above.

2.2.1.1 *Initial stage of cutting*

Fedorov [54] in 1951 observed that there is a material consolidation and defection process in the rock with a further surface deformation before the failure happens. Successively, in 1972, Moscalev [55] reported that the surface destruction induced the formation of the destroyed layers and then the crushed rock. I. Evans (1981) and Australian Tunnelling Society (2007) [6, 56] reported that in sharp penetrations with a point attack bit, a three-dimensional stress region is formed, as shown in Fig. 2.1. In this region, increased force induces the gradual densification of the porous rock followed by a series of radial cracks, which radiate away from the axis of the bit. Those radial cracks are not sufficiently dominant to develop big fragments but lead to a high potential for methane ignition. Respirable dust may be produced by microstructures of cut rock, in which rock is more easily to be pulverized into micro or nano particles.

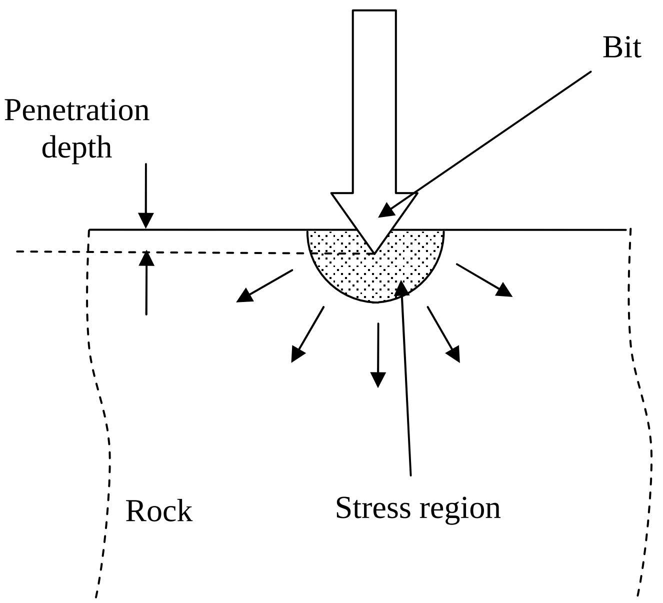

Fig. 2.1 Pressure Bulb during penetration

2.2.1.2 *Crush zone and dust generation*

Following the densification process of the rock, the stress region is enlarged and then transited into a crush zone [56]. Then researches were carried out to clarify the formation of the crush zone. Zeuch [57] (1985) specifically described that the fractures are nucleated in the rock in advance of the bit tip to form an apparently crushed and powdered region at the trailing edge of the fragment. He also supposed that the formation of the crush zone might reflect the dominance of the intense tri-axial compression, which is relevant to the shear behaviour. Lindqvist [58] pointed out that the crushed zone in sandstone and granite is formed with inelastic deformation by the shear action and brittle fracture. Blokhin and Nikiforovsky's work in [59-60] further demonstrated that the shear failure over the slip lines results in the crush zone.

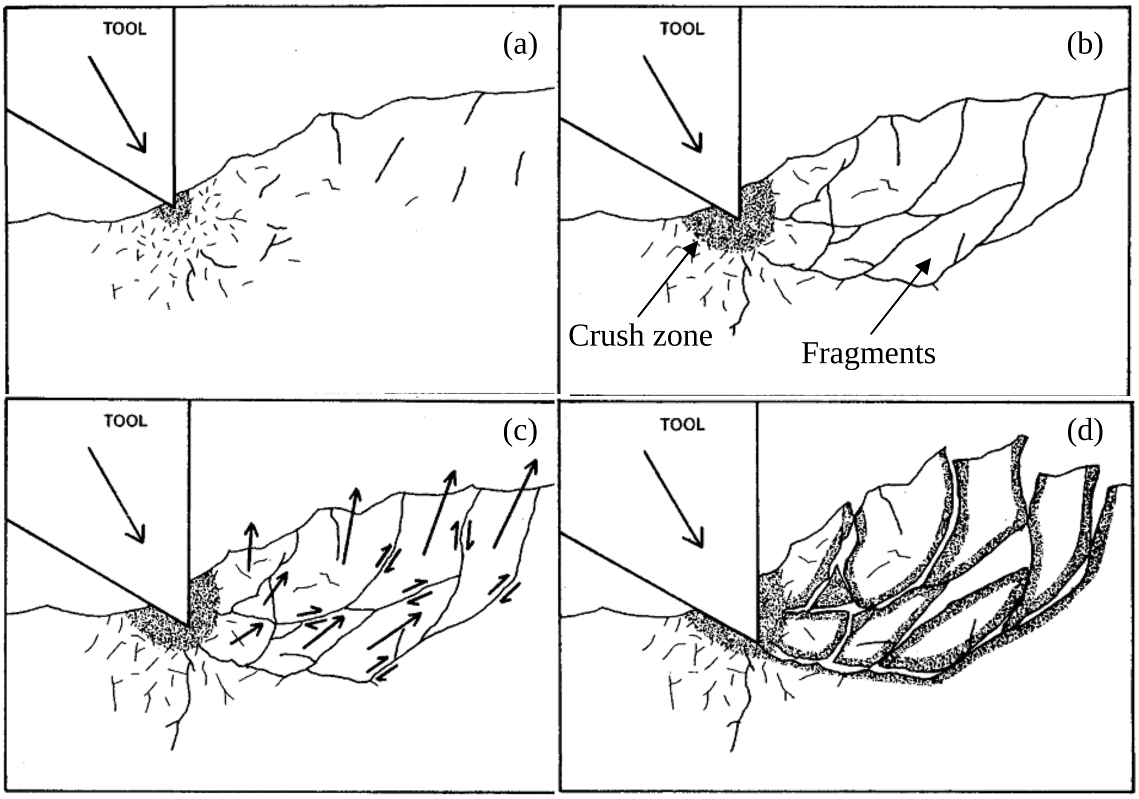

Fig. 2.2 Evolution of crush zone and fragments [61]

During crushing, dust and fine grains are generated: Evans [62] conducted rock cutting experiments to explore the internal mechanism of the crush zone and he found that the radial cracks lead to fine fragments. Howarth and Bridge [63] further pointed out that dust or fine fragments were specifically induced by two major processes: the crushing near the bit tip and the shear fracturing on the macrocrack surfaces, as shown in Fig. 2.2. Zigf also supposed that rubbing contact between the bit and macrocrack surfaces is a major source of fine grain creations [61]. Moreover, Zigf [64] further pointed out that fine grain generation is also affected by the size of the crush zone which was dominated by bit geometry and attack angle. Therefore, it is of interest that observation and comparison of the fine grains can be used to evaluate the efficiency of the bit.

2.2.1.3 *Crack and chip formation*

It is noteworthy that crushing is hard to be avoided as the cutting bit creates a major crack until the crush zone expands to a certain level. Then research work has been carried on relating to the formation of the crush zone, crack propagation and chipping failure in the past 50-60 years. In 1958, I. Evans [65] proposed that rock chipping is induced by the action of tensile stress. Hood [5] re-indicated that the drag bit induces tensile cracks to form fragments. While, in 1962, Gray [66] considered that the chipping trajectory takes a logarithmic contour and the initial cracks are formed by shear stress. Later, in 1995, Mishnaevsky [53] demonstrated that the chipping crack is a tensile and shear mixed mode. Although there are different claims regarding the causation of crack and failure, tensile or shear failures are the major standpoints related to the crack mechanism, including crack initiation and propagation.

Therefore, further understanding of the crack mechanism became crucial, due to its relevance to chip formation. Experimental and numerical investigations were undertaken to explore the crack mechanism using the drag bit [67-75]. Zeuch [68] stated that the crack follows a path 45° angled with the horizontal surface at the beginning of chipping and then flattens out to the end of a chip by conducting experiments on granite and marble. Hook [75] found a curved crack propagation path in indentation of rock predicted by the model of an inclined pre-crack in the stress field, showing the effective application of Griffith’s theory. Lindqvist [76] found that the prediction of crack propagations can be realized by stress analysis during chipping by simulated tests of cutting. Besides, numerical methods were also used in attempts to explore the fundamental mechanism of crack. Wang [67] and Saouma [73] found that the finite element method can be well applied to simulate the crushing, cracking and chipping process. Korinets [69] successfully used DIANA method to simulate the crack propagation of rock indentation. Tang [70], Kou[71] and liu [74] set up 2D models to plot the crack path with consideration of Mode I and II stress intensity factors for the mixed mode fracture and they confirmed that fracture mechanics can be a good utensil to investigate rock fracture. Integrating all features from previous researches on simulation of rock fragmentation, Guo [72] successfully predicted the crack path at different rake angles with a good match to the stress calculations, based on the set up of a linear rock cutting model using a displacement discontinuity method using linear elastic mechanics. As a whole, experimental and simulated results demonstrate that theoretical stress calculations can be used to analyse the crack path during rock chipping.

When crack propagates to a certain length, it becomes unstable [77] and the chip is formed. In order to examine the relationship between chip dimensions and other variables, such as cutting force and energy, Evans [78], Finnie [79], Roxborough [80] and Nishimutsu [81] approximated the chip geometry to model the peak cutting force with two basic assumptions: all broken chips have the same geometry and the top rock surface is smooth without preceding cuts. Thus, by focusing on one chip formation, the cutting force can be formulated by bit and chip geometry, and rock properties with the validation of the experimental results on some rock specimens. However, in continuous cutting, their assumptions are no longer valid. The rock surface, to a large extent, was affected by previous cuts and it was hard to quantify the influence. Even in a homogeneous rock there will be chips in many different shapes and sizes. Instead of using a deterministic description of the rock chips, Ranman [82] statistically analyses the chip dimensions, in which the chip surface was described by a mathematical function. Poisson's distribution was found to be suitable to describe the distribution of chip size. The chips may be regarded as group similarity and therefore, the total fracture surface area can be calculated using the mathematical function and the size of the group. It demonstrates that statistical analysis could be a way of linking chip size and total fracture surface area, which is closely related to the fracture energy based on Griffith's theorem. Hence, cutting efficiency can be investigated by the total fracture surface energy in relation to the total cutting energy.

In summary, the deep understanding of the formation of cracks in relation to chipping paves the way to further investigations on the cutting process of brittle and porous rocks in relation to cutting force modelling and specific energy prediction.

2.2.2 Investigations on cutting force and specific energy

2.2.2.1 *Attack angle*

For one single chip formation, the corresponding force increases from zero to a peak value, at which the failure happens. The force axis is always angled with the cut surface in order to change the ratio of normal and tangential components for obtaining efficient cutting. This angle is called the attack angle, the angle between the rock surface and the bit axis [83] as shown in Fig. 2.3, with the rake angle (values in relation to the strength of the rock) on top of it and the clearance angle (to clean the rock fragments during cutting) at the bottom of it. Experiments were set up for finding out the optimum angle in the cutting process [6, 22, 84-90], for achieving the most efficient ratio between the normal and tangential components. Hurt [6, 22, 40, 85-86, 89, 91] conducted a series of experiments on rock cutting at different attack angles, different depths of cut and different rock specimens, and found that the minimum cutting forces were exhibited by the conical point attack bit at an attack angle of 50° corresponding to a back clearance angle of 12° with bit angle of 75°. From the above literatures, it can be deduced that that the attack angle plays a key role in determining cutting efficiency.

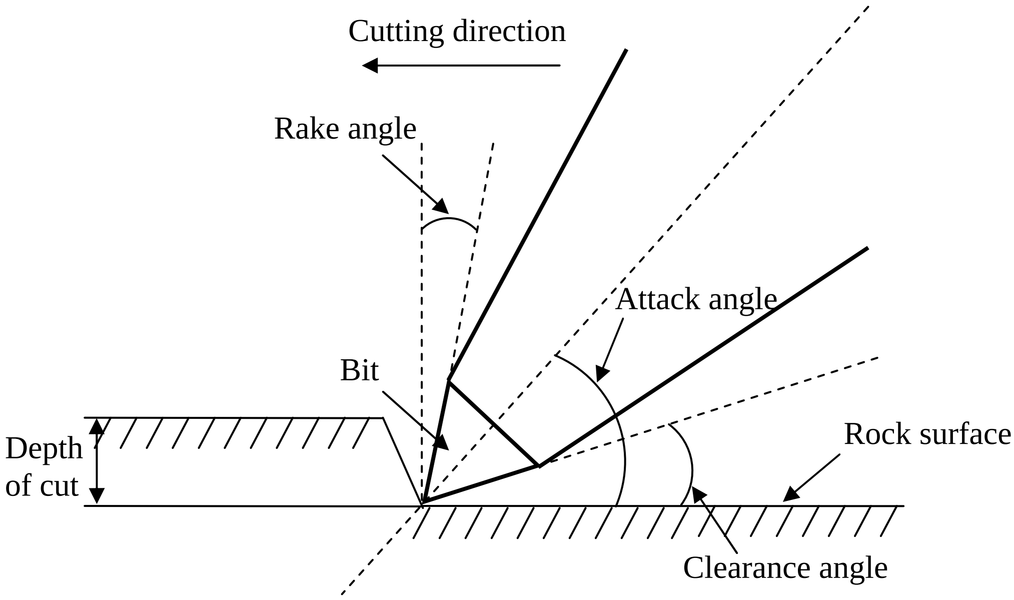

Fig. 2.3 Schematic of linear cutting

2.2.2.2 *Cutting force researches*

Application of a mechanical excavator is often limited by its rotary and force capacity [2, 5, 17-18] as there is no accurate way of selecting the most suitable power for the machine, which results in costly test facilities and time-consuming test processes, although the cutting forces may be measured through full-scale or scaled laboratory cutting tests. Also, in the discussions in Section 2.2.2, it was demonstrated that the cutting force is a vital parameter as it is crucial for the determination of machine power and selection of machines related to suitable rock [2].

Cutting force is mainly used for forming the crack and removing the chip. It is the tangential component of the resultant force, which consists of another two components, normal and lateral. Specifically, in practice, two types of cutting forces were estimated: the peak force, which is defined as the average of three highest amplitudes in one cutting process, and the mean force which is the average of all amplitudes in one cutting process [92]. An example of the raw data recording the cutting force is shown in Fig. 2.4. Both mean cutting force and peak cutting force are significant as mean cutting force possesses a direct relation to energy consumption and peak cutting force could predict the highest amplitude which may damage the machine [92]. Peak cutting force can be evaluated by stress calculations in terms of different fracture criteria, such as maximum shear stress [81] and maximum hoop stress [7, 93]. A quantitative ratio '3' of peak and mean cutting forces [94] helps to easily calculate the mean cutting forces if peak force is determined, although the mean cutting force cannot be directly obtained.

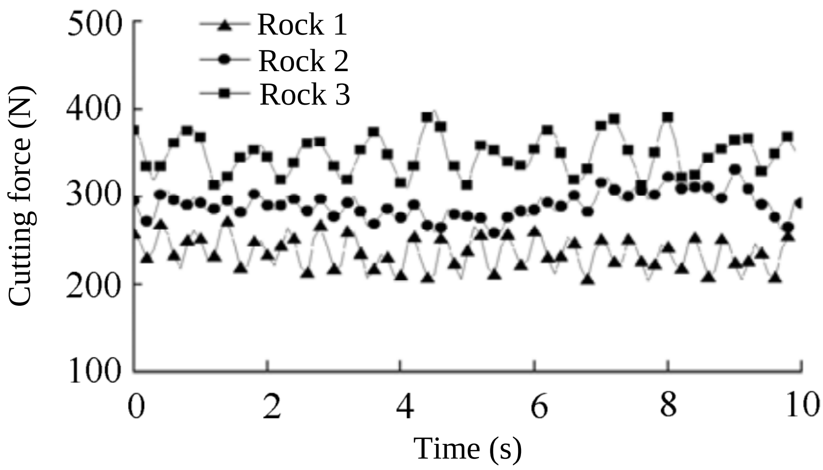

Fig. 2.4 Cutting forces of three kinds of rock [95]

Therefore, theoretical and experimental investigations were set up to model the peak cutting force of the point attack bit [7, 14, 16-17]. Evans' model [7] firstly built up the relationship among the cutting force, rock compressive and tensile strengths, depth of cut and half angle of the bit tip, with the assumption that the penetration of a point-attack bit produces radial compressive stress in the material to cut, without friction. This model was based on another assumption that the penetration of a point-attack pick produced radial compressive stress in the material to cut, without friction. When the hoop stress in the material reaches its tensile strength, breakage happens and a symmetric, V-shaped chip segment is produced. The model also assumed that the normal contact pressure between the pick and the material was distributed uniformly circumferentially along an imaginary cutting hole. It was then claimed that the total penetration force was equivalent to the normal force between the material and the pick, leading to the following calculation of the maximum penetration force of the pick to break the material:

$$F_c = \frac{16\pi\sigma_t^2 h^2}{\sigma_c \cos^2 \psi_0} \tag{2.1}$$

where F_c is the peak cutting force, σ_t and σ_c are the tensile strength and 'unconfined' compressive strength of the material respectively, h is the depth of cut, and ψ_0 is the half angle of the point-attack bit. This formula set up the fundamental theory of the peak cutting force on the bit and successfully predicted the peak cutting force on coal.

However in deriving Eq. 2.1, the stresses on the V-shaped chip do not represent the actual situation, and the determination of the imaginary cutting hole size is not properly justified [7, 96], which leads to further improvements. Thus, several researches on improving Evans' model were attempted: Roxborough and Liu [14] and Goktan [16] considered that the inconsistency could be partly due to the effect of friction which

Evans had ignored. Based on this, Roxborough and Liu [14] formulated a new equation empirically adding friction angle to it, as shown in Eq. 2.2:

$$F_c = \frac{16\pi\sigma_t^2\sigma_c h^2}{\left[2\sigma_t + \sigma_c \cos\psi_0 \left(\frac{1+\tan\psi_f}{\tan\psi_f}\right)\right]^2} \tag{2.2}$$

While Goktan [16] brought about

$$F_c = \frac{4\pi\sigma_t h^2 \sin^2(\psi_0 + \psi_f)}{\cos(\psi_0 + \psi_f)} \tag{2.3}$$

where ψ_f (in degrees) is the friction angle between the pick and the material to cut. Roxborough and Liu [14] claimed that their model, Eq. 2.3, could predict well the peak forces in cutting Grindleford Sandstones. Nevertheless, Goktan and Gunes [17] found that the predicted peak cutting force still significantly underestimated the real measurements in the full-scale laboratory experiments, although the friction angle was considered. They postulated that ignorance of the attack angle effect (asymmetrical cutting condition) in these two models led to the mismatch of the results. Then they empirically added the rake angle (geometrically related to attack angle, which is defined as an angle between the tool axis and the tangent of the cutting path, as shown in Fig. 2.3 [83]) to Evan's formula based on the curve fitting results from their full-scale experimental data, which is expressed in Eq. 2.4:

$$F_c = \frac{12\pi\sigma_t h^2 \sin^2\left[(90-\alpha_0)/2 + \psi_0 + \psi_f\right]}{\cos\left[(90-\alpha_0)/2 + \psi_0 + \psi_f\right]} \tag{2.4}$$

where α_0 is the rake angle of a point-attack bit.

However, the peak cutting forces predicted by these models remain different from the successive experimental results [2]. The need for detailed and deep analyses on the formulation is mandatory due to the crucial importance of the attack angle on optimizing the cutting efficiency reported in [6-7, 22, 84-90] in mining practices. Therefore, to deeply investigate the attack angle effect on cutting force became necessary. From the above analyses, although those models are not perfect, at least, we understand the peak cutting force may correlate with attack angle, depth of cut, bit geometry and rock properties, which somehow provides a way of assessing the mean cutting force in relation to the energy consumption.

2.2.2.3 *Specific energy*

Mean cutting force possesses a direct relation to specific energy, which is defined as the work done by the cutting force to excavate a unit volume of rock and is another important factor in estimating the cutting efficiency. Besides the straightforward calculations from the definition, specific energy can also be predicted by other parameters such as rock properties and operational parameters: in view of its significance, Hughes [97] and Mellor [98] theoretically formulated specific energy in relation to elastic modulus and compressive strength. Detailed rock cutting tests, however, show that specific energy is not only a function of rock properties but also closely related to operational parameters such as rotational speed, cutting power of excavation machines and tool geometry: Bilgin [99] conducted various rock cutting experiments held on 22 different rock specimens with the compressive strength varying from 10 to 179 MPa and demonstrated that there is a linear relationship between the uni-axial compressive strength with optimum mean cutting force and specific energy respectively, which was in line with the previous research [6, 72, 93, 100-102]. While, Roxborough [103-106] reported that specific energy decreases dramatically to a certain level with increasing depth of cut and decreasing tool angle. It is noticed that mean cutting force and specific energy vary with other factors, such as operational features and rock properties. Thus, the multi variable effect on specific energy is of interest for finding out the cutting conditions for optimum cutting efficiency.

2.2.3 Bit wear

High efficiency of mechanical performances of underground road-header machines is crucial to profitability and productivity in modern mining sites. However, bit wear seriously affects the advance rate of the machines under arduous cutting conditions, which leads to cost increases and project delays.

Research has been carried out to obtain a suitable bit with optimum shape and optimum abrasive material in order to extend its life under different cutting conditions. In [107], two bit shapes, wedge and point-attack types, were chosen as the comparable testing tools. The results demonstrated that the point-attack bit induced larger cutting forces but suffered less wear than the wedge bit. In spite of this, asymmetrical wear and damage happened to the point-attack bit and this was largely due to its severe rubbing contact with the wall of the cut grove (ridges/lands). The corresponding wear mechanism can be adhesion, abrasion, oxidation, or diffusion, depending on the cutting conditions [44].

Further studies were undertaken in order to identify the wear factors for the WC point-attack bits. Investigations [108] indicated that bit wear highly depended on the temperature that a bit experienced during cutting, of which cutting velocity was the main factor. In order to minimize the temperature effect, PDC material (Polycrystalline

Diamond Composite), with a PCD layer sintered on a WC base, was attempted to form a bit [109-114], to take advantages of the PCD's high temperature endurance. However, different thermal expansion properties of the WC base and the PCD layer often led to the ripping off of the PCD layer at a higher cutting temperature [115]. Hence, it is necessary to apply pure PCD point-attack bits to conduct a comparable test against WC bits to assess the wear resistance in rock cutting.

2.3 Edge chipping of brittle materials

An in-situ test in mining is often costly and time consuming and it is difficult to acquire accurately necessary data such as cutting forces and rock/coal fragmentation mechanisms. Hence, sensitive laboratory testing methods need to be developed. Edge chipping, to some extent, is close to rock cutting due to their similar cutting configurations as shown in Fig. 2.5.

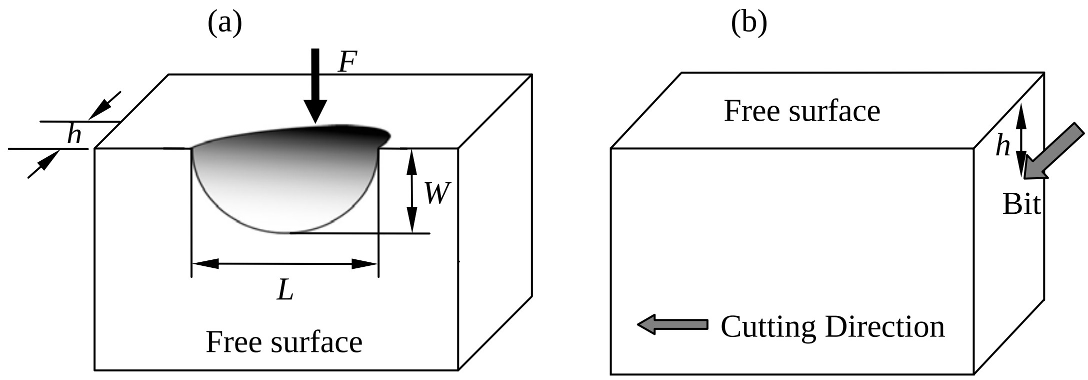

Fig. 2.5 Edge chipping and rock cutting

If the force direction in an edge chipping process is regarded as the cutting direction of the cutting bit and the free surface in edge chipping is viewed as the cutting surface, then edge chipping is similar to linear rock cutting. A concentrated force (F) is applied at the distance (h) from the indenting point to the free surface in an edge chipping, which is equivalent to the depth of cut in rock cutting. Following an increase of the force, a volume of material with length (L) and width (W) is then excavated. In laboratory, an easy-controlled edge chipping test can be a good way of analysing the rock cutting mechanism. It will be convenient to exploit edge chipping method to analyse the details for rock chipping.

2.3.1 Basis of edge chipping

Intuitionistic schematic specification of edge chipping is shown from a side view in Fig. 2.6. d is the penetration depth, corresponding to the increased force F as shown in Fig. 2.6(a). An example of the quantitative relation between the change of force and distance is illustrated in Fig. 2.6(b). F increases followed by increment of d until it reaches a peak value F_{pp}. Then, the catastrophic fracture happens, leading to a chip formed in the end. d_{pp} is the maximum penetration depth before fracture. The area of O, d_{pp} and the peak point represents the total energy consumed in the chipping process. As an edge chipping test can easily be applied in labs, it will be a convenient way to explore the nature of the chipping process.

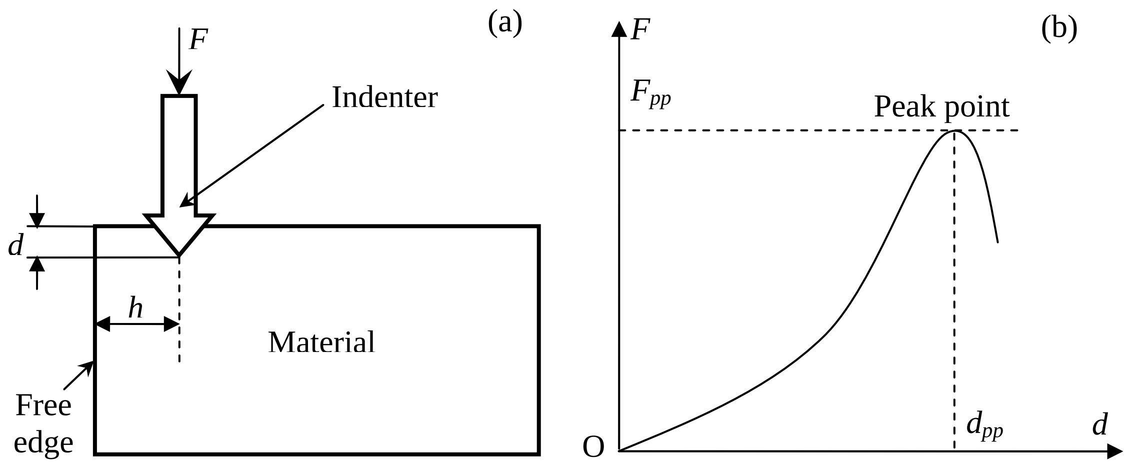

Fig. 2.6 (a) Side view of edge chipping process; (b) Force-depth relation

2.3.2 Crack and chip formation

For obtaining a good understanding of chipping mechanisms with different bits, such as the Rockwell cone and Vicker's, several attempts have been tried: Morrell [116] built up a two-dimensional analytical model for investigating edge fracture using a conical bit. The results showed that the maximum hoop stress around the indentation trace occurs at two symmetrical points on the circle close to the free edge and crack linearly extends to the free side on the top surface. Chai and Lawn [117] used a Vicker's bit to conduct several edge chipping experiments on soda lime glass and they got some important findings: cracks are initiated along the two vertexes of the pyramid (as shown in Fig. 2.7 (a)-(b)) and following the increase of force, crack propagates until fracture happens (a big drop of force) after some time with a chip formed in the end; the half penny shaped median crack is the predominant pattern throughout the whole chipping process, as shown in Fig. 2.7 (c) (cracks were those darker lines) and before crack becomes unstable, crack approximately extends in a plane and the plane contains the force axis. Those phenomena were also observed in other experiments on glass [118-

123]. From the above findings, it is noteworthy that the edge chipping process contains the processes of crack initiation, propagation and immediate fracture with a half penny shaped median crack dominant in the whole process when sharp bits are applied.

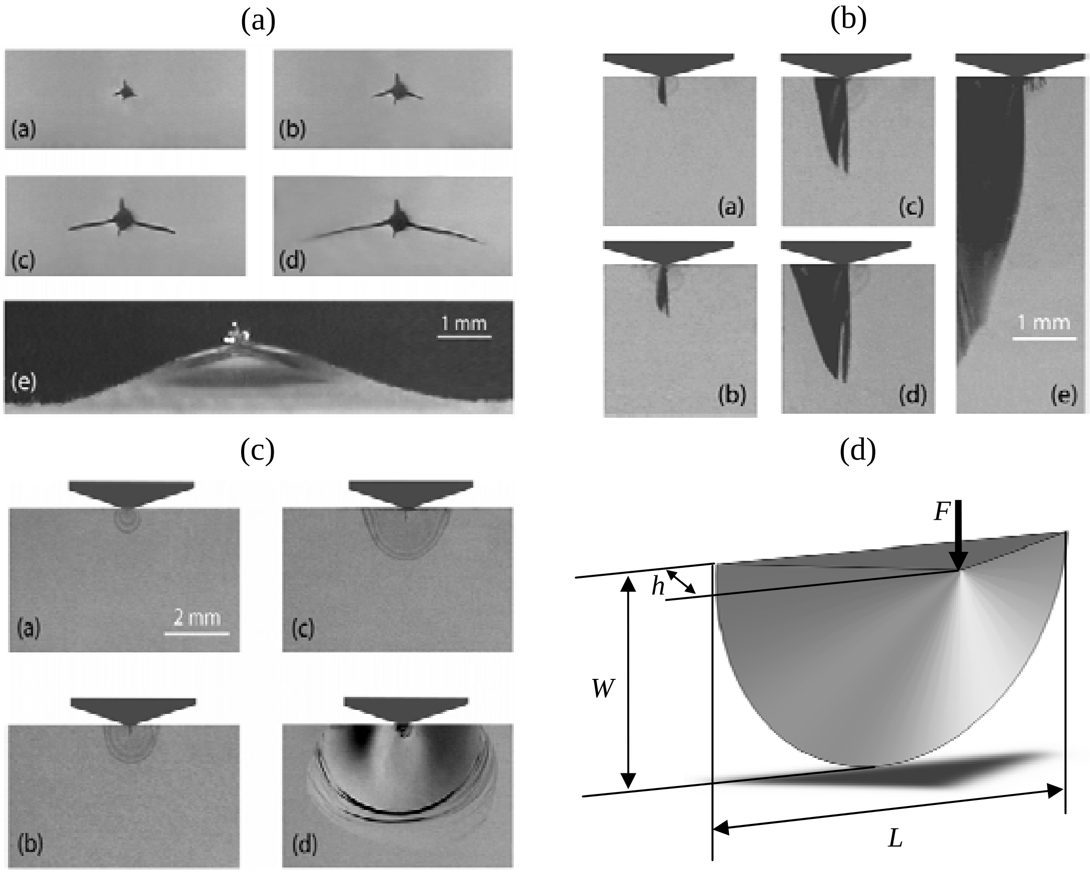

Fig. 2.7 Crack morphology in chipping glass [117]: (a) Crack top view; (b) Crack side view; (c) Crack front view; (d) Profile of a conchoidal chip

After the abrupt fracture, a chip with conchoidal shape is formed [124-131], as shown in Fig. 2.7 (d). Although early in the Stone Age, people already exploited this chipping method to knap flint or fabricate stone tools [132-135], no one became aware of the essential relations of chip dimensions until Almond [136] first discovered the linear relationships between *L*-*h* and *W*-*h* respectively, reflecting the geometrical similarity of the chip dimensions. Subsequent researchers enlarged the scope of the test specimens to glass and ceramics and found the same law still applied [117, 124-125, 137]. With input from previous analyses of peak cutting force, the chip geometrical similarity may possess the power of illuminating the relation between the chip and force, which may also provide a basis for the further calculation of the energy consumption in relation to force.

2.3.3 Peak chipping force

Besides straightforward observations of chipping tests, the mechanical behaviours of the material can be investigated by the application of external force. Due to its convenient acquisition, chipping force can be used for understanding the chipping mechanism, which is correlated with the crack features. Thus, the evaluation of the relation between peak chipping force and depth of cut has attracted many researchers.

In the early stages, researchers attempted to set up the force-depth relation by applying the cantilever beam model with a pre-crack at the end point of the depth of cut [124, 133, 137]. Cotterell [133] formulated the chipping force using a transited point load and bending moment with the consideration of Mode I and II stress intensity factors. He also found that the chipping force is determined mainly by the stiffness of the material. Thouless [137] revealed that general trends in cracking are broadly consistent with the predicted chipping force from crack location, crack propagation, and onset of chipping by conducting experiments on glass and PMMA. In an analytical and numerical investigation, Chiu [124] built force models considering the nonlinear effect generated from a moment during the chip bending. This research provided an introduction to the theoretical investigation of edge chipping problems. However, in edge chipping, there is no prescribed crack, which demonstrates a significant defect from the above model as the stress field underneath the bit without a prescribed crack is dramatically different from one that cracked. Therefore, further experimental work was conducted strictly under the real edge chipping conditions: apply a continuous point force on the intact material surface near a free edge until a chip is formed.

Danzer [138] and Gogotsi [139-143] conducted a series of edge chipping experiments on various kinds of brittle solids such as glass, alumina, flint, zirconia and quasi-brittle metals and found that the chip geometrical similarity is material independent, whilst the chipping force required to produce a chip had a strong material dependency. They further pointed out that there is a constant quotient between peak chipping force (F_{pp}) and depth of cut (h), which is defined as the edge toughness (ET) of the material to evaluate the resistance of an edge to damage. Later, Gogotsi [144-146] noticed that ET is found to be linearly correlated to the fracture toughness K_c, an important material property for evaluating fracture resistance.

In succession, from Quinn's experiments [129] on ceramics, whose structure is closer to rock than glass, the F_{pp} - h relation was not found to be linear, instead, the linear relation only exists in the high force region and the regression lines mismatch the original point. Instead, a power relationship between force and depth of cut with an average exponent of 1.3 fitted all experimental data and curves passed the original point. Even though a new power relationship was obtained, the lack of analytical explanation would motivate the further researches. Interestingly, Quinn also found that from dimensional analysis, K_c would be dependent on the normal force divided by edge distance powered by 1.5, eg. $K_c \propto F / h^{1.5}$.

In fracture mechanics [147], the Mode I stress intensity factor is equivalent to K_c at crack equilibrium. In terms of the Griffith energy-balance condition [148], Atkinson [149] and Swain [150-151] built up the relationship between crack size and force in indentation of a brittle solid. The derivation was based on the calculation of the total external mechanical energy and fracture surface energy considering the characteristic crack dimension, c (see Fig. 2.8) and the strain energy density. The final expression gives rise to:

$$F^2 / c^3 = const.(\gamma, E) \tag{2.5}$$

where γ is the fracture surface energy of the material and E is the Young's modulus.

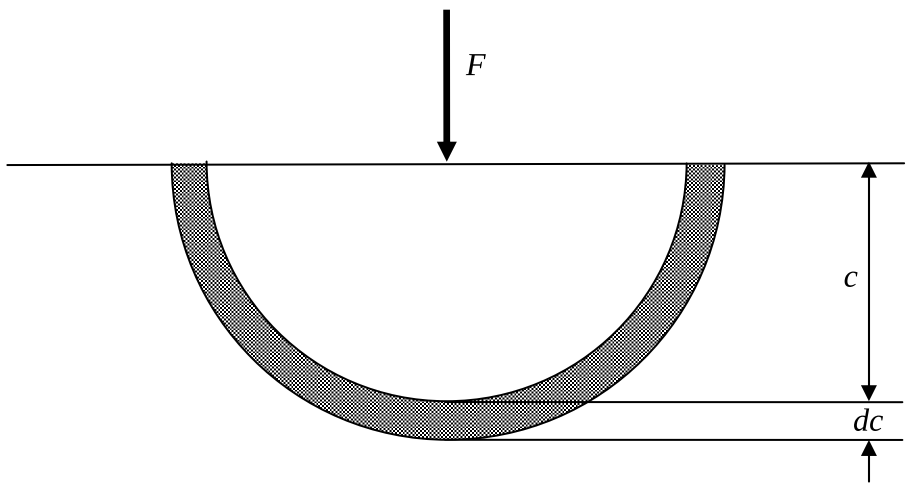

Fig. 2.8 Crack extension with point force under sharp indentation

From the fracture mechanics handbook [152], Lawn [153] rewrote Eq. 2.5 in full with the consideration of fracture toughness K_c, given the prevailing stable propagation of the crack at sustained force F :

$$K_c = \chi F / c^{1.5} \tag{2.6}$$

where χ is a dimensionless constant relevant to the bit geometry. Based on Eq. 2.6, Chai and Lawn [117] theoretically and experimentally demonstrated its validity based on Lawn's research of the configuration of median crack under sharp indentation on soda lime glass and various ceramics (eg. Rockwell, Vicker's and Knoop indentations) [153]. They further extended the relationship between the peak chipping force F_{pp} and crack dimension c into F_{pp} and depth of cut h by normalizing $c^{1.5}$ with $h^{1.5}$ by introducing a dimensionless function f_c, which was used for describing the crack evolutions.

$$F_{pp} = \beta_0 K_c h^{1.5} \tag{2.7}$$

where $\beta_0 = \frac{1}{\chi}(\frac{c_F}{h})^{1.5} f_c(\frac{c_F}{h})$ is a dimensionless constant independent of material and c_F is the crack length at the peak point. Then the force-distance relation powered by 1.5 matched the dimensional analysis of K_c.

Chai and Lawn's derivation provides a way of simply measuring the fracture toughness, depending on the fitted coefficient β_0. Especially, Eq. 2.7 possesses its dominance: at least, it is based on a real chipping model with consideration of the free edge effect. Also the application of fracture mechanics makes the formulation more reasonable.

Moreover, the free edge effect is supposed to be related to the power difference of the force-depth relations. In summary, it is worth taking a whole look at the previous power relations on peak force and depth of cut, which are 1, 1.3 and 1.5 respectively. Quinn's results demonstrate a 1.3 power relationship between the force and depth of cut for fine-powdered brittle ceramics. While, Chai and Lawn demonstrated a strong power relation with an exponent of 1.5, based on experimental observations of soda lime glass and ceramics. Those relations may need to be modified when applying to multiphase mineral composites with different grain sizes. Hence, it can be hypothesized that the exponent of power relation for rock materials should be close to 1.3 and located in the range from 1.3 to 1.5.

2.3.4 Fracture toughness of brittle materials

As discussed in Section 2.3.3, fracture toughness K_c, related to the force-depth relation, is a fundamental issue in modern fracture mechanics based on Griffith's work. In materials science, fracture toughness is a material property to assess the ability of a material to resist fracture, and is one of the most important properties of any materials for designing applications. Fracture toughness is also a quantitative way of expressing material resistance to brittle fracture when a crack is present [154]. Therefore, measurement of fracture toughness becomes more emphasized in researching crack behaviour and making reliable structural designs. Since crack propagation is the major failure mechanism of rock materials in many cases [155-156], fracture toughness, resistance to crack initiation and crack propagation, has become one of the most important parameters in analysing the failure of rock materials, designing rock boring equipments, predicting rock drilling and excavation forces etc [157-160].

Based on fracture mechanics in brittle solids, fracture toughness can be determined experimentally and theoretically. In order to enforce the consistency and accuracy of experimental results, ISRM (International Society of Rock Mechanics) suggested three specific experimental methods for rock materials [161]: short rod (SR) method, chevron bend (CB) method; and chevron-notched Brazilian disc (CCNBD) method. In addition, indentation test [149, 162], radial cracked ring test [163], round compact disk in tension test [107] etc were also adopted, circumventing the difficulties in producing a prescribed notch in brittle material (such as rocks, ceramics) and in measuring the crack size accurately. Another attempt to determine fracture toughness was to relate the fracture toughness with other material properties, such as tensile strength, compressive strength and brittleness [164-166], which were much easier to measure in laboratories. Although these relations could be rigorous in theory, the experimental results however varied from case to case especially in rock mechanics [164-166]

Because of its convenience and easy control, edge chipping methods can be applied in testing the fracture toughness of various kinds of ceramics, glasses and quasi-brittle metals [118, 130-131, 136, 139-140, 167-170]. Edge chipping of glass and ceramics correlates fracture resistance to toughness [142-143, 145, 171]. In Gogotsi's works, the fracture toughness K_c is linearly related to the quotient of the peak chipping force and the corresponding depth of cut [144]. However, few literatures have been reported for measuring rock toughness using edge chipping. Owing to its close relationship with chipping force, simplicity in experimental setup and direct relation to rock cutting, edge chipping can become an alternative approach to study the fracture mechanics of rocks. In combined consideration with the chipping force analyses in Section 2.3.3, the power relation between the peak chipping force and depth of cut is vital for determining the toughness. Hence, determination of the exponent of this power relation becomes a necessity.

2.3.5 Inclined edge chipping

As discussed above, although there are abundant researches in edge chipping, most of the work focuses only on perpendicular force application and little has been done regarding the inclined chipping mechanism except a few literatures [115, 172]. Quinn [172] conducted experiments on soda lime glass and reported that the inclined angle has effects on the scar morphology and peak chipping force. It was found that greater force is required to form a chip when the force is with larger attack angles and the quantitative analyses of chip geometrical changes could enable back calculation of the peak chipping force. Although there are detailed discussions referring to the experimental observations of the inclined chipping mechanism, deeper explanations for such phenomena are also needed.

For the sake of obtaining an explanation of the inclined chipping mechanism, Chai and Lawn [115] analytically formulated the relationship (see Eq. 2.8) among peak chipping force, depth of cut, inclined and sidewall angles based on the crack geometrical relations (as shown in Fig. 2.9).

$$F_p = \beta_0 K_c h^{1.5} \left(\frac{\cos\theta_s}{1+\kappa\sin(90^\circ-\alpha+\theta_s)}\right)^{1.5} \tag{2.8}$$

where α is the attack angle, l is the distance from the critical point of the crack to the free side, θ_s is the angle between sidewall and vertical line, F_p represents the general peak chipping force and κ is the ratio of c_F and h, mentioned in section 2.2.4. They successfully identified the inclined sidewall effects on the peak force with perpendicular force application by conducting chipping tests with a Vicker's bit near the edges of glass blocks. From the above researches, we may find that the peak inclined force is closely related to crack information and the peak inclined force still possesses a power relation with depth of cut.

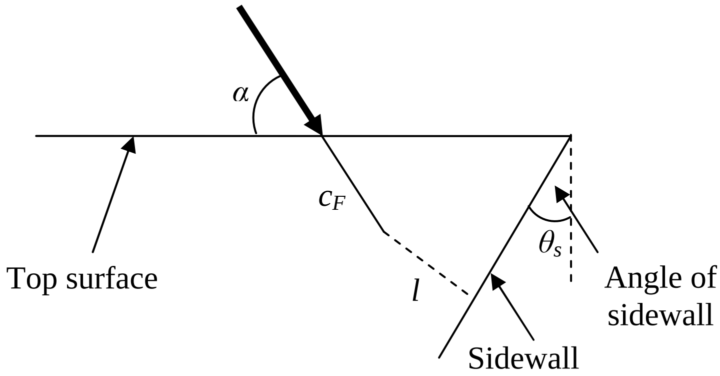

Fig. 2.9 Schematic of inclined chipping with non-normal force and non-orthogonal free surface at critical point

2.4 Concluding remarks

A comprehensive literature review of relevant researches provides a fundamental understanding of the internal mechanism of rock chipping and the relevant parameters focused on in rock cutting, such as cutting force and specific energy. It also reveals the relationship between edge chipping and rock cutting and the feasibility of applying edge chipping methods for investigating rock cutting in relation to verification of the availability of the cutting bit.

The factors involved in the rock cutting process such as fine grain generation, cutting force and specific energy, are suitable for comparing the bit cutting performances. With the investigation of the crack path in relation to the rock chipping mechanism, it is noticed that in Guo's research [72], the initial crack was assumed to be at 45° to the direction of stress. In real cases the crack inclination angle is not always the same as be assumed. Especially, when tangential force is applied in the real cutting process, the initial crack inclination angle may vary following the attack angle change. Therefore, it may be necessary to foresee the suitable crack direction in another way. For Evans' formulation, the size determination of the imaginary cutting hole was not properly justified with the comparison of the expansion cavity model [96]. This may result in inaccuracy in analysing the chipping process. Although other researchers further modified the formula considering friction angle and attack angle, the basic assumption and deductions were still from Evans' model. Hence, it is necessary to find a more reliable way of deducing the force formula with the consideration of attack angle and depth of cut effects.

In the analyses on edge chipping, most of the experiments focused on glass. Thus, for other brittle materials, such as ceramics or rock, there are no verifications that may have the same crack mechanism as glass. It is also noted that most work was focused on the chipping mechanism with Vickers bit and even though there are a few cases using other bits such as Rockwell conical and Knoop bits, the comparison of distinct mechanisms formed by different bits is still unclear. And especially, there have been no further explorations on different orientations of the effect of the pyramidal bit on chipping and the corresponding force. For the investigation of chip geometrical similarity, almost all researches concentrated only on the results with perpendicular force application, although quite a few studies, e.g. the experimental research on soda lime glass in [173], assumed this similarity could be extended to the chipping situation with inclined force application. But the lack of experimental verifications has become a defect.

Moreover, for the analyses of the peak chipping force in the perpendicular edge chipping test, there are still several concerns: following the increase of the depth of cut the linear relationship between the peak chipping force and depth of cut seems inaccurate, which was also reported in Quinn's experiments. Although Quinn found that the exponent of the power relationship is averagely 1.3, there is no elucidation on its causation. Furthermore, for the exponent of 1.5 in testing soda lime glass, Eq. 2.7 was formulated from the experimental curve fittings although it was based on the theoretical deduction of Eq. 2.5, with the assumption that the Mode I crack would exist all through the whole chipping process; all observations of the crack were from soda lime glass, which may not be appropriate for analysing the crack in other brittle materials, e.g. rock. Therefore, an explanation clarifying the exponent is necessary. Furthermore, the establishment of a relation between toughness and directly obtained parameters such as peak force and depth of cut should be highlighted, so as to bring about a simple method to predict rock toughness. This work is necessary due to the inaccurate measurements and complex fabrication of the specimen in the current rock toughness testing methods.

Finally, further exploration of the inclined chipping mechanism becomes crucial in order to theoretically discuss the attack angle effect in rock cutting. From the analyses in Section 2.3.5, it is known that, in the analytical result from Chai, there was no experimental verification of the attack angle effect on chipping force. Moreover, the formulation was based on the assumptions that the Mode I crack type would still be available through all the inclined chipping tests and also the chip geometrical similarity would be extended to the inclined case. Thus, the lack of experimental verifications of the relationship might result in uncertainty about whether those assumptions could also be suitably applied to chipping other brittle materials, such as ceramics and rocks. Hence, experiments on chipping rock should be conducted in order to check the accuracy of the assumptions and a new relationship between peak force and attack angle might be set up to suitably adapt to rock chipping. As in rock cutting, attack angle is within the range of 0-90 degrees, to the focus will be on the angles within this range.

In relation to the above analyses in this thesis, specific tasks will be undertaken and are listed below:

- Apply an edge chipping method to obtain a deep understanding of the rock chipping mechanism in relation to fine grains, crack path and chip morphology and then compare the results from both the conical and the new pyramidal bit, considering fine grain generation, chip dimensions, peak chipping force and energy consumption. For the pyramidal bit, different orientation effects on the chipping force and energy also need to be investigated.
- Theoretically analyse the peak chipping force with and without attack angle effect and attempt to clarify the relationship among force, depth of cut, attack angle and rock property. Apply an edge chipping method for measuring the rock toughness based on the relation of toughness and other relevant parameters, such as peak force and depth of cut. Explain the similarity and differences between the previous results and those in this research.
- Based on the experimental findings and the corresponding theoretical analyses, bit design can be improved by conducting linear rock cutting tests. Cutting

performances in relation to cutting force, specific energy, chip mass and wear can be compared in order to check the availability of the improved cutting bit. Peak and mean cutting forces can also be compared with the theoretical results. Multi variable effects on cutting performance can also be considered.

Chapter 3

Experimental studies on edge chipping of rock

3.1 Introduction

As discussed in Chapter 2, bit geometry affects cutting efficiency. Consequently, it is necessary to find a new bit profile, as changing the included angle of the bit was the previous major way of improving the cutting efficiency. Moreover, for validating and further improving a new bit design, detailed investigations into rock chipping mechanisms will be necessary and helpful. Thus, choosing a suitable and convenient method for assessing the chipping behaviour of rock with the new bit is crucial. To date, an in-situ test in mining is usually costly, time consuming and it is difficult to acquire accurately necessary data such as rock/coal fragmentation mechanisms and cutting forces.

Therefore, sensitive laboratory testing methods need to be developed. An easy-controlled edge chipping test can be conducted to simulate the rock cutting process, due to similarity to the cutting operation in mining. However, investigations into the edge chipping of rock materials are not extensive in the literature, although some analyses of the chipping processes and crack mechanisms [97-98, 117, 124-127, 129-130, 136, 174] have been carried out on glass and ceramics. Based on observations of crack initiation and propagation in soda lime glass, Chai and Lawn [117] investigated the relationship between the indentation fracture and the edge chipping crack, concluding that the fracture toughness of these brittle materials could be approximately obtained from an edge chipping test. McCormick [126] and Almond and McCormick [136] reported that the chip/flake shapes are geometrically similar under varying depths of cut. Thouless et al. [130] conducted a theoretical analysis on the edge flaking of glass and Lardner et al. [174], Chiu et al. [124] and Quinn et al. [129], based on two fracture toughness modes, carried out some experiments to ascertain the edge toughness and crack mechanisms in both indentation and edge chipping. Morrell [127] reported that the flakes of brittle materials from quasi static and impact chipping tests are geometrically similar. It is worthwhile to point out that in all the above studies, the bits used were very small in comparison with any mining cutters, and the bit shapes were the Vickers and Rockwell cone, different from the geometry of a mining cutter. The sample materials used in their laboratory tests were glass and ceramics, rather than rocks.

Clearly, there is a need for a deeper understanding of the edge chipping process with considerations of crack mechanism, chip morphology, fine grain generation and energy consumptions [103, 105, 175-177] to compare the cutting performances of pyramidal [178] and conical bits. Therefore, this chapter firstly introduces a new bit with a pyramidal profile. Then a practical investigation is undertaken to compare the cutting performances of both bits based on the exploration of the chipping mechanism of rock.

3.2 Initial bit design

3.2.1 Hypothesis

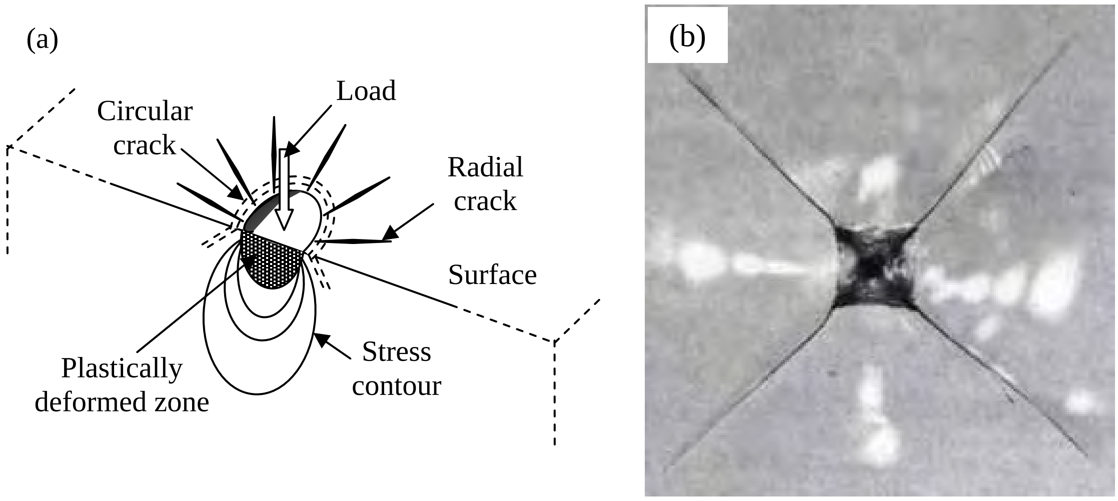

Fig. 3.1 (a) Conical indentation [179] and (b) Pyramidal indentation [180]

The hypothesis was derived from observations of the fracture mechanisms in both the Rockwell cone and Vicker's indentation. A schematic image describing the Rockwell cone indentation on glass as shown in Fig. 3.1(a): The bit penetrated into the material with a plastic deformation region created underneath the bit. Radial cracks on and below the top surface and a spherical crack in the median plane emanated in the process [179]. In the process of forming the radial cracks, continuous bit squeezing and material densifying induced the generation of small fragments and fine grains. More radial cracks and fine fragment bursting resulted in the increment of energy consumption. Fig. 3.1(b) displays the indentation fracture on glass by the pyramidal bit. Instead of creating a large number of radial cracks, the Vicker's pyramid brought about major spherical median cracks initiated and propagated [181-182] along the four vertexes, due to stress concentrations.

3.2.2 Designed profile

From the above observations and analyses, stress concentration of the pyramidal profile may be helpful in cracking the material. So a pyramidal bit [178] was attempted in order to check whether the cracking performances of the pyramid were as predicted above and to assess the performance in comparison to the currently used conical bit. The standard of designing the pyramidal bit was based on the same cross sectional areas at the same penetration depth for both bits. However, compared with the half included angle of $38°$ for the conical bit, the pyramid possessed an included angle between the two lateral surfaces of approximately $68°$. The top parts of both bits were the effective parts during cutting, with heights of 4.3mm for the cone and 3.5mm for the pyramid. The diameters of the top sphere were 1.2mm and 1mm for the conical and pyramidal bits respectively. For the sake of comparative assessment on the cutting performances of the pyramidal and the currently-used conical bits, the fabrications of both the conical bit [183] (Fig. 3.2 (a)) and the pyramidal bit (Fig. 3.2 (b)) were in half real size for the requirements of the lab test.

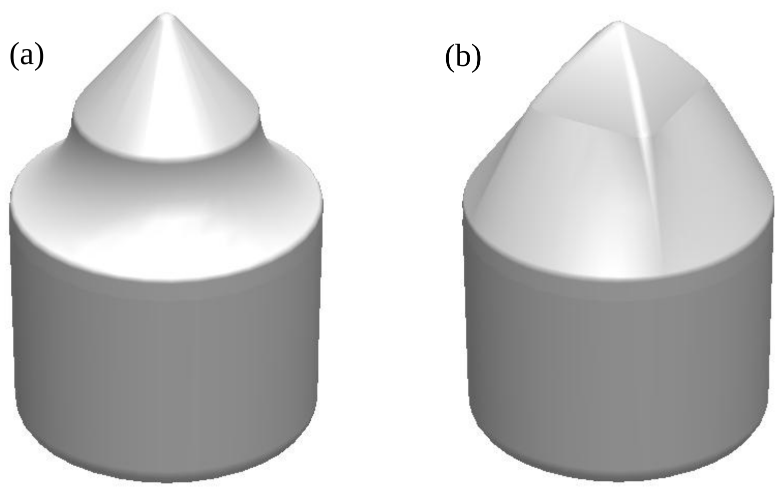

Fig. 3.2 (a) Conical bit; (b) Pyramidal bit

3.3 Experimental setup

An edge chipping test scheme is shown in Fig. 3.3(a), where h is defined as the depth of cut from the edge and d is the penetration depth of the bit. Underneath the bit tip, a major crack initiates and propagates with the increase of force. The crack propagation becomes unstable as the peak force is reached with the consequence of catastrophic failure and formation of a chip. The relation between force and penetration depth was schematically plotted in Fig. 3.3(b), where F_{pp} and d_{pp} denote the perpendicular peak force and the corresponding penetration depth respectively and W_t, the shaded area, is the total external work in this process, which is equivalent to the total energy consumption E_t majorly for crushing and forming a chip.

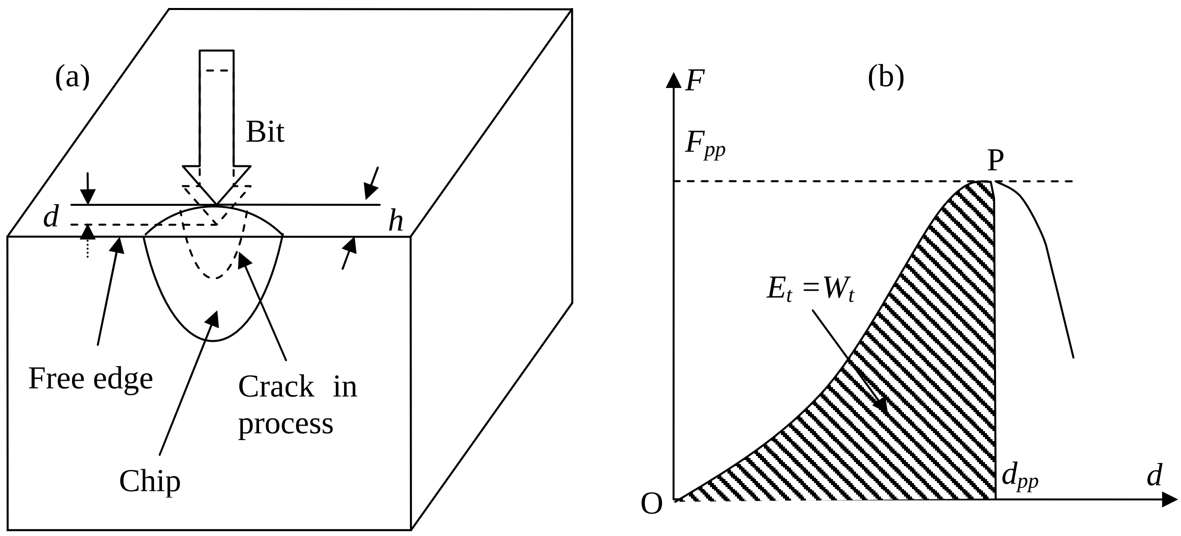

Fig. 3.3 (a) Edge chipping process; (b) Force depth curve

Universal INSTRON machines of 5567 and 8504 were used to implement the perpendicular and inclined chipping tests, which are shown in Figs. 3.4 and 3.5. Three special components were also applied for experimental assistance: the bits, the inpurpose holder for mounting the bits, and the clampers for fixing the rock samples. A 30kN load cell was employed to measure the force and displacement signals and a holding plate was used to fix the samples to restrict their possible horizontal movements during test.

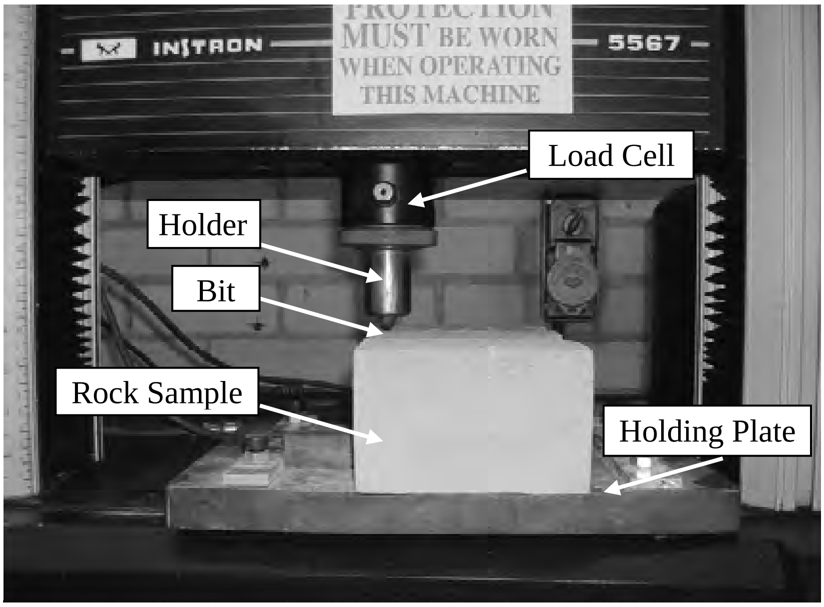

Fig. 3.4 Schematic setup of perpendicular edge chipping

The depths of cut in the perpendicular tests were from 4mm to 25mm respectively. In the inclined chipping tests, the depths of cut were fixed at 10 and 15mm, while the attack angles were selected from 70° to 90° for different materials. Below 70°, the shoulder of the holder will inevitably touch the rock surface, inducing inaccurate data. Specifically, attack angles in the tests were adjusted by placing quadrangular blocks with various cross-sectional areas on one side of the rock specimen, as shown in Fig. 3.6. The other side of the rock block was prevented by another block from moving forward. The inclined angle could then be determined by the ratio of L' and h'. Angle gauge was also used for a double measurement. Loading rate was set to be 1mm/min throughout the tests. Unloading was applied when force dropped over 50% compared with the previous peak point as the failure.

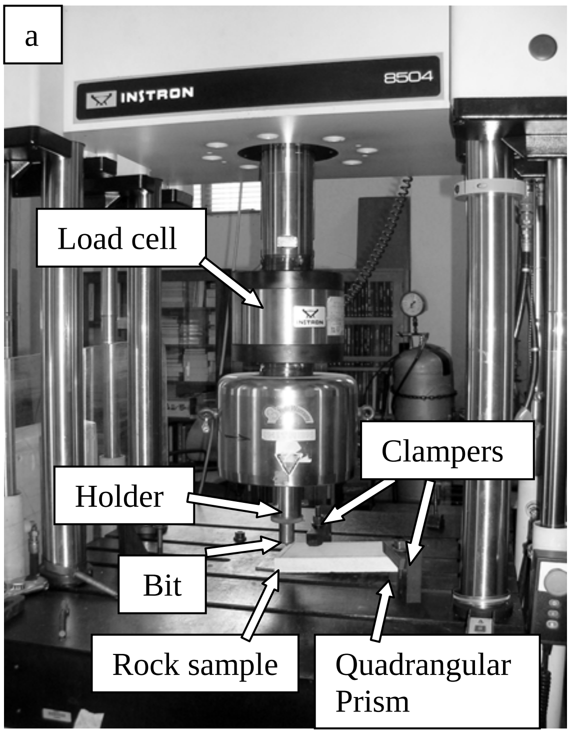

Fig. 3.5 Schematic setup of inclined edge chipping

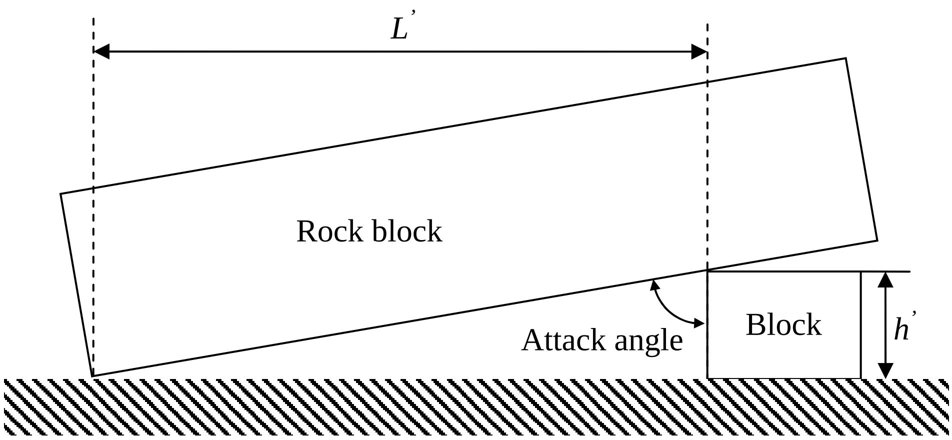

Fig. 3.6 Determination of inclined angle

Four kinds of sandstone produced in New South Wales of Australia, namely Bauhaus, Littlewood, Appin and Pyrmont, were selected for the tests, and the material properties are shown in Table 3.1. Prior to conducting the chipping tests, the rock blocks were cut into rectangular shape with the dimensions of length (mm) × width (mm) × thickness (mm) = 220 × 90 × 40, 215 × 100 × 80, 217 × 76 × 74, 219 × 118 × 74, 218 × 120 × 71, 220 × 118 × 73, and 150 × 150 × 150, respectively, based on the availability of the sandstone geometries. To minimize the effect of surface morphology, the specimen surfaces were ground to R_a=92μm with a parallelism tolerance of 1mm. Since the mechanical properties of sandstone are greatly influenced by its content of moisture, to obtain a uniform moisture control the samples before edge shipping tests were baked in a Labmaster oven at $70°C$ for 24 hours.

Table 3.1 Material properties of rocks

Type of material	Littlewood	Pyrmont	Appin	Bauhaus
Toughness ($MPam^{1/2}$)	1.15	0.91	0.82	0.72
Young's Modulus (GPa)	3.26	2.3	2.2	5
Poisson Ratio	0.23	0.3	0.25	0.25
Bulk density (ton/m^3)	2.21	2.28	2.18	2.25

Fig. 3.7 shows the pyramid (a) and cone (b), which were made from tungsten carbide (18% of cobalt). In a test with the pyramidal bit, its square-base diagonal was arranged to be either perpendicular to or parallel with a sample's side surface or with 45° and 135° respectively in order to apply two extreme conditions.

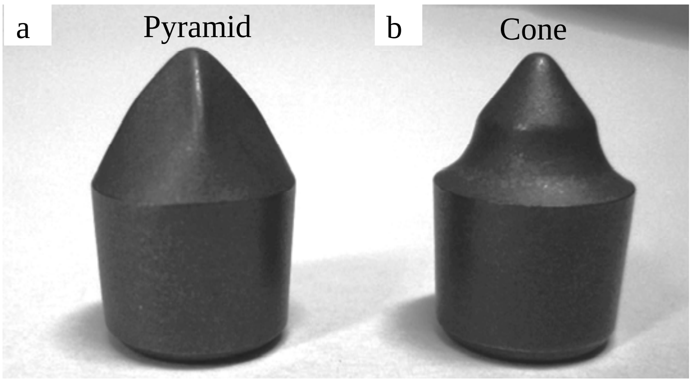

Fig. 3.7 Pyramidal and conical bits

3.4 Results and discussions

3.4.1 Crack mechanisms

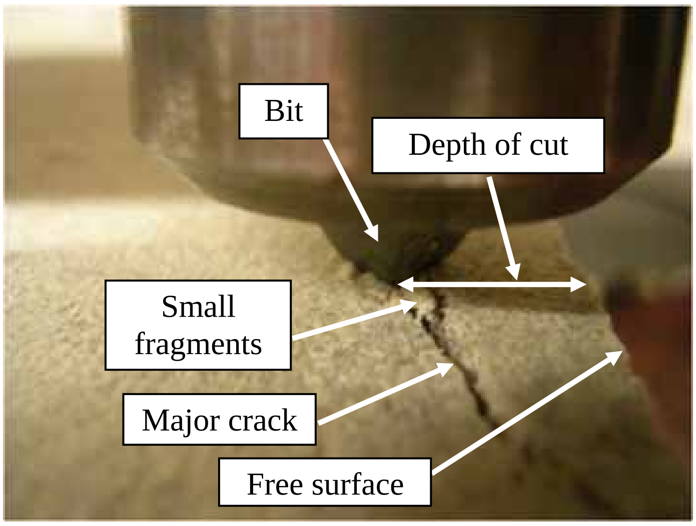

Fig. 3.8 Chipping induced by pyramid

Conical and pyramidal bits lead to different crack initiation circumstances. An example of crack induced by a pyramidal bit is shown in Fig. 3.8. When the bit penetrated to a certain depth, a major crack started along the two vertexes due to the strong stress concentration and then deviated almost linearly to the free surface in a tiny interval with a final chip formed in the end. Due to the fast crack initiation and propagation, brittle fracture may be predominant throughout the process. It was also qualitatively pointed out that the stress field underneath the bit was modified by elastic relaxation of the free edge, which led to the easy crack propagation and chip formation after the peak force was reached [17].

Fig. 3.9 (a) shows the top view of the final groove generated by the pyramidal bit with diagonals perpendicular and parallel to the free surface. Crack started from Points A and B, where stress concentration happened. Then it propagated along the linear trajectories represented by the two white lines. This may demonstrate the wedge drives the crack propagation after its initiation, like peeling the chip from the specimen. When the pyramid was reoriented at a position of two diagonals with 45° and 135° to the free side, stress concentration happened at the two adjacent vertexes as shown in Fig. 3.9(b). It is of interest to notice that a critical orientation of the pyramid may lead to ease of crack propagation and chip formation, reflecting minimum force and energy consumption.

Fig. 3.9(c) shows the scar generated by a conical bit. The major crack on the top surface emerged when penetration depth reached a certain value, and abruptly propagated to the free side. Instead of the causation from the stress concentrations, the serious squeezing forced the chip to burst from the rock sample. The major cracks happened at points A and B on the circular trace, which matched McCormick’s theoretical analyses on the crack system with a conical bit [125]. It demonstrated that the maximum hoop stress around the circular indentation takes places at two symmetrical points, A and B, as shown in Fig. 3.9(c). During penetration, a large number of radial cracks (see Fig. 2.2) were generated in the crush zone underneath the surface, which resulted in more energy consumption.

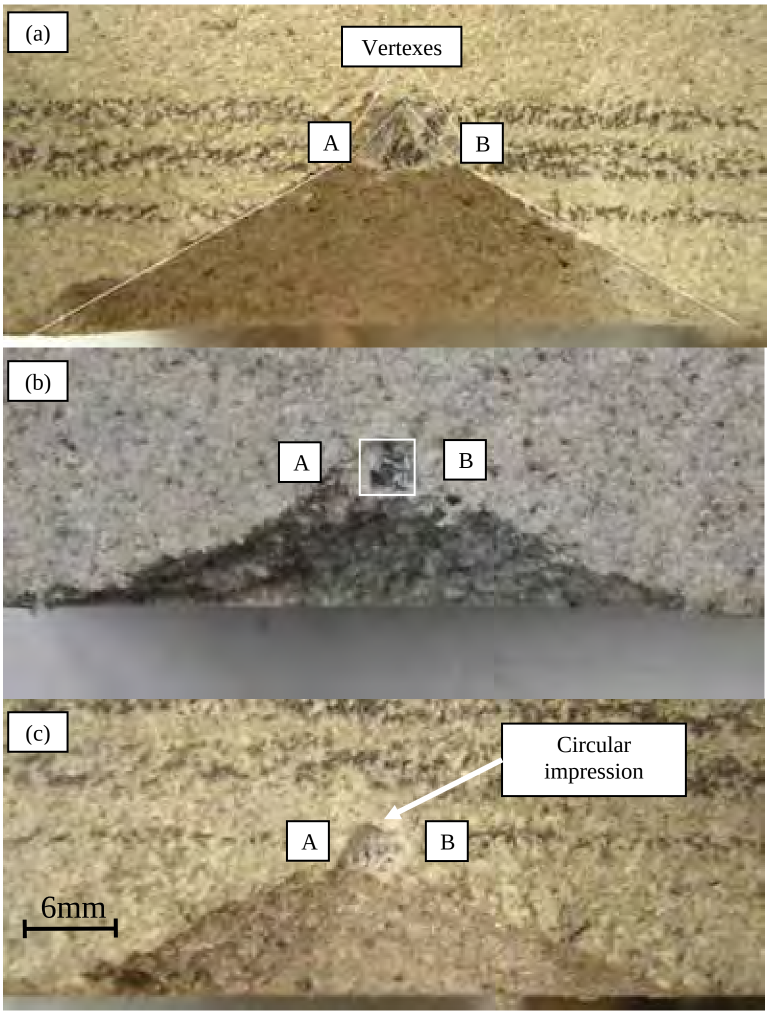

Fig. 3.9 Top view of the grooves generated by pyramidal (a) & (b) and conical bits (c)

Therefore, after a comparison of the above three crack mechanisms, the chipping process by a conical bit may consume more energy to form the radial cracks and burst the small fragments. The chipping mechanisms induced by two extreme orientations of the pyramid are majorly due to the stress concentration at two vertexes. Thus, we propose that the pyramid may consume less energy and the different bit orientations may lead to different force reactions and energy consumption.

3.4.2 Fine grains

The fine grains and fragments generated in crushing can be regarded as the source of dust in rock cutting. Hence, in this test, it is of interest to investigate the amount of fine grains and small fragments in a comparison of the bit cutting performances. Fig. 3.10(a) and (b) show the fine grains and small fragments induced by the pyramidal and conical bits respectively. It is comparatively observed that circumferential squeezing and abrading are the predominant cause of the creation of small fragments and fine grains by the conical bit; while, due to the stress concentration for the easy cracking, the pyramidal edges may cut the material to assist the bit to penetrate. Thus, fine grains may be less formed except in the part generated by the lateral surface compressions.

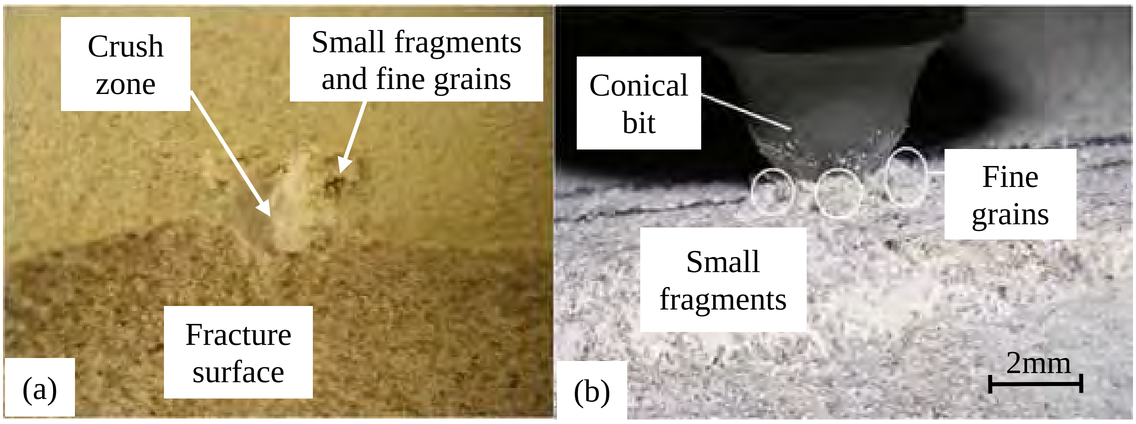

Fig. 3.10 The crush zone generated by the pyramidal (a) and conical (b) bits

More fine grains seem to be generated by the conical bit due to the different crushing mechanisms, and the compared result for fine grain generation can be assessed by gauging the weight of the fine grains, created in the whole process, including those in the crush zone and those attached to the bit surface. The ratio between the mass of the fine grains and the small blocks, and that of the major chips (under the same amount of mass) is considered as the comparison standard. Figs. 3.11 and 3.12 show the fine grains generated in the tests with both bits. The pile on the left hand side is for the conical chipping process, while the one on the right hand side is for pyramidal chipping. The size of the small blocks with the pyramidal bit is a little larger, about 2-3mm, than those with the conical bit, about 1-2mm. And the ratio with the conical bit is about 2.56%, while, for the pyramidal bit at both orientations of diagonals parallel and perpendicular to the free surface or diagonals with 45° and 135° to the free surface, the ratios are 1.38% and 1.41% respectively, about a half. It demonstrates that in the quasi-static rock cutting tests, dust generation with the pyramidal bit is less than that with the conical bit, which confirms to the previous hypothesis. The reason for this result might be due to the different crack mechanisms of both bits as discussed in Section 3.4.1. The pyramidal bit will generate stress concentrations for the major cracks along each vertex, instead of squeezing the surrounding materials to abrade more fine grains, like the conical bit.

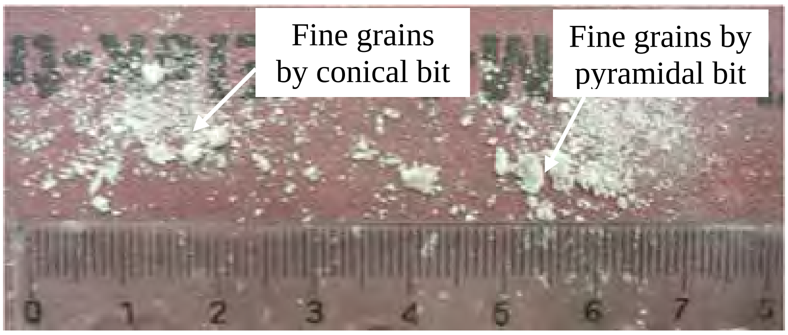

Fig. 3.11 The fine grain generated by both bits in perpendicular chipping on Bauhaus

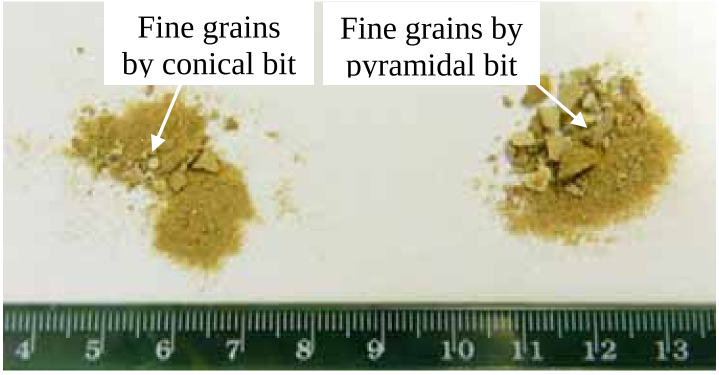

Fig. 3.12 The fine grain generated by both bits in inclined chipping on Littlewood

3.4.3 Crack path and crack deviation angle

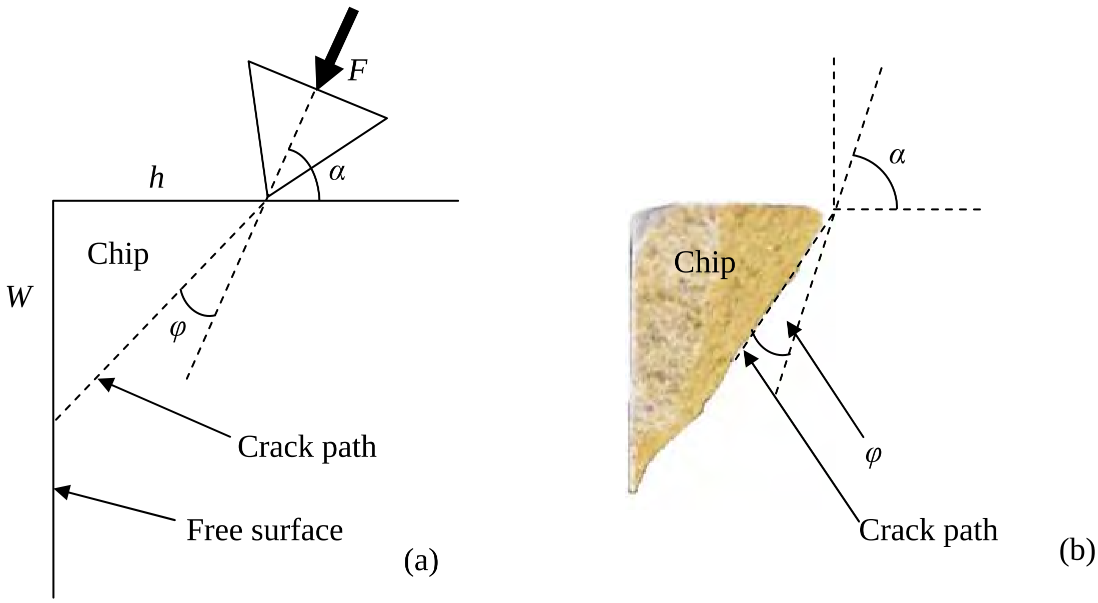

Fig. 3.13 Crack path (a); a real case of crack path (b);

During chipping, major cracks symmetrically propagate from the indentation point downwards and towards the free side surface. In terms of this symmetry, we investigated the crack trajectory on the median plane from the side view of the chip as shown in Fig. 3.13(a). An example of crack path characterization is shown in Fig. 3.13(b). It was observed that the crack starts from a small crush zone and extends straight downward and towards the free surface, in close to a straight line. This might be explained as: after the formation of the initial crack during crushing, brittle fracture happens, which leads to crack propagation along the path with a deviation angle to the previous crack direction [72, 184] in a very short period of time. This is probably the reason for the straight line-shaped crack trajectory. It was also found that the direction of major crack is not along the axis of the force, and instead, the propagation orientation deviates from the force axis with an angle φ for all kinds of sandstone in this research. This phenomenon does not confirm Chai and Lawn's experimental observations on soda lime glass [173], as they proposed that the major crack path followed the force axis. Therefore, it is necessary to find a suitable way of predicting the crack path and investigate the differences. From the above analyses, especially, we may formulate the chip width W in relation to depth of cut h, based on the geometrical feature of the crack, which gives rise to:

$$W = h \tan(\alpha - \varphi) \tag{3.1}$$

The relative change between φs and the corresponding α s is shown in Fig. 3.14. The angular elements of the major crack paths (solid black lines) demonstrate the effects on the elongation and foreshortening of W at different α s. Different from the crack mechanism of glass, there does not appear to be a strong trend to the adjacent free side as it was hardly to notice the deviation of direction from the preceding path was hard to notice after a critical time of propagation. Instead, the linear extension of the crack starts at the beginning and remains almost straight throughout the whole cracking process. With the increase of α , φ is also incremented but with a slower growth rate. A linear fit between α and φ was plotted, as shown in Fig. 3.15.

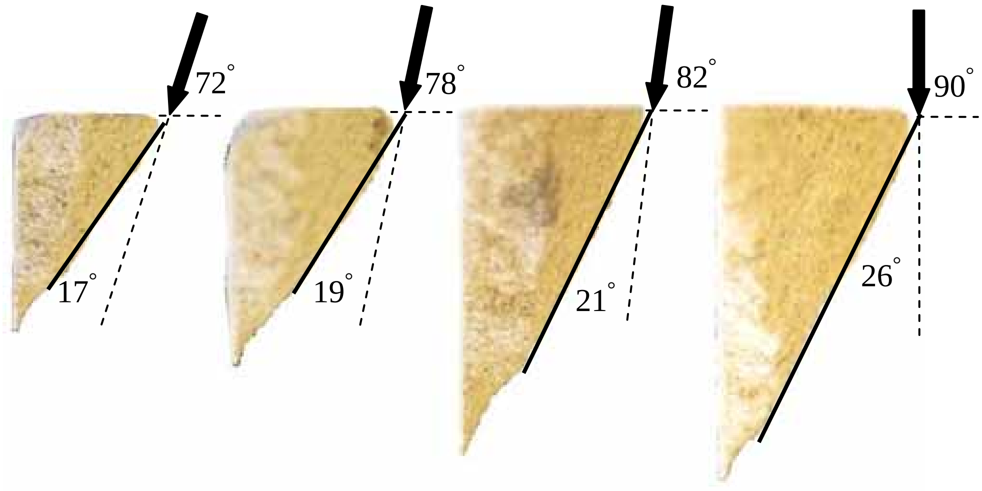

Fig. 3.14 Different φs at different α s

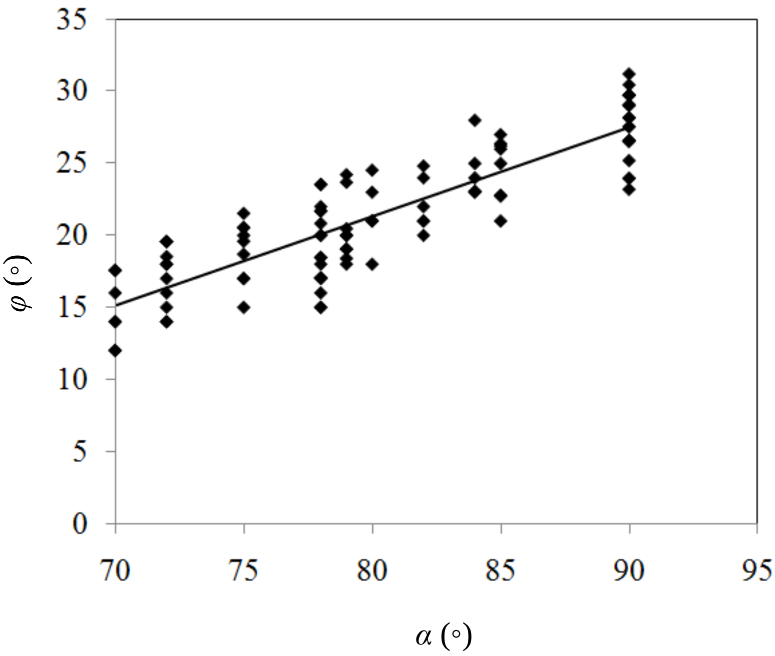

Fig. 3.15 α vs φ

3.4.4 Chip morphology

A typical conchoidal-shaped chip, with 15mm depth of cut, is shown in Fig. 3.16(a) while a simplified chip geometry schematically is shown in Fig. 3.16(b). L denotes the chip length respectively.

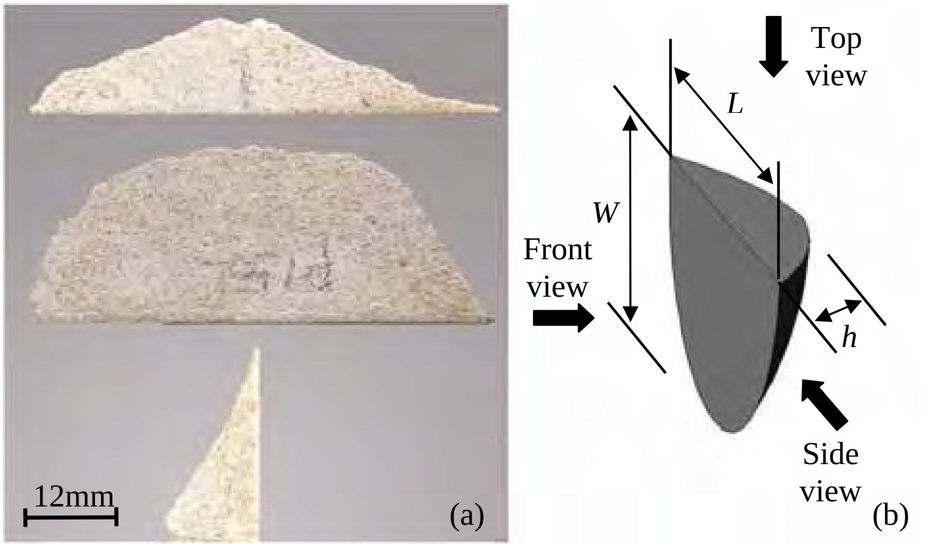

Fig. 3.16 A typical chip

3.4.4.1 *Chip appearances at different depths of cut and attack angles*

Two groups of chips in perpendicular chipping tests were selected, as shown in top, front and side views, in Fig. 3.17(a) for pyramidal bit and Fig. 3.17(b) for conical bit. Fig. 3.17(a) shows the chips with cutting depths of 8mm, 15mm, and 20mm, while Fig. 3.17(b) shows the chips with cutting depths of 8mm, 10mm and 15mm. It was found that L and W simultaneously increase while h is incremented. The shape of the chip front is similar to a half ellipse in Fig. 3.17(a), which may refer to the penny shaped median crack type for fracture. Moreover, the homogeneity and uniformity of the rock may give rise to asymmetry of the top surface of the chip.

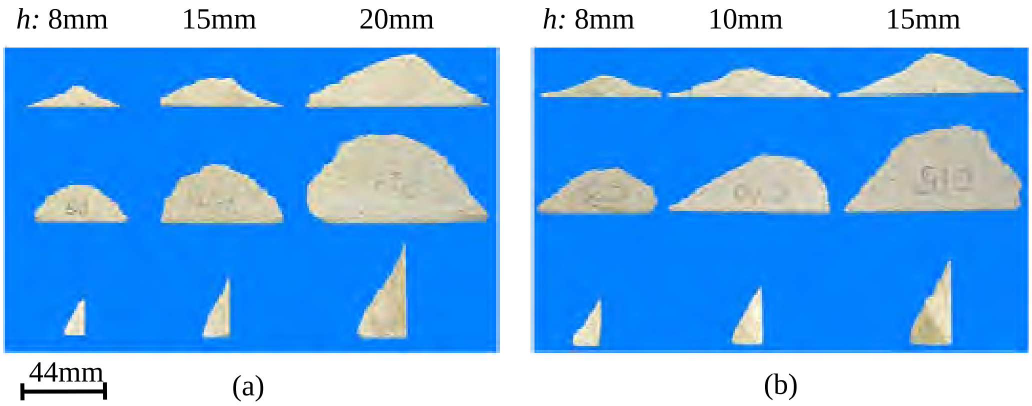

Fig. 3.17 Chips formed with pyramidal bit (a) and conical bit (b)

Fig. 3.18 shows a group of Littlewood chips with pyramidal bit at 10mm depth of cut and various attack angles, 72°, 78° and 82°. The chips are still in conchoidal shape. Compared with the top views of Bauhaus chips, those of Littlewood chips appear more symmetrical, which may demonstrate that Littlewood sandstone possesses a more uniform and homogeneous texture. Meanwhile, the front views show that the decrease of the attack angle induced the reductions of L and W. It further indicates that different attack angles alter the directions of the crack paths: the smaller the angle is, the shallower the chip is dug.

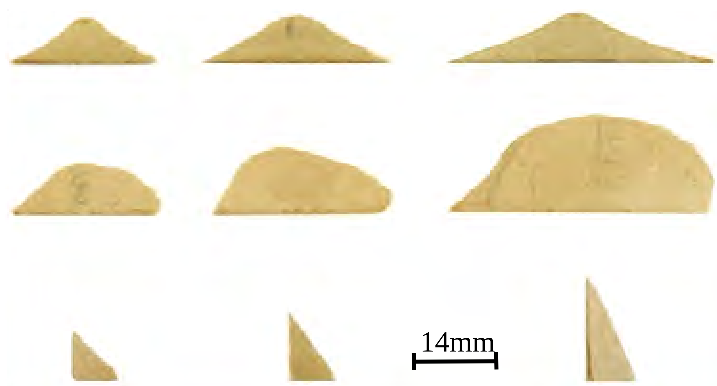

Fig. 3.18 Top, front and side views of chip morphology (Littlewood sandstone) at different inclined angles with pyramidal bit, from 72° (left) to 82° (right).

3.4.4.2 *Regression analyses of chip dimensions*

Based on the previous observations, a statistical analysis was adopted for a deep understanding of the essence of chip morphology. Plotting L and W versus h as shown in Fig. 3.19 for different bit shapes and materials, results for the chips in perpendicular chipping tests demonstrated strong linear relationships: $L \propto h$ and $W \propto h$. L/h and W/h are respectively 4.2 and 1.8 for the conical bit and 4.8 and 2.0 for pyramidal bits at two orientations. It is noteworthy that for each kind of bit these ratios do not vary with different rocks tested, which is consistent with findings in [117, 124-125, 127-128, 136]. The geometrical similarity implies that the chipping process involves a self-similar crack initiation and propagation process. The causes of the self-similarity are twofold. Firstly, both conical and pyramidal bits are sharp bits with the indentation area proportional to the square of penetration depth, which implies self-similarity of the strain field in a uniform material [185]. Secondly, the rock can be regarded as uniform and isotropic material in the macroscopic scale since the particle size in these rocks is much smaller than that of chips. It should be pointed out that L/h and W/h depend not only on bit geometry but also on the material structure. For soda lime glass indented with a pyramid bit [117], $L/h = 8.0$ and $W/h = 5.1$. However, for rocks, owing to the similarity in microstructures, the chip geometry remains similar across different kinds of rocks as shown in Fig. 3.19, which then brings about great convenience in analysing the fracture energy of rocks. With given experimental conditions, i.e., the depth of cut h and the bit shape, as well as the load-depth curve, one can easily estimate the energy per unit area consumed for creating the fracture surface, which provides a link to the toughness of the material, due to the relation between the material properties of specific fracture surface energy and fracture toughness in brittle materials.

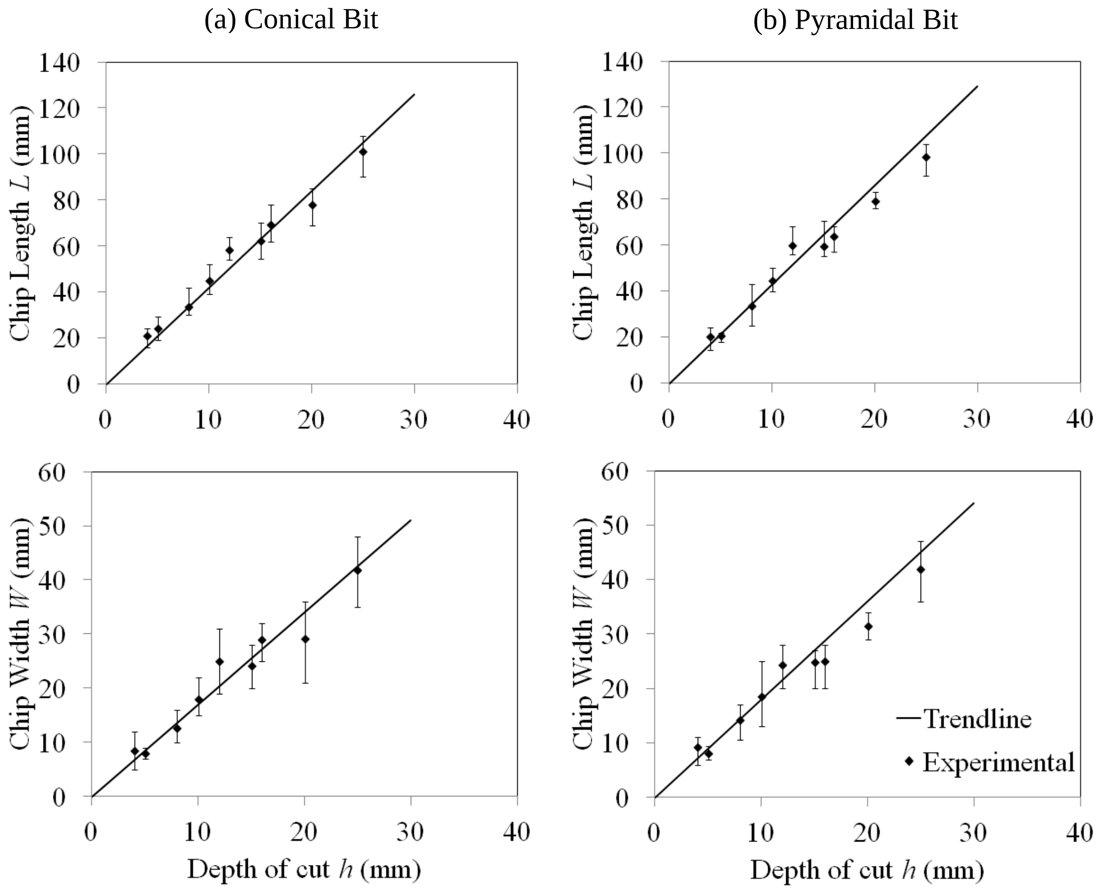

Fig. 3.19 Geometrical similarity of different sandstones

Considering all test conditions including inclined and perpendicular chipping, the statistical information for chips from all kinds of rocks on the ratio between L and W displays a constant around 2.6 for both conical and pyramidal bits as shown in Fig. 3.20, which then implies the chip geometrical similarity could be extended to the inclined chipping mechanism due to the insensitivity of the angular effects on the ratio of L/W. Based on Eq. 3.1 and the succeeding derivation based on $L/W = Const.$, L/h and W/h in relation to α s can be plotted, as shown in Fig. 3.21. Such plots focus the data on universal angular functions within scatter points. It is a fact that the experimental data can be fitted via the universal functions, which may be regarded as validation of the extension of geometrical similarity. As a result, the chip morphology observed in the experiments reveals a certain geometrical similarity, which is independent of material. Even for the inclined chipping configuration, the constant of L/W corresponds to the extension of the geometrical similarity when considering the angular component.

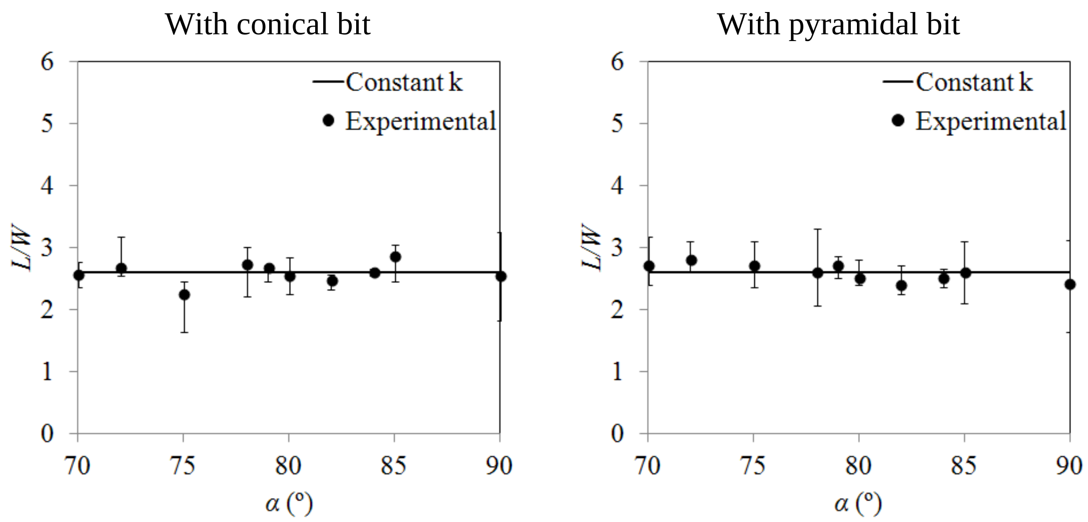

Fig. 3.20 Ratio between L and W for both bits on all kinds of rocks

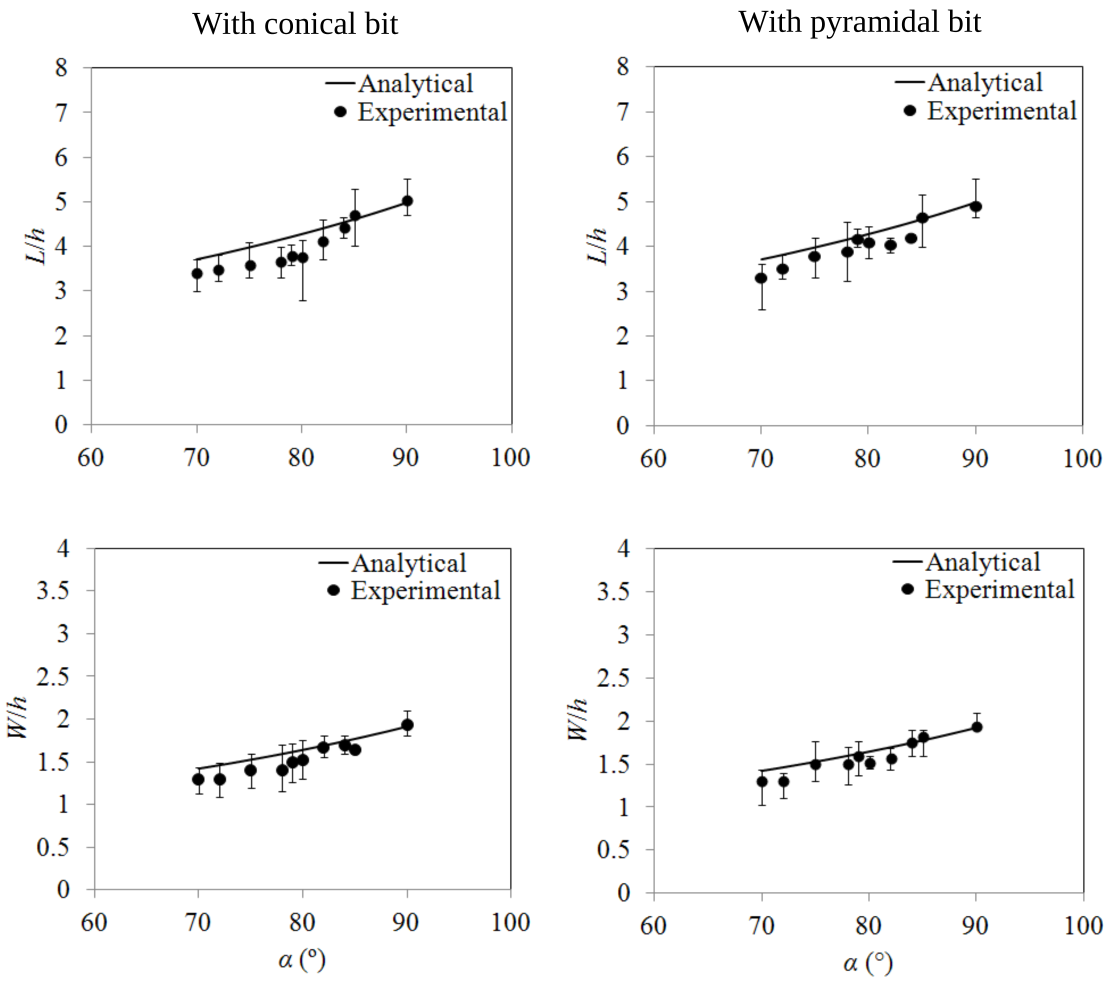

Fig. 3.21 Relationships between L/h, W/h and α with both conical and pyramidal bits

3.4.5 Peak chipping force and total energy consumption

To investigate the quantitative relations to the previous experimental observations, the curves related to the chipping force and the depth of cut were plotted for both conical and pyramidal bits, which could be easily obtained from the data acquisitions. From a curve in Fig. 3.3(b), the peak cutting force can be easily traced and the total energy consumption can also be obtained by the area between the curve and the horizontal axis.

3.4.5.1 *Peak force of different orientations of the pyramidal bit*

We investigate two extreme orientations of the pyramidal bit: two diagonals of the cross area parallel and perpendicular to the free surface or with 45° and 135° to the free edge as shown in Fig. 3.22. Experimental curves in perpendicular edge chipping tests on Bauhaus sandstone in Figs. 3.23 and 3.24 quantitatively show the orientation effect for the two extreme conditions. It was found that at different hs, $h = 10mm$ and $h = 15mm$, pyramidal diagonals with 45° and 135° consumed less energy compared with the other extreme orientation. It infers the possibility of an optimum orientation of the pyramid during cutting.

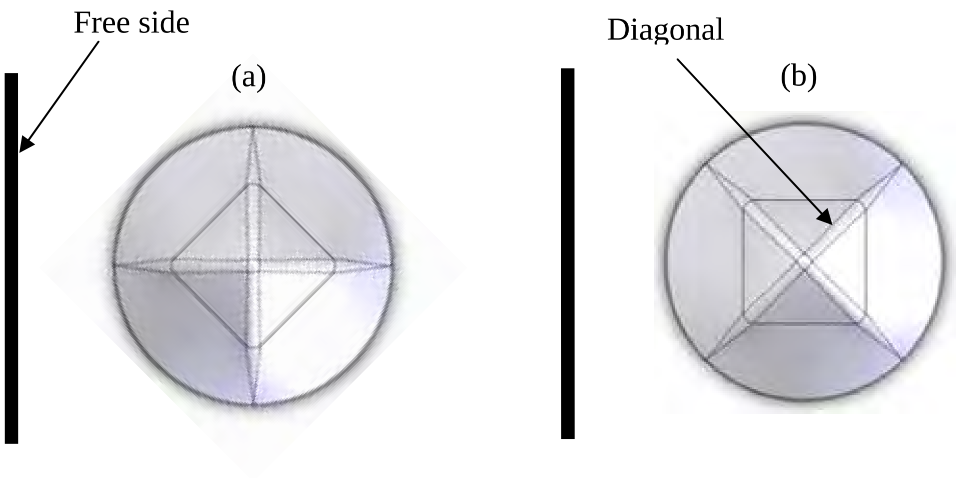

Fig. 3.22 Bottom views of different orientations of pyramid relative to free surface: (a) one edge perpendicular to free surface; (b) one diagonal with 45° to free surface

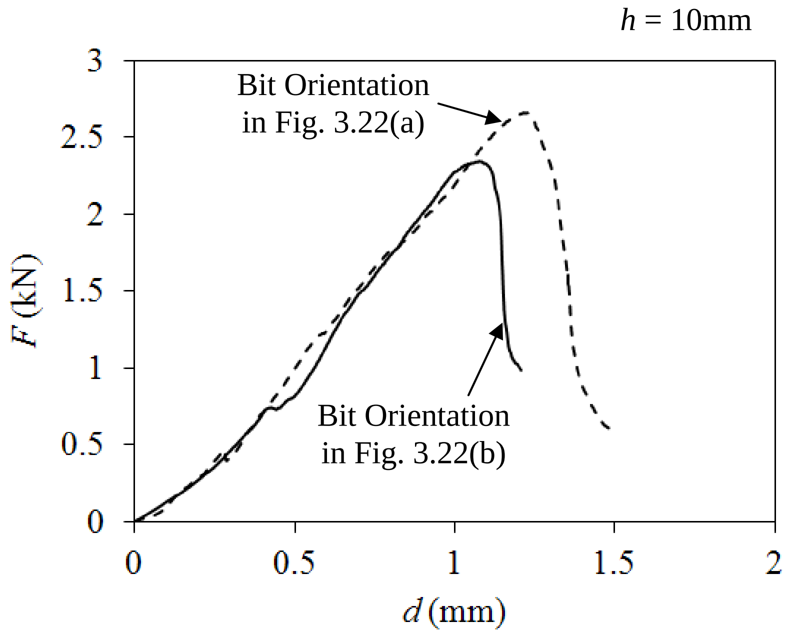

Fig. 3.23 Orientation effect of pyramid at $h = 10$mm

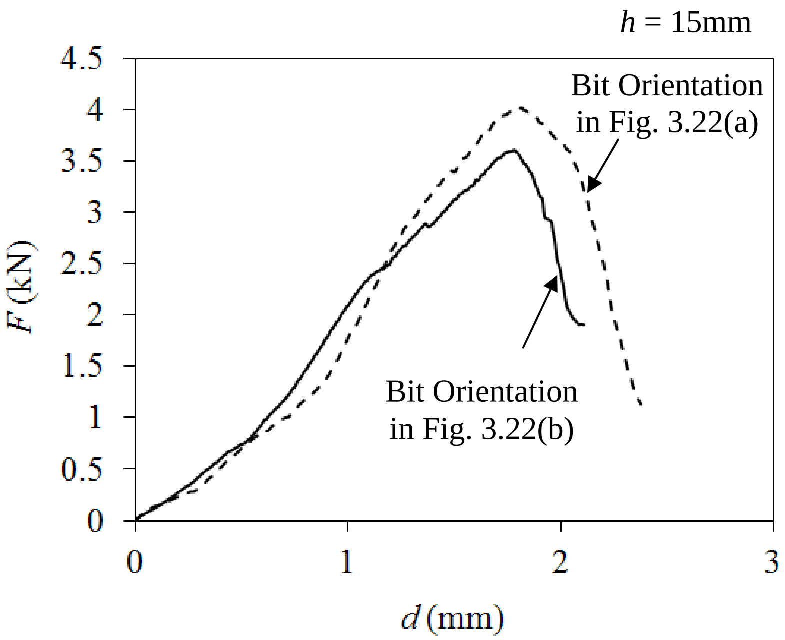

Fig. 3.24 Orientation effect of pyramid at $h = 15$mm

Verifications by simulations from my colleague are shown in Figs. 3.25 and 3.26. It was noticed that when diagonals are perpendicular and parallel to the free side, the cracks start at two stress-concentrated points and along a paralleled path to the free side, shown as the red area in Fig. 3.25. While, when diagonals were with 45° and 135° to the free side, after crack started, they propagated along a path angled with the free side. It infers that for the orientation in Fig. 3.26, the crack should spend less time in reaching the free side and create fracture, which further elucidates the force should be smaller according to the crack mechanism. It confirms the previous experimental observations. Moreover, even in the inclined chipping test, we also found the same phenomenon, which can be seen in Figs. 3.27 (a) and (b).

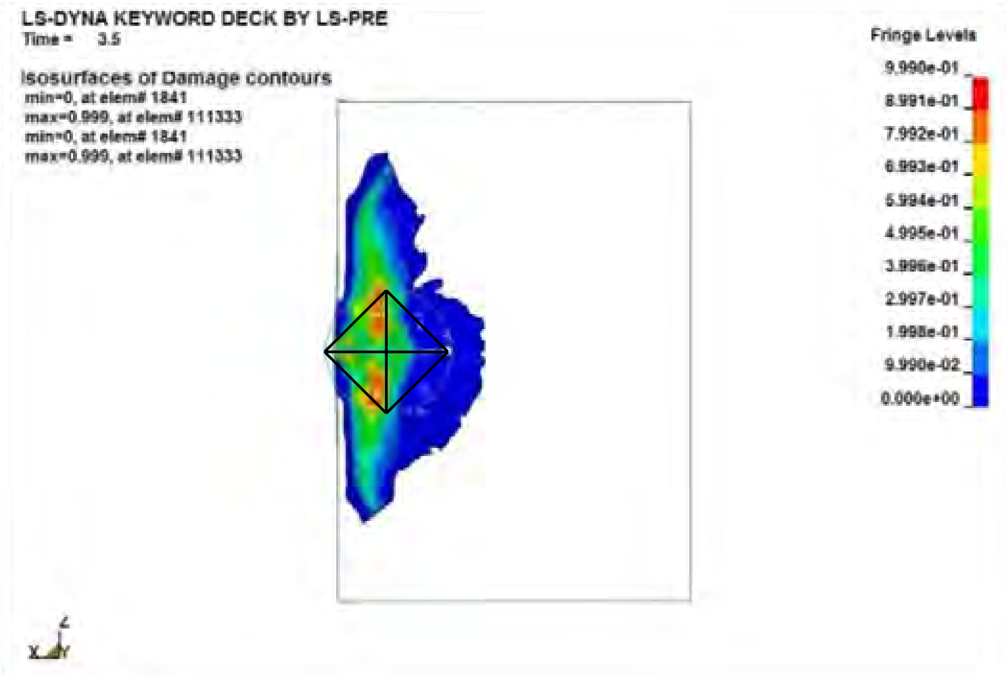

Fig. 3.25 Orientation as shown in Fig. 3.22(a)

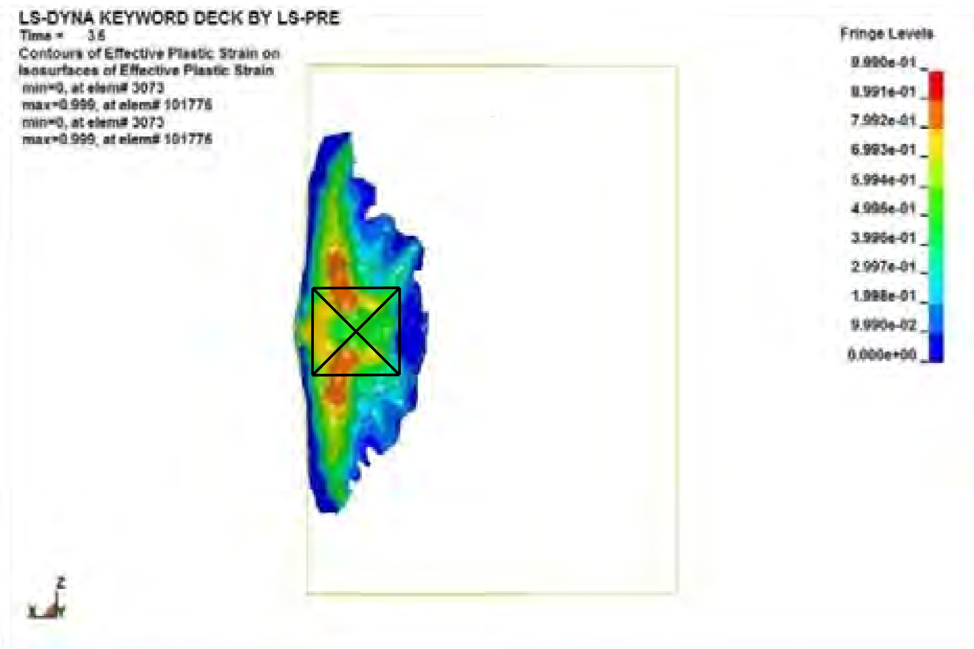

Fig. 3.26 Orientation as shown in Fig. 3.22(b)

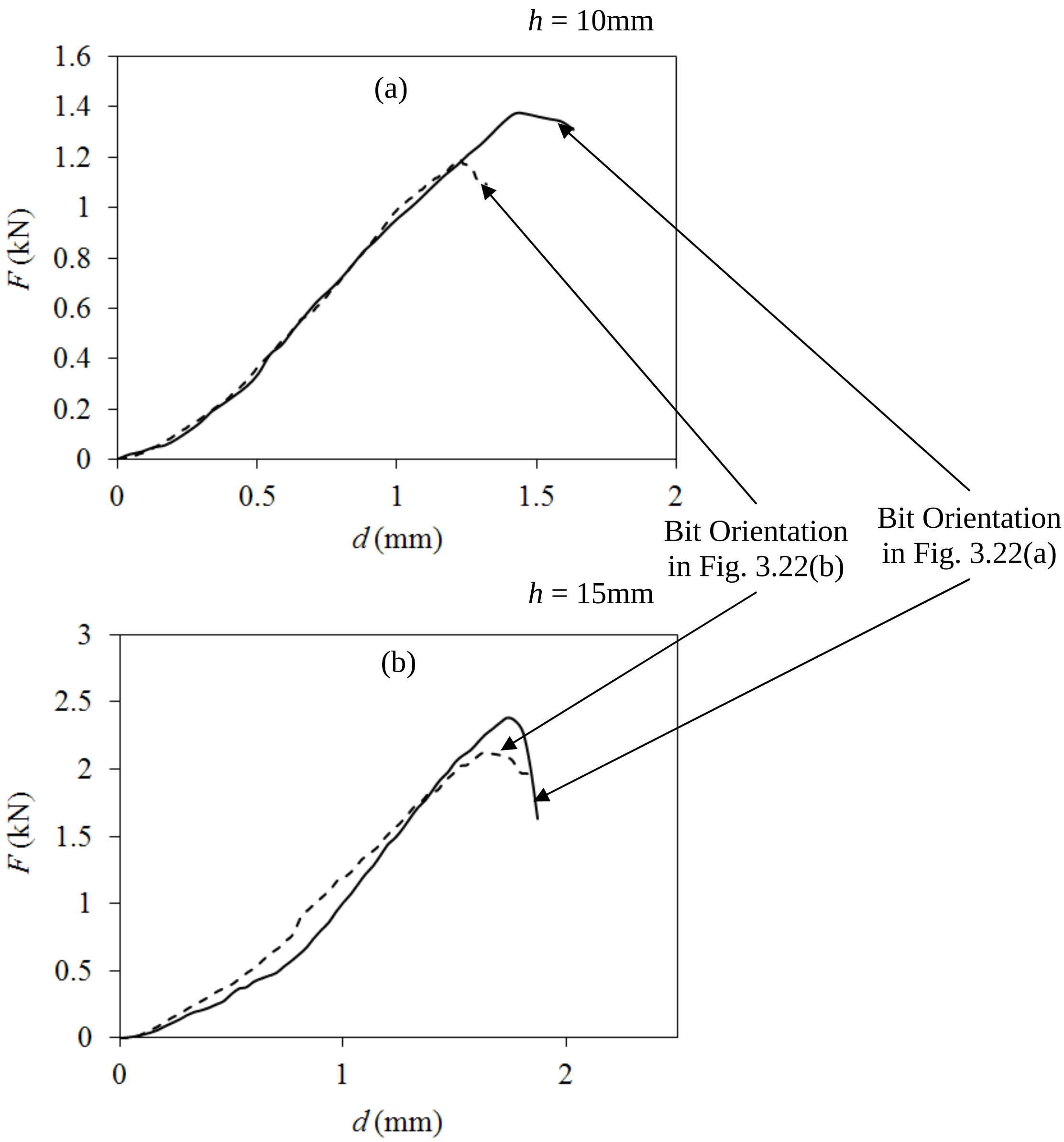

Fig. 3.27 Orientation effects at h = 10mm (a) and 15mm (b) at 80° on Bauhaus

3.4.5.2 *Relation between edge chipping and indentation*

Fig. 3.28 shows the plots of chipping force against the indentation depth for the test on Bauhaus with conical bit at depths of cut 10, 20, and 60 mm, respectively. For a sufficiently large depth of cut (e.g., h = 60 mm) and a small indentation force, the boundary effect becomes negligible. The situation approaches the perfect indentation problem. With further indentation, the indentation force approaches one or several local peaks associated with local crushing, inducing small fragments/powders around the bit. The maximum chipping force is followed by a catastrophic drop associated with the formation of a large conchoidal chip. Both the local crushing and the major edge chipping dissipate the elastic strain energy. The energy consumed in local crushing can be significant as observed by Carroll [186], who demonstrates that the energy consumed in forming the main fracture surface only takes a small fraction of the total energy.

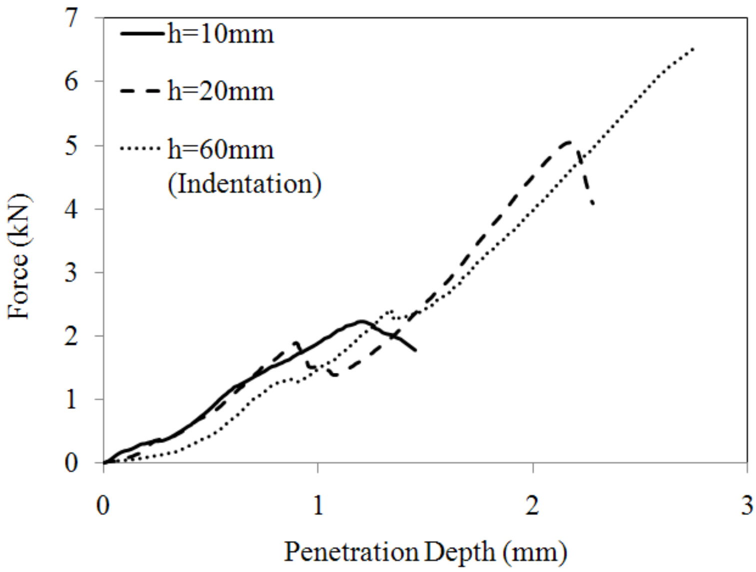

Fig. 3.28 Relationship between indentation and edge chipping

Fig. 3.29(a) and (b) plots the chipping forces versus indentation depths on Littlewood sandstone with conical and pyramidal bits respectively. It is noted that the peak chipping force increases with the depth of cut. Since the soaring parts of the curves resemble the indentation curves, we fit these curves with the quadratic equation:

$$F = \lambda H d^2 \tag{3.2}$$

where F is the indentation force, λ is a geometrical coefficient, d is the penetration depth and H is the indentation hardness. The quadratic fitting curves were drawn with the λH = 2.1GPa for a conical bit and λH = 1.9GPa for a pyramidal bit respectively. λH varies in material and bit shape. In Table 3.2, we listed λH s for all the cases.

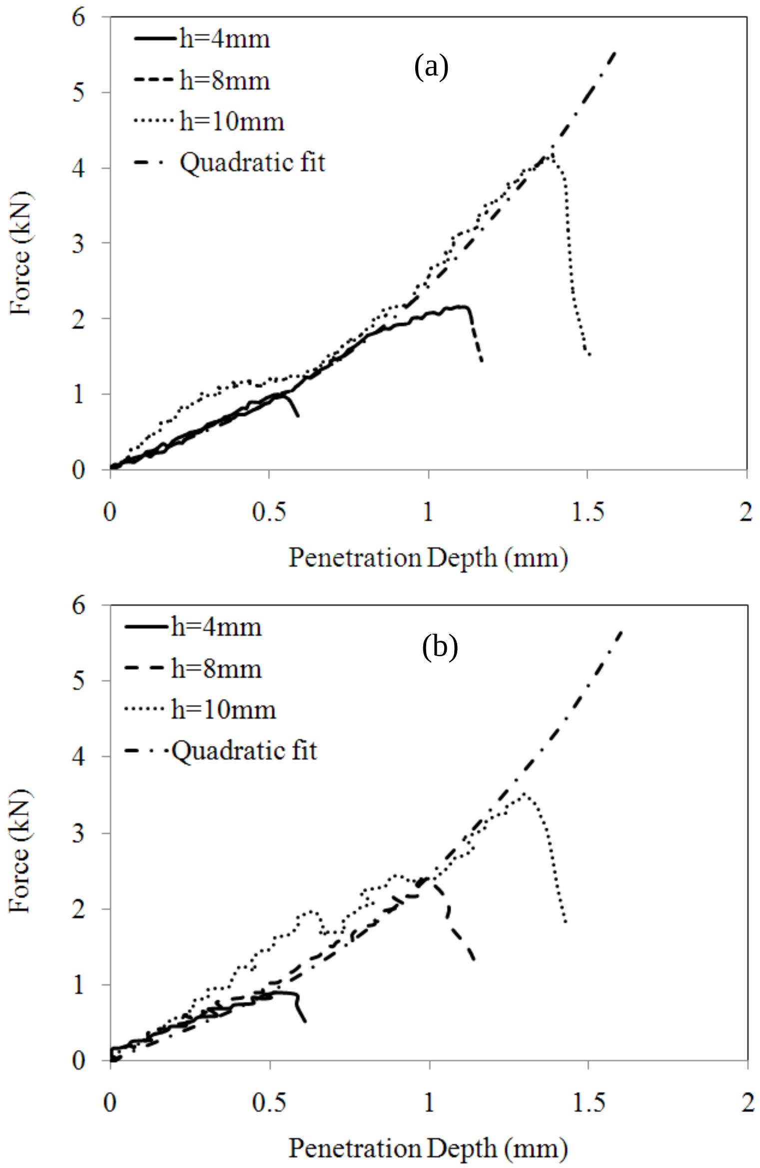

Fig. 3.29 Edge chipping curves with conical (a) and pyramidal (b) bits

Table 3.2 Measured values of λH

Material	Littlewood		Appin		Pyrmont		Bauhaus	
Bit	Cone	Pyramid	Cone	Pyramid	Cone	Pyramid	Cone	Pyramid
λH (GPa)	2.1	1.9	1.7	1.56	1.46	1.22	1.9	1.7

Moreover, in inclined experiments on Littlewood sandstone, the force-penetration depth curves at different attack angles also fit the quadratic trajectory. Fig. 3.30(a) and (b) shows the data curves at $h = 10mm$ and different attack angles from 72° to 90° with conical and pyramidal bits respectively, which demonstrates that Eq. 3.2 can also be applied in inclined chipping. At the same depth of cut, with the decrease of the attack angle, the peak inclined chipping force was also reduced. In terms of the same quadratic relation with the perpendicular force, it may further illuminate that the peak inclined chipping force F_p should be the product of the peak perpendicular chipping force F_{pp} and the triangular function $f(\alpha)$ in relation to the crack geometry, which can be simplified as $F_p = F_{pp} f(\alpha)$. The attack angle does not affect the force-penetration depth relation and instead, it only takes effect on the value of the peak force.

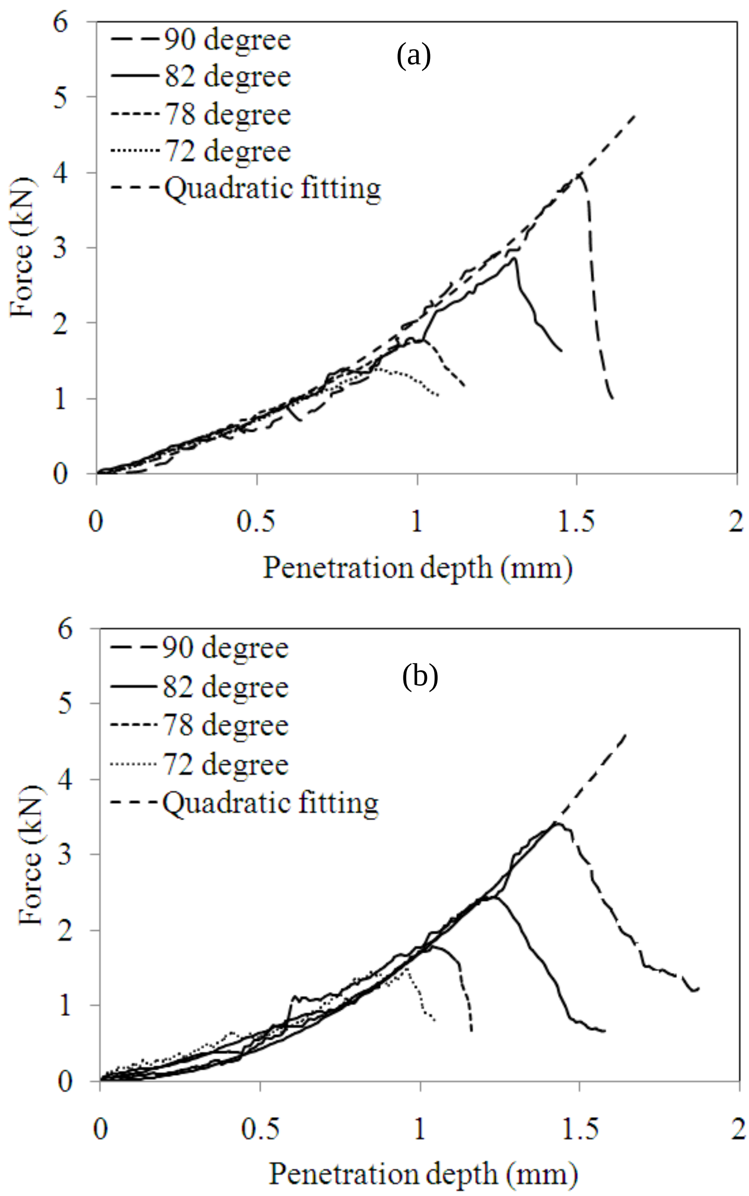

Fig. 3.30 Force and penetration depth curves with conical (a) and pyramidal (b) bits at h=10mm and attack angles of 72°, 78°, 82° and 90° on Littlewood

3.4.5.3 *Power relation between peak chipping and depth of cut*

As the peak inclined force is the product of the perpendicular peak force and the attack angle function, we may conduct an investigation on the relationships between the peak force and depth of cut with perpendicular force application. Recall the power relationships between the peak force and depth of cut mentioned in Chapter 2 and the fitting can be used to assess the availability of the previous results in reference. Then, we take an example of the fitting results on Bauhaus with a pyramidal bit to show the results.

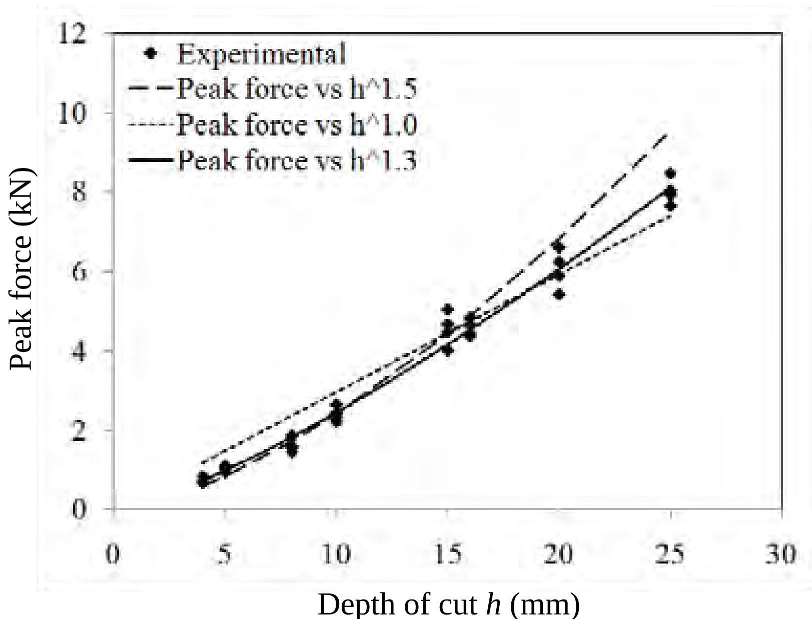

Fig. 3.31 Fitting results for the peak force with pyramidal bit

Fig. 3.31 shows the results of the different relationships between the peak force and depth of cut of $F_{pp} \propto h$ [125-126, 138, 141-143, 171, 187], $F_{pp} \propto h^{1.3}$ [129], and $F_{pp} \propto h^{1.5}$ [117]. For the linear relationship, it is found that at smaller depths of cuts, the fitting result is greater than the experimental while at larger depths, the fitting result is smaller. The mismatch may somehow imply the linear relationship does not reflect the chipping features. It is noteworthy that at smaller depths of cut ($h \le 10mm$), the 1.3 and 1.5 power curves are close to each other. Following the increase of h, the concomitant rise of F_{pp} is higher for $F_{pp} \propto h^{1.5}$. It is then found that the relation of $F_{pp} \propto h^{1.3}$ best matches the experimental results. However, there is no theoretical explanation for this chipping feature. It may simply demonstrate the difference of the chipping mechanisms between glass and rock.

3.4.5.4 *Total energy consumption*

From the above peak force analyses, the chipping features can become more understandable if energy consumption is analysed in one edge chipping process. Recall the quantitative relationship of penetration force and depth and the area between the curve and horizontal axis stands for the total energy consumption E_t, which contributes to forming a single chip. It could be numerically calculated from the integration of the force depth curve. As previously discussed, the peak force F_{pp} possesses a power relationship with the depth of cut h. Therefore, power regression is attempted to correlate E_t to h, and fitting results still on Bauhaus are shown in Fig. 3.32.

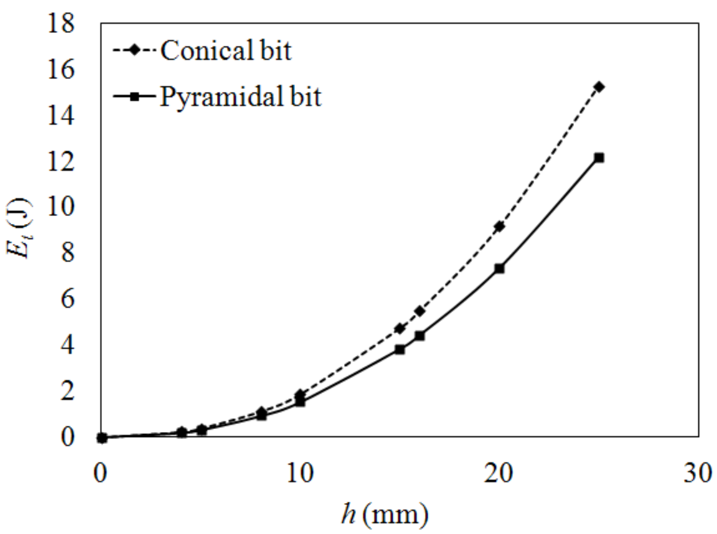

Fig. 3.32 Fitting results for the total energy consumption with conical and pyramidal bit

It is immediately noticed that the pyramidal tip consumes less energy than that of the conical, but the difference becomes greater only when the depth of cut gets large. Meanwhile, fitting results demonstrates the strong power relationship between total chipping energy E_t and depth of cut h and specifically for Bauhaus in this case: $E_t \propto h^{2.29}$ (cone) and $E_t \propto h^{2.26}$ (pyramid). With further investigation of the power relations of all materials, we found that the power values were in a range from 1.85 to 2.29. Especially, for the conical bit, the average power value is $2.07^{+0.22}_{-0.13}$, while for the pyramidal bit, it is $1.98^{+0.28}_{-0.13}$. The fluctuation of the power values may be due to the local chipping and internal sub-cracking during the major chipping process, which can be noticed in the small drop of the curves shown in Fig. 3.28 at $h = 20mm$ and $h = 60mm$. This indicates that for the edge chipping tests with the same depth of cut, the micro cracking process can be different due to the inhomogeneity and anisotropy of the sample materials, but the macroscopic behaviour/response of the material in edge chipping still reflects the essential mechanism. It is also of interest to notice the strong power relation for E_t and h, which may demonstrate the interrelation between total energy consumption and peak force. Moreover, depending on the discussion in Section 3.4.5.1, the total energy consumption of the pyramidal bit at the orientation of diagonals with 45° and 135° to the free surface should be the least, which further infers the optimum orientation of the pyramid during cutting.

3.5 Conclusions

From the analyses of the crack mechanism and the chip formation, the application of the pyramidal bit can be determined, as the stress concentration results in the quick generation of the initiation of the radial and median cracks and the symmetrical fracture surfaces as well, which, to some extent, might assist the crack to propagate easily. For the chips, they still have similarities in shape, but the ratios between chip length (width) and cutting depth are different from those in the previous research for glass and ceramics, which may be due to the internal properties (porosity and uniformity) of the material, although glass, ceramics and stone all belong to brittle material. The amount of the fine grains generated and collected in the test predicts the capacity of the dust in a real mining site could be smaller for the pyramidal bit. Meanwhile, the indentation force was found to be equivalent to the edge chipping force. The inclined chipping force and the perpendicular chipping force also possess this relation, which indicates the peak inclined force can be expressed by the product between the peak perpendicular force and the angular function. It was also noticed that the orientation of the pyramidal bit affected the peak force value, which may be helpful for uncovering the optimum mounting condition of the pyramid. Moreover, the regression results on both the peak force and energy consumption demonstrate a strong power relationship with depth of cut, and it was found that the force-depth relation of $F_{pp} \propto h^{1.3}$ well matched the experimental results and the power value between the energy consumption and depth of cut should be located in the range from 1.98 to 2.07 for both bits. However, there are also some limitations in this research: 1) the tests were in quasi static mode so the wear rate could not be measured; 2) real cutting is in dynamic mode and the fracture formation would be different from that in the static mode; 3) the attack angle in this paper is 90 degrees, however, in a real mining site, it would be less than 90 degrees, which will cause the stress field to change. Nevertheless, this research demonstrates the potential application of the pyramid-shaped bit as the cutting pick in a real mining site.

Chapter 4

Modelling of edge chipping

4.1 Introduction

Mechanical excavation by point attack bit is crucial for the productivity of rock cutting. Accurate prediction of the cutting force helps improve cutting efficiency and estimating the cutterhead torque and machine power for different rock types [1-5]. Therefore, prediction of the cutting force becomes salient, which has attracted many mining researchers and experts to work on that. Evans developed a cutting force model [7] with the assumption that frictionless penetration of a point-attack bit gave rise to radial compressive stress and hoop tensile stress in the material. When hoop stress in the material reaches its tensile strength, breakage happens, inducing a symmetric, V-shaped chip in the end. He also assumed that the normal contact pressure between the bit and the material should distribute uniformly and circumferentially along an imaginary hole. The simplification of the complex cutting process brought about theoretical contributions to the practical mining field, in which, at least, the predicted force could be considered as a reference to select the suitable power of roadheaders and longwall shearers [7, 72, 82, 92, 94, 184, 188-191]. However, from some succeeding rock cutting tests, it was found that the estimated force deviated considerably from the measurements in [2, 7, 14, 16].

Therefore, several attempts were undertaken in order to improve Evan's model: Roxborough and Liu [14] and Goktan [16] considered that the inconsistency could be partly due to the effect of friction which Evans had ignored. But Goktan and Gunes [17] found that although the friction angle was considered, the predicted peak cutting force is still much lower than the real measurements in full-scale laboratory experiments. They demonstrated that ignorance of the effect of attack angle (asymmetrical cutting condition) in these two models led to the inconsistency. Then they added the rake angle (geometrically related to the attack angle, which is defined as an angle between the tool axis and the tangent of the cutting path [83]) empirically to Evan’s formula based on their full-scale experimental data. However, a fundamental understanding of the chipping mechanism is lacking. Many succeeding studies in the mining practices [6-7, 22, 84-90] have corroborated the importance of the attack angle and it is now considered as a crucial geometrical parameter in optimizing cutting efficiency. However, the incorporation of attack angle effect in estimating the cutting force remains empirical.

To a great extent, an inclined edge chipping test is similar to the cutting operation in mining, as sketched in Fig. 4.1. Due to the easy control and application of the experiments, edge chipping tests were also widely adopted in laboratories for studying the fracture mechanisms of glass and ceramics [117, 136, 139, 142-144, 192]: Almond [136] discovered the similar geometrical relation of the chip dimensions; Gogotsi [139, 142-144, 192] set up the relation between edge toughness and fracture toughness and its applications in odontogical ceramics. Chai [117] applied an edge chipping method to measure the toughness of glass and ceramics.

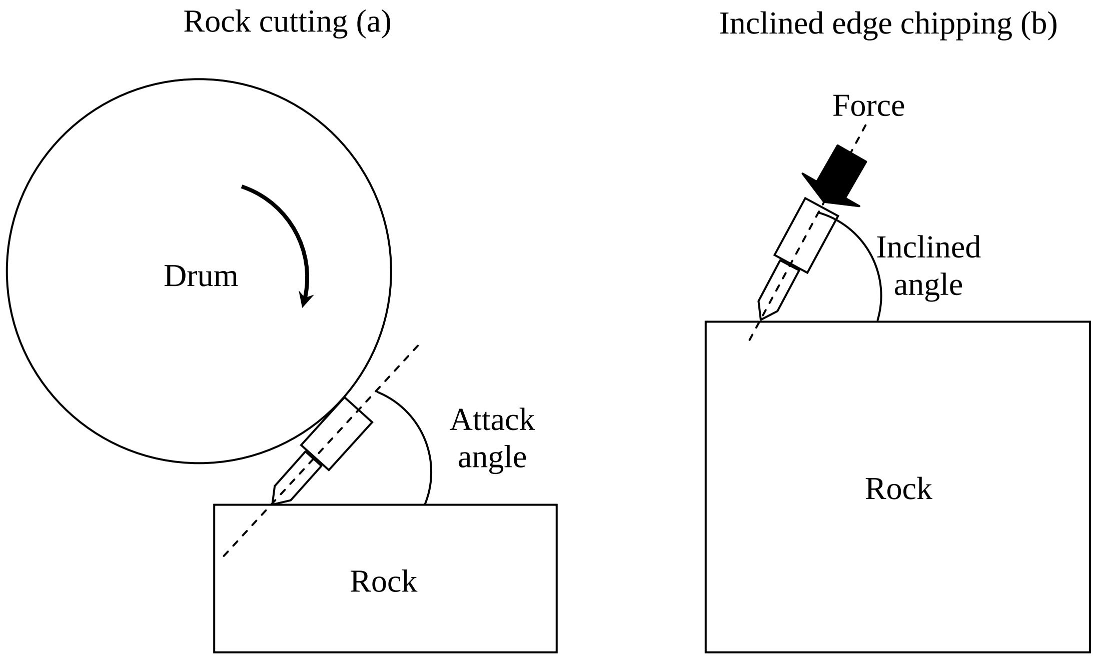

Fig. 4.1 Rock cutting and inclined edge chipping

However, these works mainly focused on the perpendicular loading process and only a few of them discussed the inclined chipping mechanism. Quinn reported the effects of the attack angle on the peak chipping force of glass [163]. Chai and Lawn investigated the relationships among the peak inclined chipping force, the indenting distance (depth of cut) and the angle of the sidewall of the tool based on crack morphology. Their formula successfully explained the inclined sidewall effects on the peak force. But the lack of experimental verifications on the relationship between the peak inclined force and inclined angle and whether this formula could be suitably applied to other brittle materials, such as ceramics and rocks, were undetermined. It is also noteworthy that Chai's model [193] was based on the assumption that the crack path is in line with the force axis, which leads to the mode I crack formed at the very beginning of the contact. From our experimental observations on rock chipping in Chapter 3, there was a deviated angle between the force axis and the crack path in the side view of the chip. Hence, this chapter aims at setting up a new relationship between peak inclined force and attack angle in rock chipping in order to investigate attack angle effects on rock cutting force.

4.2 Theoretical considerations

4.2.1 Basic assumptions

From the experimental observations in Chapter 3, we proceed with our theoretical considerations based on the following assumptions:

Firstly, based on the geometrical similarity of the chips, the total area S of the new surface of the chip is proportional to $h^2 \tan^2(\alpha - \varphi)$, which gives

$$S = \chi' h^2 \tan^2(\alpha - \varphi) \tag{4.1}$$

where χ' is a geometrical factor independent of material properties but related to the bit geometry. Secondly, the fracture energy E_f associated with the new surface of the chip is a constant fraction of the total energy consumption (E_t) from the total external mechanical work (W_t) (as shown in Fig. 3.3(b)), i.e.,

$$E_f = \mu E_t \tag{4.2}$$

where μ represents the ratio of E_f and E_t. In rock cutting and drilling, the energy contributed to forming the fracture surface, E_f, occupied only 8-10% of the total energy E_t [194-195]. In view of the large uncertainty of the properties of rocks, the narrow range of the variation of μ allows us to assume that this fraction is independent of material properties of rocks.

Based on the observations in Chp. 3, we may extend the quadratic relationship between indentation force and penetration depth to edge chipping, which is expressed as:

$$F_p = \lambda H d_p^2 \tag{4.3}$$

where F_p is the peak chipping force and d_p is the corresponding penetration depth

4.2.2 Formulation of the inclined cutting force

Recall γ as the material fracture surface energy mentioned in Chapter 2, and since the total fracture surface area associated with a chip is $2S$, we related E_f and γ through

$$E_f = 2\gamma S = 2\gamma\chi' h^2 \tan^2(\alpha - \varphi) \tag{4.4}$$

While, E_t is expressed as:

$$E_t = W_t = \int_0^{d_p} F(x)dx \tag{4.5}$$

Substituting Eq. (4.3) into Eq. (4.5) gives:

$$E_t = \frac{1}{3}\frac{F_p^{3/2}}{(\lambda H)^{1/2}} \tag{4.6}$$

Then, substituting Eqs. (4.2) and (4.4) into (4.6) gives:

$$F_p = \eta(h\tan(\alpha - \varphi))^{4/3} \tag{4.7}$$

where $\eta = (\frac{6\gamma\sqrt{\lambda H}\chi'}{\mu})^{2/3}$.

4.3 Experimental verifications

4.3.1 Relation between the perpendicular peak force and inclined peak force

As shown in Fig. 3.27, although the attack angles were different from each other, all force depth curves almost followed the same trajectory. It implies a relationship between the perpendicular peak force and the inclined peak force. Therefore, it is of interest to investigate the internal correlation, which may provide a simple way of validating Eq. 4.7, due to the unknown coefficients of $\chi^{'}$ and γ.

When $\alpha = 90^{\circ}$, Eq. 4.7 is recast as

$$F_{pp} = (\frac{6\gamma\sqrt{\lambda H}\chi^{''}}{\mu})^{2/3} h^{4/3} \tag{4.8}$$

where $\chi^{''} = \chi^{'} \cot^2 \varphi$. Then, with a comparison of Eqs. 4.7 and 4.8, we obtain:

$$\frac{F_p}{F_{pp}} = (\frac{\chi^{'}}{\chi^{''}})^{2/3} \tan^{4/3}(\alpha - \varphi) \tag{4.9}$$

Eq. 4.9 verifies the internal correlation of F_p and F_{pp} in Section 3.4.5.2: $F_p = F_{pp} f(\alpha)$.

4.3.2 Verifications of the power relation between F_{pp} and h

We divide the verification of Eq. 4.7 into two steps: (i) the relationship between the peak force and depth of cut; and (ii) the relationship between peak chipping force and attack angle. In this section, we validate the relation between peak force and depth of cut at a certain attack angle, e.g., $\alpha = 90^{\circ}$. Figs. 4.2-4.5 show the peak force versus the penetration depth with logarithmic coordinates for all kinds of sandstones. After linear regression, the exponent of *h* is shown in Table 4.1.

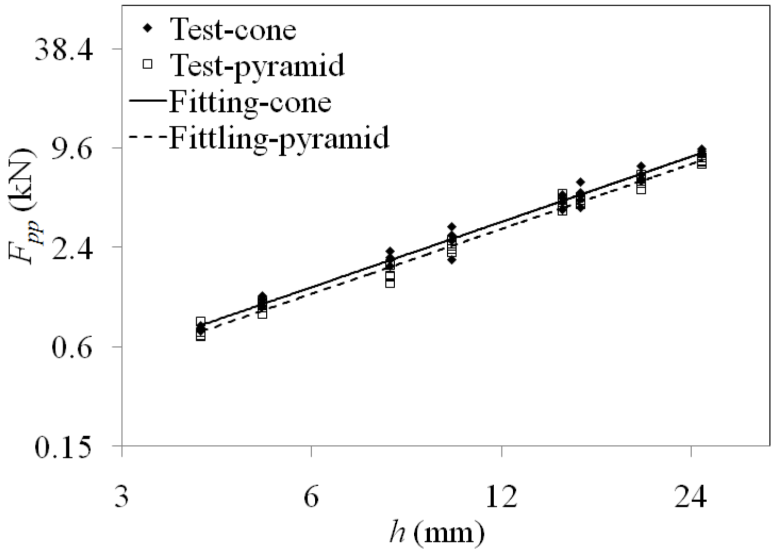

Fig. 4.2 Relationships between peak perpendicular forces and depths of cut for Bauhaus sandstone

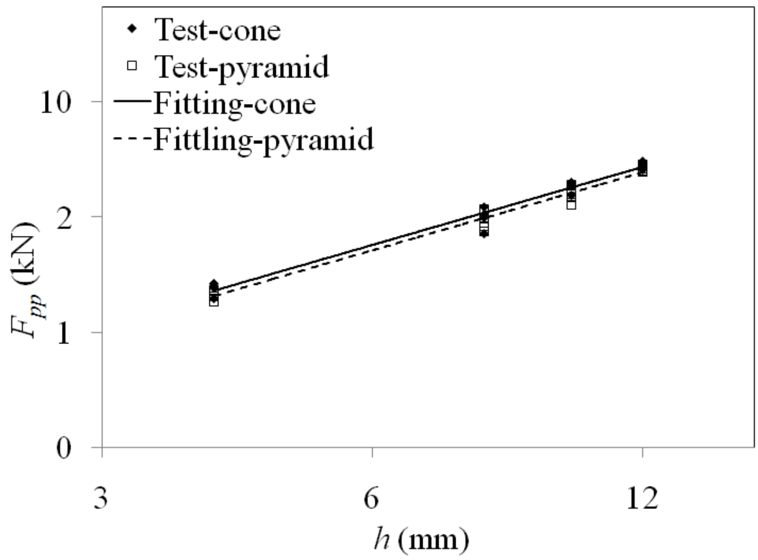

Fig. 4.3 Relationships between peak perpendicular forces and depths of cut for Littlewood sandstone

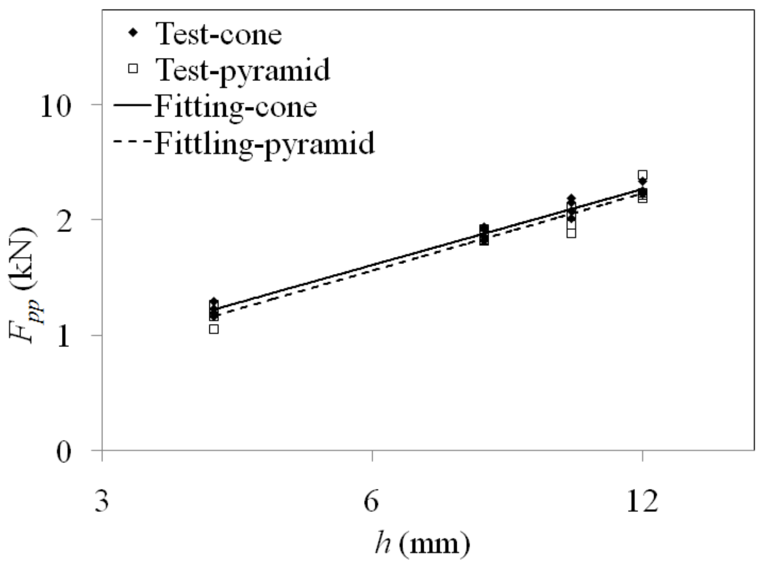

Fig. 4.4 Relationships between peak perpendicular forces and depths of cut for Appin sandstone

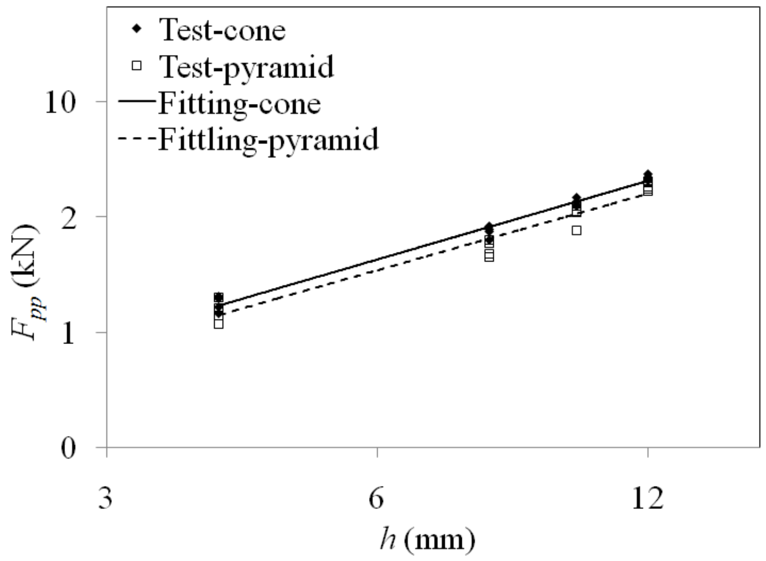

Fig. 4.5 Relationships between peak perpendicular forces and depths of cut for Pyrmont sandstone

Table 4.1 Exponent of h

Sandstone	Bauhaus	Littlewood	Appin	Pyrmont
Power of h for cone	1.313	1.3504	1.3261	1.3631
Power of h for pyramid	1.3076	1.3535	1.3414	1.3228

It was found that the exponents were very close to the theoretical result 1.33 for all kinds of sandstone with both conical and pyramidal bits. From the comparison of the experimental and the predicted results, we can conclude the power relations between the peak perpendicular force and depth of cut have been validated. And this power relation is also consistent with Quinn's experimental result [129], which then theoretically explained her finding.

4.3.3 Verifications of the relation between F_p and α

Given the verification of the power relation between the peak force and depth of cut, it is encouraging to verify the validity of the relation between the peak force and attack angle. Note that a crack deviation angle φ is needed in Eq. (4.9). Recall the relationship between α and φ in Section 3.4.3.Although it is an empirical fitting, we may expect that α should be the function of φ. First we use the fitted α-φ curve. Figs. 4.6 and 4.7 plot $\frac{F_p}{F_{pp}}(\frac{\chi^{''}}{\chi^{'}})^{2/3}$ versus the attack angle α, which shows that the predicted relation between the peak force and the attack angle (the solid line) agrees with the experimental results (all points) well. The dashed line shows the theoretical calculations of the crack deviation angle φ using the trajectory of the maximum shear stress, which will be specifically discussed in Section 4.4.

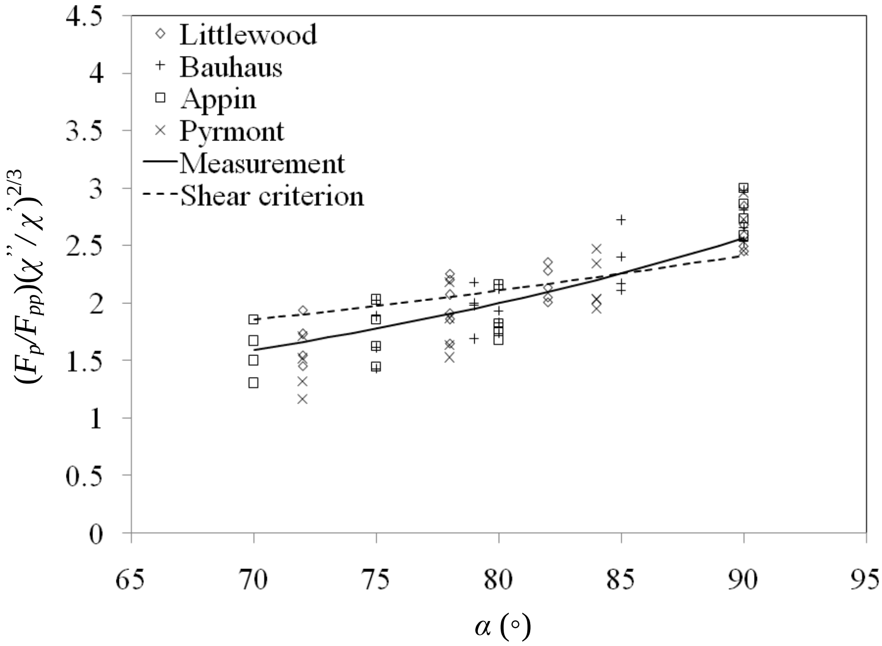

Fig. 4.6 Relationships between peak forces and attack angle for all kinds of sandstone with conical bit

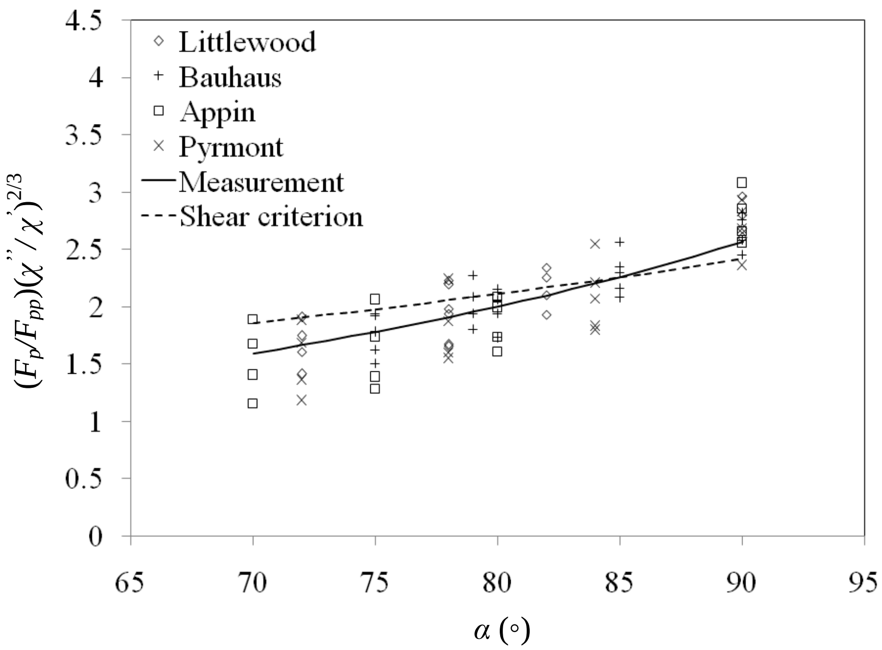

Fig. 4.7 Relationships between peak forces and attack angle for all kinds of sandstone with pyramidal bit

4.4 Discussions

4.4.1 Calculations of crack deviation angle φ

As discussed in the above section, the crack deviation angle φ is an important parameter to evaluate the peak cutting force. Although the latter can be predicted reasonably well for different αs, this was only based on the empirical fitting results. Hence, a mechanism for understanding the crack propagation is greatly desired. In this section, we aim at an interpretation of the trajectories of the crack path at different attack angles. We assume that the rocks are brittle materials and fracture happens immediately after crack initiation.

Crack formation is closely related to the stress state underneath the indenting bit. We assume that at the initial stage the rock surface is intact and Boussinesq stress distribution formulations can be applied. Due to the symmetry of the stress field, we focus on the crack trajectory in the median plane, which gives rise to $y=0$ and $\rho=\sqrt{x^2+z^2}$ as shown in Figs. 4.8 (a) and (b).

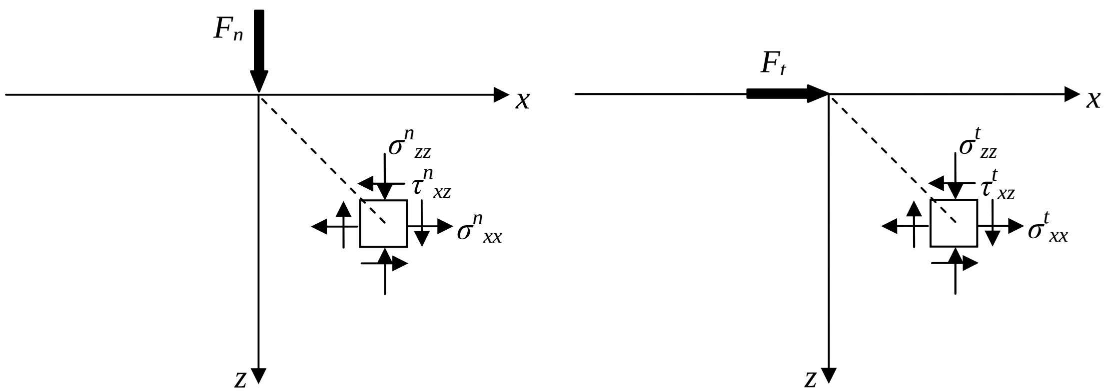

Fig. 4.8 The stress status with normal (a) and tangential (b) forces

From analytical results for the Boussinesq stress distribution on a half elastic space with both normal and tangential force, we obtain the normal and shear stresses with the equations below:

For normal point force,

$$\sigma_{xx}^{n} = \frac{F_n}{2\pi}\left(\frac{1-2\nu}{x^2}\cdot\left(1-\frac{z}{\rho}\right)-\frac{3zx^2}{\rho^5}\right) \tag{4.10a}$$

$$\sigma_{zz}^{n} = \frac{F_n}{2\pi}\left(-\frac{3z^3}{\rho^5}\right) \tag{4.10b}$$

$$\tau_{xz}^{n} = \frac{F_n}{2\pi}\left(-\frac{3xz^2}{\rho^5}\right) \tag{4.10c}$$

For tangential point force:

$$\sigma_{xx}^{t} = \frac{F_t}{2\pi}\cdot\left(\frac{-3x^3}{\rho^5}+(1-2\nu)\cdot\left(\frac{x}{\rho^3}-\frac{3x}{\rho(\rho+z)^2}+\frac{x^3}{\rho^3(\rho+z)^2}+\frac{2x^3}{\rho^2(\rho+z)^3}\right)\right) \tag{4.11a}$$

$$\sigma_{zz}^{t} = \frac{F_t}{2\pi}\left(-\frac{3xz^2}{\rho^5}\right) \tag{4.11b}$$

$$\tau_{xz}^{t} = \frac{F_t}{2\pi}\left(-\frac{3x^2z}{\rho^5}\right) \tag{4.11c}$$

Then in order to obtain the stress components with an inclined force at an angle in between 0° and 90°, superposition can be applied as the following equations:

$$\sigma_{xx} = \sigma_{xx}^{n} + \sigma_{xx}^{t} \tag{4.12}$$

$$\sigma_{zz} = \sigma_{zz}^{n} + \sigma_{zz}^{t} \tag{4.13}$$

$$\tau_{xz} = \tau_{xz}^{n} + \tau_{xz}^{t} \tag{4.14}$$

Therefore, depending on Eqs. 4.12 to 4.14, different fracture criteria can be exploited to investigate the crack path.

4.4.1.1 *Maximum tensile circumferential stress criterion*

An easy starting point for investigating the crack path in a brittle rock is to consider the maximum tensile circumferential stress sustained in the material immediately prior to fracture. This approach is common for brittle solids [196-199] and is predicated on the idea that: crack is controlled by tensile failure and fracture happens at the point where maximum circumferential stress locates. Although it is simple, this method successfully explains crack initiation, propagation and fracture causation of various brittle materials [200-203], especially rock [204-208]. Therefore, it is of specific interest to employ this method for finding out the crack mechanism in edge chipping. Based on the hypothesis in Section 4.2.3, we may further assert that a small initial crack is generated in the Boussinesq stress field and it deviated with an angle to the direction of the initial crack due to the penetration of the bit tip. With a small bit penetration depth (far smaller than the depth of cut), the stress field can be assumed to be the case of an inclined crack in a tensile field, after which the brittle crack happens and propagates along the same direction to the free side.

As Boussinesq stress components have been obtained, we can calculate the direction of the initial crack using the maximum tensile circumferential stress criterion. As the circumferential stress can be easily expressed in Polar coordinates, we then firstly transit the stress components in Cartesian coordinates into Polar coordinates so as to acquire the expression of tensile circumferential as shown in Fig. 4.9, where σ_θ denotes the circumferential stress component. Then, we transfer the Eqs. 4.10-4.11 in Cartesian coordinates into equations in Polar coordinates with $x = r\cos(-\theta)$, $z = r\sin(-\theta)$, where, $\theta \in [0, \pi/2]$ and $\rho = \sqrt{x^2 + z^2} = r$.

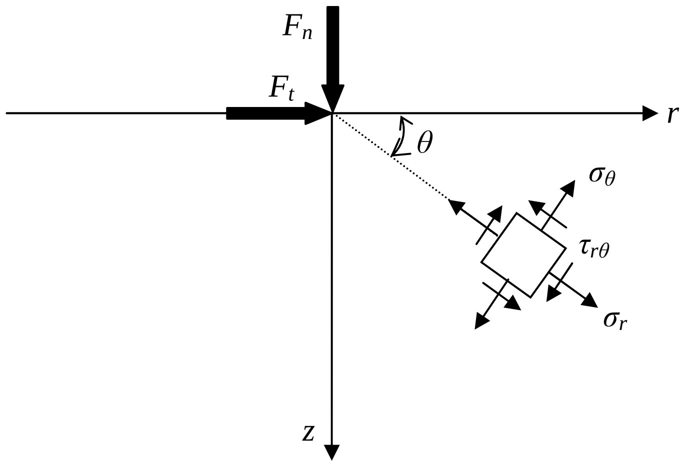

Fig. 4.9 The hoop stress generated by resultant force

For normal point force,

$$\sigma_{xx}^n = \frac{F_n}{2\pi r^2}\left(\frac{1-2\nu}{\cos^2\theta}\cdot(1+\sin\theta) + 3\sin\varphi\cos^2\theta\right) \tag{4.15a}$$

$$\sigma_{zz}^n = \frac{F_n}{2\pi r^2}3\sin^3\theta \tag{4.15b}$$

$$\tau_{xz}^n = \frac{F_n}{2\pi r^2}(-3\cos\theta\sin^2\theta) \tag{4.15c}$$

For tangential point force:

$$\sigma_{xx}^t = \frac{F_t}{2\pi r^2}\left(-3\cos^3\theta + (1-2\nu)\left(\cos\theta - \frac{3\cos\theta}{(1-\sin\theta)^2} + \frac{\cos^3\theta}{(1-\sin\theta)^2} + \frac{2\cos^3\theta}{(1-\sin\theta)^2}\right)\right) \tag{4.16a}$$

$$\sigma_{zz}^{t} = \frac{F_t}{2\pi r^2}(-3\cos\theta\sin^2\theta) \tag{4.16b}$$

$$\tau_{xz}^{t} = \frac{F_t}{2\pi r^2}(3\cos^2\theta\sin\theta) \tag{4.16c}$$

With superposition of the stress, we obtain the circumferential stress expression in the Polar coordinates:

$$\sigma_\theta = \frac{\sigma_{xx} + \sigma_{zz}}{2} - \frac{\sigma_{xx} - \sigma_{zz}}{2}\cos 2\theta - \tau_{xz}\sin 2\theta \tag{4.17}$$

Then, with $\frac{\partial \sigma_\theta}{\partial \theta} = 0$, the direction of the initial crack (angle θ) can be determined. Then, from theoretical calculations, it was found that the angle between the initial crack direction and the perpendicular line changed in a small range from 0° to 7° when $\alpha \in [70^\circ, 90^\circ]$. Meanwhile, from the experimental observations, the average change of that angle was also small from 26° to 35°. It may somehow imply that the effect of the tangential component was small for inducing the next crack direction. Moreover, we also noticed that the crack propagation after the initial crack was close to the mode I type, as the squeezing behaviour of the bit became dominant. This might be the reason why the crack propagation path did not change a lot in the experiments.

Along with the formation of the initial crack, the stress field has been changed. And the case is close to an oblique crack in a tensile stress field, where the crack will deviate to another direction as it is the mixed Mode I and II crack type. Therefore, from the analytical result, we may calculate the next crack propagation angle with the stress intensity factors listed in [209].:

$$K_I = \sigma\sqrt{\pi a_c}\sin^2\psi \tag{4.18}$$

$$K_{II} = \sigma\sqrt{\pi a_c}\sin\psi\cos\psi \tag{4.19}$$

where σ is the external stress, a_c is the half crack length and ψ is the smaller angle between the direction of the initial crack and the stress, as shown in Fig. 4.10. Then, the next crack direction can be determined by calculating the inclination angle θ_0, based on Eqs. 4.18 and 4.19 and the circumferential stress component at the crack tip:

In Mode I:

$$\sigma_{\theta I} = \frac{K_I}{(2\pi r)^{1/2}}\cos^3\frac{\theta}{2} \tag{4.20}$$

In Mode II:

$$\sigma_{\theta II} = \frac{K_{II}}{(2\pi r)^{1/2}}(-3\sin\frac{\theta}{2}\cos^2\frac{\theta}{2}) \tag{4.21}$$

Then, combine Eqs. 4.17-4.21 at $\frac{\partial\sigma_\theta}{\partial\theta} = 0$, the second inclination angle θ_0 can be obtained based on the initial crack angles for each attack angle application. Depending on the geometrical features, the resulting crack deviation angle φ can be obtained using this method and plotted in Fig. 4.11, in relation to α. It is found that the predicted curve by the maximum tensile circumferential criterion significantly scales out the trend of the experimental results. A second serious problem with this method is revealed by the difference of the predicted and tested φs at $\alpha = 90^\circ$. The crack path determined by φ is almost along the same direction as the force axis, implying that the mode I crack is predominant throughout the whole process, which may be due to ignorance of the free side effect. Besides, the stress field will inevitably change, which leads to the unsecured continuous application of the above approach. Accordingly, the analytical calculations using the tensile circumferential criterion may not be sufficient to explain the experimental observations, as the free side effect may become more evident when bit penetrates deeper inside the rock or a different fracture mechanism may be more predominant in forming the crack.

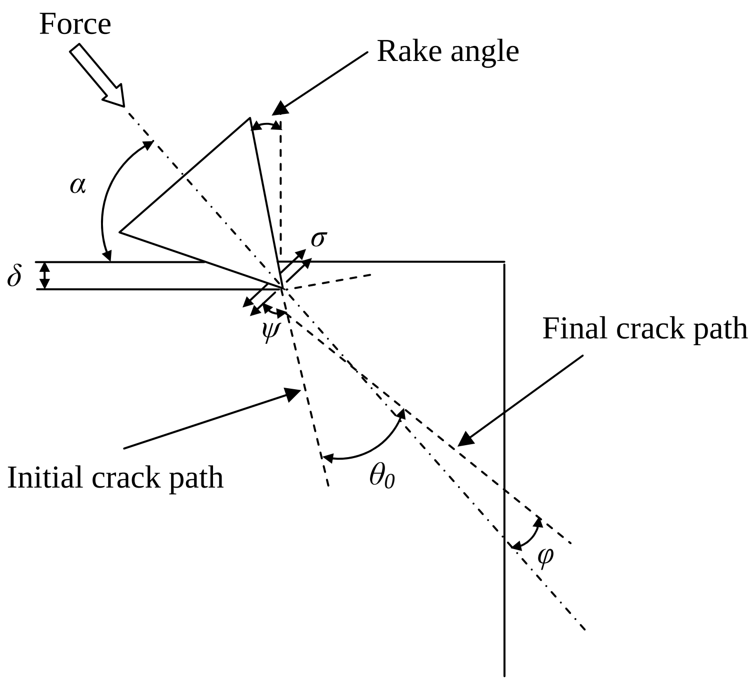

Fig. 4.10 The cracking process

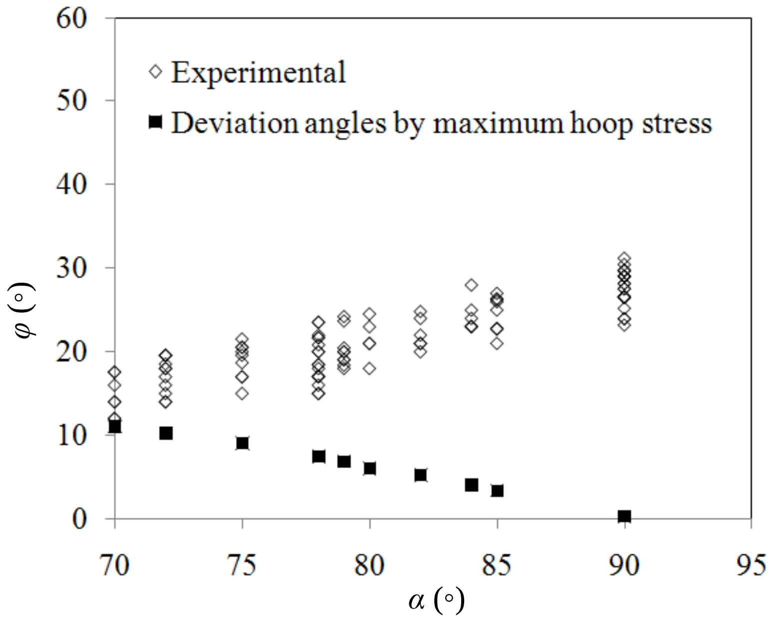

Fig. 4.11 φ vs α using maximum circumferential criterion

4.4.1.2 *Shear failure trajectory*

In our view, the failure of the above approach indicates that the crack mechanism in rock is not tensile failure but probably shear failure. It has been pointed out for many years [81, 151, 187] that the major median crack fell on the trace of the maximum shear stress ($\sigma_1 - \sigma_3$) during indentation fracture of rock. In what follows, we examine the maximum shear stress to predict the potential fracture trajectory in the Boussinesq stress field. In order to calculate the maximum shear path, we firstly assume that the crack path can be described analytically by a path function $f(x,z)$. We then have

$$df(x,z) = \frac{\partial f}{\partial x}dx + \frac{\partial f}{\partial z}dz \tag{4.22}$$

where ($\partial f/\partial x, \partial f/\partial z$) is the direction of maximum shear. Starting from any point (x_0, z_0), the maximum shear direction can be determined and the curve f can be numerically found. The maximum shear angle is given by

$$\alpha_t = \frac{1}{2}\tan^{-1}(\frac{\sigma_{xx} - \sigma_{zz}}{2\tau_{xz}}) \tag{4.23a}$$

or

$$\alpha_t = \frac{1}{2}\tan^{-1}(\frac{\sigma_{xx} - \sigma_{zz}}{2\tau_{xz}}) + \frac{\pi}{2} \tag{4.23b}$$

We then have

$$\frac{\Delta f}{\Delta x} = \sec\alpha_t \tag{4.24a}$$

$$\frac{\Delta f}{\Delta z} = \csc\alpha_t \tag{4.24b}$$

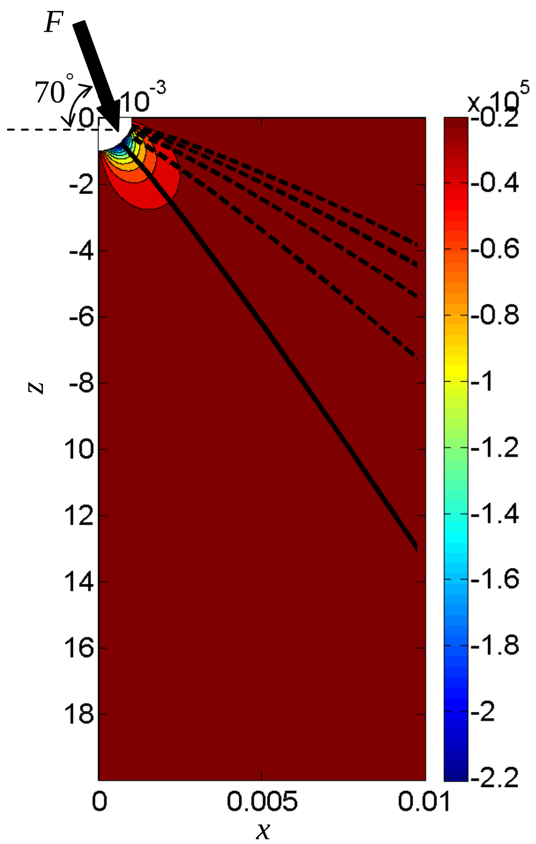

Fig. 4.12 Maximum shear trajectories at different attack angles

Fig. 4.12 shows the result of shear trajectory for $\alpha = 70^{\circ}$. The dashed lines and the solid line are all the trajectories starting from different (x_0, z_0). The solid line, which starts from the point most close to the contact point, is the most probable path as it coincides with the ridge of the shear stress contour. It is also noted that the shear trajectories of all lines are close to a straight line, which is in line with the experimental observations. Then, φ can be calculated and plotted with respect to α as shown in Fig. 4.13.

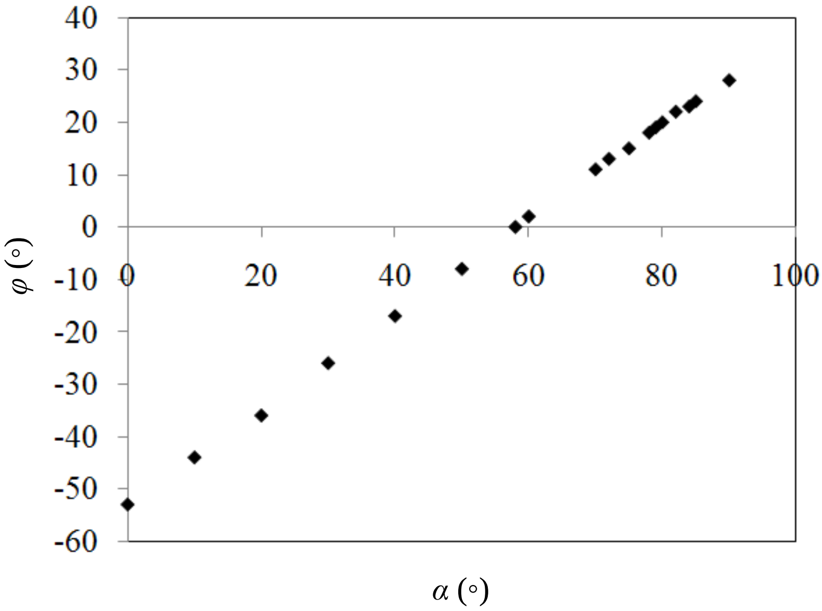

Fig. 4.13 φ vs α based on maximum shear trajectory

Following the increase of α from 0° to 90°, φ linearly changes with α and we may notice φ is almost zero at $\alpha = 58^{\circ}$. Fig. 4.14 shows the comparison of the predicted and the measured angle φ. In contrast to those in Fig. 4.11 using the maximum circumferential tensile stress criterion, the results in Fig. 4.14 are of close match with the experimental results. It is encouraging to state that this in the edge chipping of rocks, shear fracture dominates. It is to be noted that the effects of crush zone size and a bit shape are not considered in the above discussion, which would certainly introduce a more complicated scenario. However, considering the fact that the penetration depth is much smaller than depth of cut, the point contact may still be a reasonable assumption, which has indeed shed the light on the interpretation of the crack path.

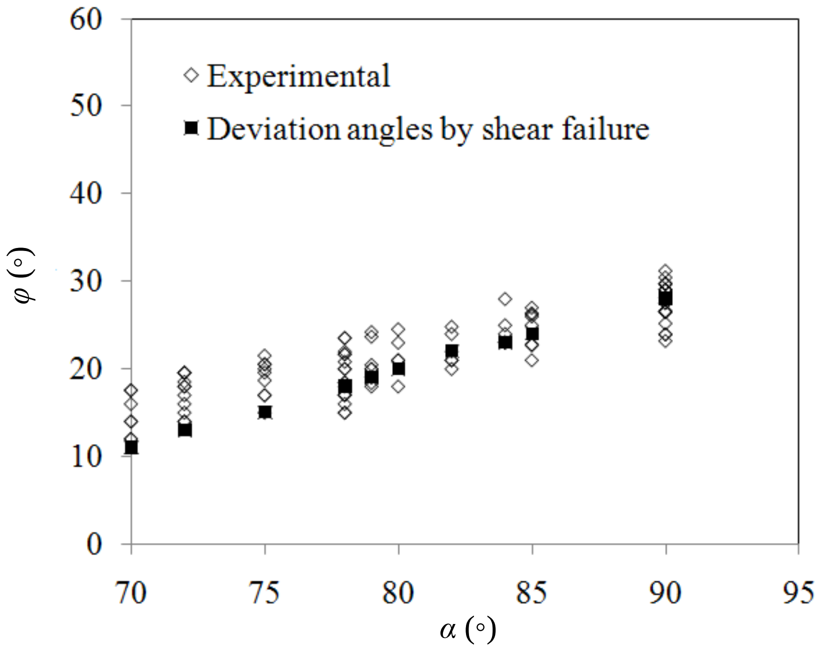

Fig. 4.14 φ vs α based on maximum shear trajectory

4.4.2 Prediction of rock toughness

In Eq. 4.7, it is interesting to notice the parameter γ, which is closely related to the energy release rate G, and the important material property, the toughness, K_c. Therefore, in this section it is of interest to set up a relationship among K_c, and the directly obtained h and F_p from the experiments. Especially, with the rationalized expression of Eq. 4.9, we obtained the relationship between F_p and F_{pp}, which led us to investigating the perpendicular case, depending on its easy control and convenient operations.

4.4.2.1 *Fracture toughness K_c derivation*

From linear elastic fracture mechanics, for brittle materials, we have

$$G = 2\gamma \tag{4.25}$$

where G is the energy release rate at stable crack propagation. In order to compare the result of edge chipping with that of three-point bending, we adopt the relationship between G and the toughness K_c under the plane-strain condition:

$$G = \frac{K_c^2}{E}(1-\nu^2) \tag{4.26}$$

Since the total fracture surface energy at $\alpha = 90^{\circ}$ can be related with G through

$$E_f = GS = G\chi'' h^2 \tag{4.27}$$

with Eqs. 4.25-4.27 and 4.6 and given that the crack remains stable before the peak force, we have:

$$K_c = \beta \frac{E^{1/2}}{(1-\nu^2)^{1/2}(\lambda H)^{1/4}} \frac{F_{pp}^{3/4}}{h} \tag{4.28}$$

where E, ν are Young's modulus and Poisson's ratio respectively. $\beta = \sqrt{\mu/3\chi''}$ is a dimensionless constant independent of material.

4.4.2.2 *Experimental verifications and analyses*

Fig. 4.15 plots all the experimental results of $F_{pp}^{3/4}$ versus *h*, where the linear regression curves have been drawn in order to find out the slope, which represents the product of K_c and $(1-\nu^2)^{1/2}(\lambda H)^{1/4}/\beta E^{1/2}$. In this research, Bauhaus was used as the model sample to quantify β. Toughness values could then be calculated from Eq. 4.28. It is found that β values for both bits are quite similar to each other, 0.084 for cone and

0.088 for pyramid. If β is asserted to be a universal constant, independent of both material and bit geometry, with a value of about 0.086, then the rock toughness values of the other three kinds of materials could be determined. For all kinds of rock materials tested in this research, Fig. 4.16 plots the toughness values from edge chipping as the function of the average toughness values obtained from three-point bend tests in the quarry. Despite the scatter of data, it verifies the applicability of Eq. 4.28 for directly obtaining the rock toughness from the edge chipping tests.

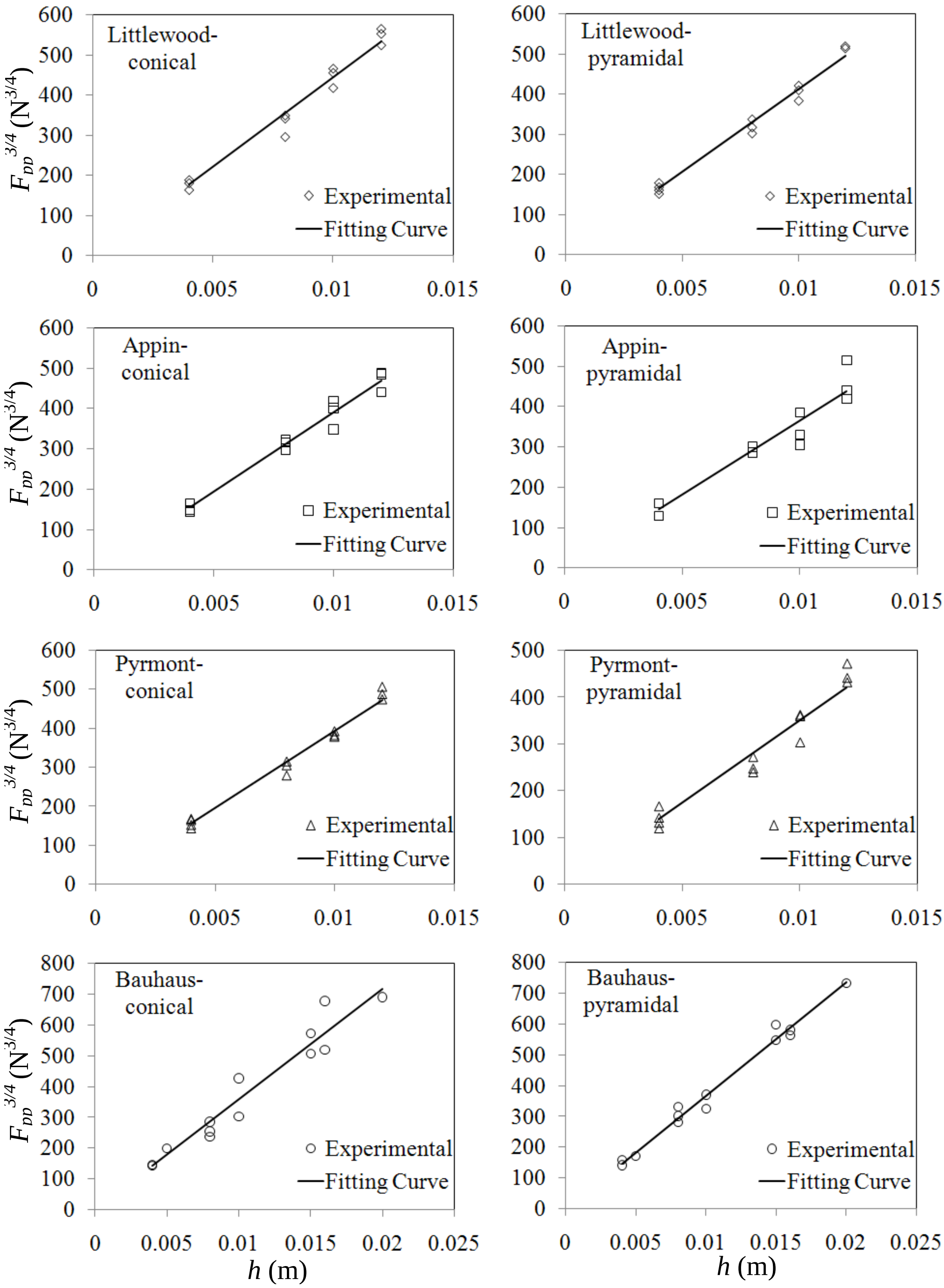

Fig. 4.15 $F_{pp}^{3/4}$ against h for each tested rock with both bits

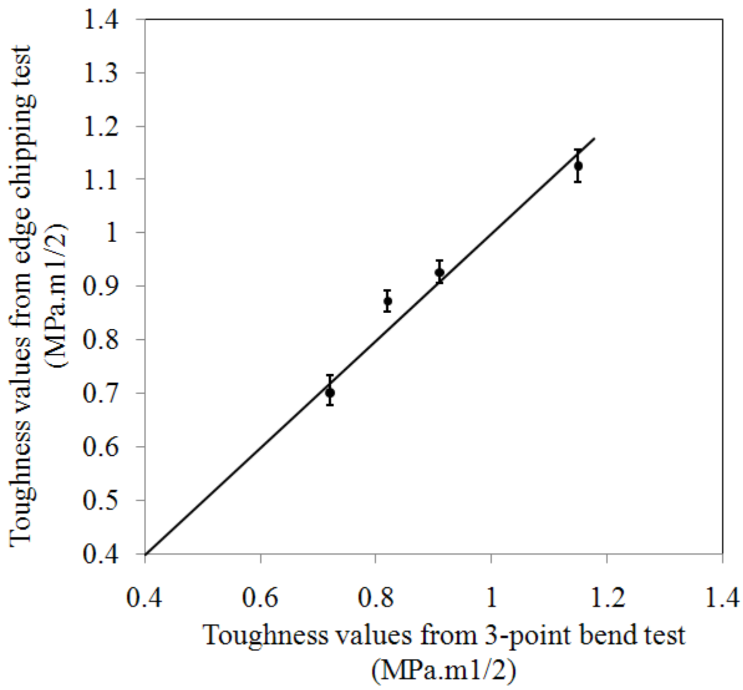

Fig. 4.16 Comparison of K_c from edge chipping and 3-point bend tests

Based on the geometrical similarity of chips and the quadric fitting of chipping force against penetration depth, the toughness is found to be a function of the peak chipping force and the indenting distance. For acquiring the toughness of brittle and opaque rock, one only needs to fabricate a block sample with polished surface and then conduct several chipping tests at different prescribed distances. Eq. 4.28 provides a convenient way of predicting the toughness of opaque and brittle rocks.

It is necessary to emphasize the significance of the chip geometrical similarity as it paves the way for deducing the peak chipping force of rock, circumventing the complex calculations for crack initiation and propagation. It further enables the specification of the universal critical force in relation to the depth of cut in a simple way based on the establishment of the proportionality between fracture surface area and the square of indenting distance, which eventually gives rise to the proportionality between the material toughness K_c and the quotient between $F_{pp}^{3/4}$ and h. A constant β is assumed by noting that $\chi^{"}$ and μ both vary in very narrow ranges. Note that β can be directly calculated if $\chi^{"}$ is determined. Assuming that the chip is a quarter of ellipsoid or an octahedron as shown in Fig. 4.17, with the ratios L/h = 4.3 and W/h = 1.9 from the experimental results in Chapter 3, $\chi^{"}$ is found to be 10.1 and 5.1 respectively. Taking μ= 0.1 [194-195], we obtain $\beta \approx 0.06$ for ellipsoidal surface and $\beta \approx 0.081$ for the flat surface. The measurement $\beta = 0.086 \pm 0.002$ then indicates that the fracture surface is close to a flat surface, which infers that the crack should propagate along the path with minimum energy consumption.

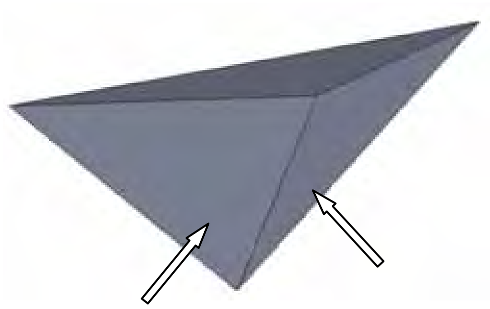

Fig. 4.17 The possible flat fracture surface

Great care is needed when extending our method to other types of materials. Firstly, the material independency of β or μ is attributed to empirical evidence on rocks, and it might not be applicable for other materials such as ceramics and glass. Secondly, the bluntness of the bit tip affects the chipping force in shallow indentations. We suggest that the indentation depth should be much larger than the tip radius. Finally, frictional force is not considered but can be influential. We therefore suggest that the sample surface must be polished and the indentation must be normal to the surface.

4.4.3 Explanations on perpendicular peak forces and energy consumption

After the analytical description of the effect from the angular component on the peak chipping force, it is found that the peak inclined force can be denoted by the product of the peak perpendicular force and the attack angle function. This further infers the analogous format of the peak force equation under both inclined and perpendicular conditions if the attack angle function is incorporated into β value. This relationship verifies the experimental observations in Chapter 3 and provides a convenient way of assessing the peak inclined force considering the attack angle in the rotary cutting process.

Considering the power relationships discussed in Section 3.4.3, $F_{pp} \propto h^{1.3}$ was found to be the most suitable to match the experimental results and from the theoretical formulation of Eq. 4.9, the power relation is about $F_{pp} \propto h^{1.33}$, which successfully elucidates the previous experimental observations. It also educes the different fracture mechanism of rock, compared with glass. Furthermore, from Eqs. 4.6 and 4.9, the power relationship between total energy and depth of cut is found to be 2, which is close to the average power value in Chapter 3. Therefore, we finished the theoretical explanations on Quinn's experimental results in [129] to explain the power relationship of the peak force and the depth of cut.

4.5 Conclusions

We have investigated the peak cutting force in relation to depth of cut and attack angle based on the edge chipping formation in different kinds of sandstone using two sharp bits. Based on the relations of edge chipping force and indentation force and cutting forces at different attack angles, an analytical description has been developed for the general case of a concentrated force delivered at an arbitrary angle α from the edge of the specimen. The formulation of the relation between peak cutting force and depth of cut considering attack angle effects is derived from interrelating the fracture energy and total energy consumption. An important element in this analysis is the interrelation between the critical force and the attack angle in Eq. 4.7. This provides a convenient way of investigating the effects on peak force from the angular component. Experimental validation has been given with a good match to the predicted results and it also demonstrated that the peak cutting force diminishes strongly with the decrease of α.

More important, the assumption of the straight crack path in rock chipping was deeply analysed based on the calculation of the Boussinesq stress field and the maximum shear trajectory was found to fit the experimental observations well, which perhaps indicates that the internal crack mechanism of rock is due to shear failure. This may be helpful for explaining the different crack trajectories in rock and glass. For greater α, the peak force is high, due to the bevelled force application inducing the immunity of the slight angular effect; while, for smaller α, the peak force was weakened, which is due to the evident assistance from the tangential component. Especially, the crack deviation angle is found to be around zero, when α falls in the range between 50° and 60°. It may uncover the possible mechanism of the optimum attack angle applied in rock cutting.

Another important feature to be noted is the derivation of the material toughness considering the easy-obtained parameters of perpendicular peak cutting force and depth of cut. Interestingly, one only needs to prepare the surface-polished rock specimen and employ any kind of cutting bit to conduct the edge chipping tests instead of accurately fabricating an initial notch in the traditional three point bending test and making the complicated calculations. Because of this, edge chipping of rock is an easier way to measure the rock toughness.

Furthermore, it also verified the best fit (1.3) of the power value for the peak cutting force in relation to the depth of cut under perpendicular chipping condition by providing an analytical elucidation of Quinn's experimental observations. Based on the simplified feature of peak force in relation to depth of cut, the power relationship between total energy consumption and depth of cut was also validated to be 2, which is similar to the experimental fitting results in Chapter 3.

We admit that there are some limitations in this research: the selected range of α is only from 70° and 90°, which is due to the experimental configurations of the holder, eg. it may touch the rock surface when α drops lower than 70°. Since a well-developed crack is driven by the exerted external surface of different cutting bits, the combo of the parameters $\beta/(\lambda H)^{1/4}$ in Eq. 4.41 should be a function of the bit included angle and there should be the different influences with different bit shapes. Therefore, further investigation is needed for demonstrating the specific formulation considering the bit angles.

Moreover, the applicability of Eq. 4.7 strongly depends on the chip forming on the front surface. However, some cases may not meet this requirement especially when a large depth of cut is applied or a small specimen is under investigation. Nevertheless, notwithstanding those limitations, Eq. 4.7 conveniently expresses the angular effects on the peak force. Hence, one may need to obtain the perpendicular peak force to calculate the certain inclined peak force based on the linear relationship between α and φ.

Chapter 5

Experimental studies on linear rock cutting

5.1 Introduction

The linear cutting method (LCM) is widely used to execute a single point cutting test due to its easy-control and convenient-configuration [210]. The forces acting on a cutter measured in linearly cut rock provides the direct information for performance assessment, machine specification, cutterhead balancing and optimization of cutter geometry [211-212]. LCM is thus regarded as a simulation of the on-site cutting process and can be employed to evaluate the performance of a cutter.

Many researches evaluating the cutting efficiency of a point attack bit with focus on specific energy and tool life have been carried out using LCM: Tuncdemir [213] and Tiryaki [212] found that specific energy is closely related to several factors, such as material properties and bit geometry. Achanti [214] pointed out that specific energy reduction is associated with an increasing amount of dust as the bit is blunted, which demonstrates that a sharper bit possesses better cutting efficiency. Fowell [215] further found that optimum cutting performance, in terms of bit life, dust generation and energy consumption, can be determined by the alteration of the bit included angle. In addition, cutting efficiency is also affected by bit wear. Roepke [108] indicated that the wear of a WC (Tungsten Carbide) bit highly depends on the temperature during cutting. In order to minimize the temperature effect, PDC material (Polycrystalline Diamond Composite), with a PCD (polycrystalline diamond) layer sintered on a WC base, was attempted to form a bit [109-114], for utilizing PCD’s high temperature endurance. However, Sneddon [115] demonstrated that different thermal expansion coefficients of the WC base and the PCD layer often led to the ripping off of the PCD layer at a high cutting temperature.

In this chapter, we used LCM to compare the performances of different cutting bits (conical and pyramid) and to investigate the effectiveness of the PCD pyramidal bit.

5.2 Ideas and analysis on the improved pyramidal bit

5.2.1 Enlightenments from the experimental observations

As discussed in Chapter 2, the profile of a bit affects the cutting performance. Therefore, it is necessary to optimize the bit shape in order to improve the cutting efficiency. Linear cutting tests were firstly set up using conical and pyramidal bits. For the pyramidal bit, two extreme orientations were considered: one flat surface at the bottom and one ridge at the bottom, in order to check the differences in cutting force and energy consumption at these two orientations. This is associated with the minimum cutting force and energy consumption when pyramid diagonals are with 45° and 135° to the free surface, compared with the condition of diagonals parallel and perpendicular to the free surface. Similarly, a pyramidal bottom flat (P1 configuration as shown in Fig. 5.3(b)) was found to be optimum as the cutting force and specific energy were minimum compared with C1 (Fig. 5.3(a)) and P3 (Fig. 5.3(c)). This implies that this configuration can be adopted when improving the shape design. Moreover, the sharper the bit, the easier bit penetration, which implies that a smaller included angle should bring about a smaller force. This then provides a reference for determining the efficient bit angle, at which total energy is minimum. Furthermore, the friction between the bit lateral surfaces and the groove surfaces leads to another source of fine grains besides crushing. Hence, reduction of the contact area would be another consideration for decreasing the amount of fine grains for dust reduction.

5.2.2 Improved profile of the initial bit

Based on the discussion in Section 5.2.1, the shape modifications of the initial pyramidal bit could be carried out in the following steps (drawings shown in Fig. 5.1(a)-(d)): 1, we adopt the bit configuration of a pyramid bottom flat; 2, the top cutting angle (as shown in Fig. 5.1(a)) is reduced to be 30°, a little sharper than the top of the initial pyramid, in order to obtain easier penetration and keep the strength of break-resistance. The bottom cutting angle is enlarged to 38° (shown in Fig. 5.1(a)), which aims at retaining the same cross sectional area when penetrating the same depth for comparison; 3, the front cutting surface is connected by a transition arc (R5 in Fig. 5.1(a)) to avoid stress concentration. Finally, two concaved profiles are employed in order to reduce the friction on the side surface, as shown in Fig. 5.1(b). Figs. 5.1(c) and (d) show the top view of 3D image of the bit respectively.

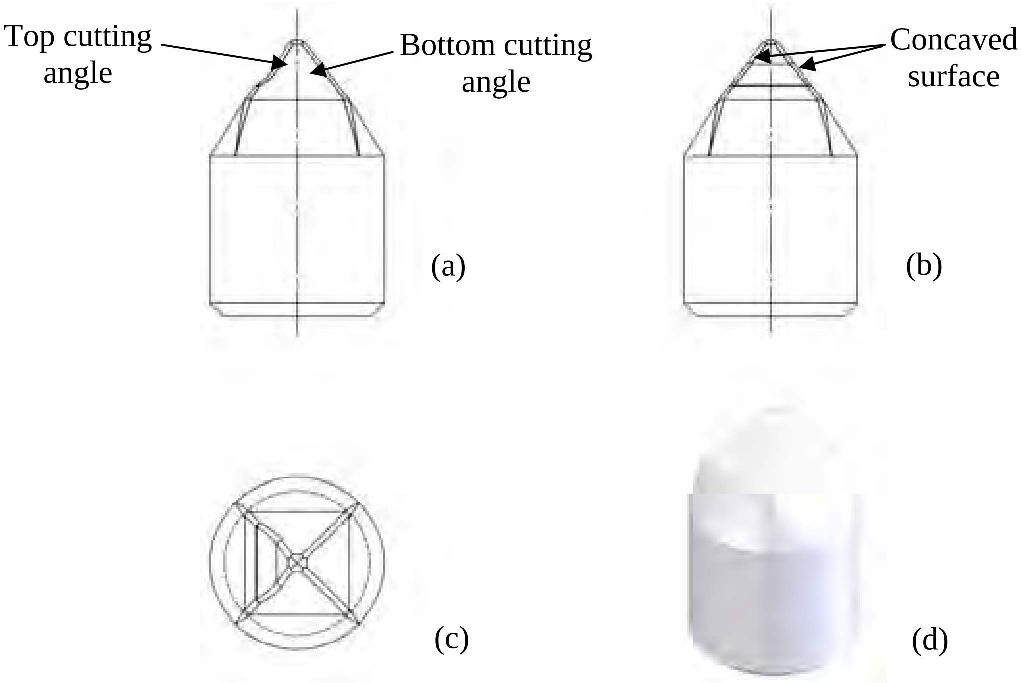

Fig. 5.1 Draft of the improved bit profile

5.2.3 Material for the cutting bit

As wear is a crucial factor that affects tool life, bit material with high wear resistance is necessary to extend the efficient cutting period. The frequently applied WC possesses a rapid wear rate, which is due to the accelerated material deformation induced by temperature rise [216]. Another widely used material is PDC, WC base coated with a high temperature endurance PCD layer to enhance wear resistance, but the layer breakage induced by different thermal expansion coefficients of the WC base and the PCD layer becomes a defect [115]. Therefore, the application of PCD material alone may potentially solve the above problems due to its high temperature endurance.

5.3 Experimental setup

Fig. 5.2 (a) shows the schematic experimental setup of the linear cutting test. A bit was held statically, while the rock sample was fixed on the machine table approaching the bit horizontally to realize the cutting. The cutting forces were measured by the dynamometers attached to the bit holder. Four configurations for the bit installation are shown in Fig. 5.3(b), C1 (conical), P1 (pyramidal bottom flat - a pyramidal surface parallel with the rock surface to cut (see section B-B)), P3 (pyramidal bottom edged - with its pyramidal surfaces in 45° with the rock surface to cut (see section C-C)) and P7 (the modified pyramid). For P1 and P3, the bits possess the same geometry and dimensions, but orientate differently to the rock surface.

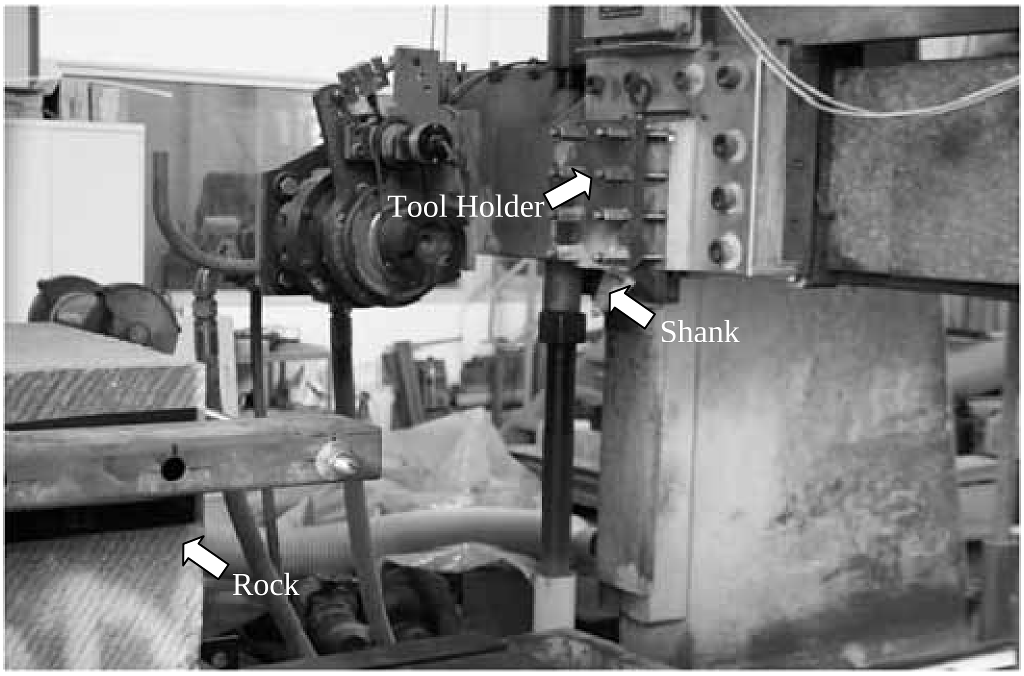

Fig. 5.2 Experimental setup

Helidon sandstone and Harcourt granite are test samples, obtained from a local quarry in Brisbane Australia with dimensions of Length × Width × Height = 1700mm × 450mm × 450mm. Material properties of both rocks are listed in Tables 5.1 and 5.2 below. In order to compare the cutting performances of the above three cutting conditions, different depths of cut (DOC), speeds of cut (SOC) and angles of attack (AOA) were used as the major parameters in the series tests: The depths of cut varied from 5 mm to 15 mm; the speed of cut changed from 0.015 m/s to 2.5 m/s and the angle of attack increased from 45° to 65°. Sandstone was mainly used for comparing the cutting performances of all bits, while granite was exploited to assess the wear performances of the bits made by PCD (Polycrystalline Diamond) or WC (Tungsten Carbide)

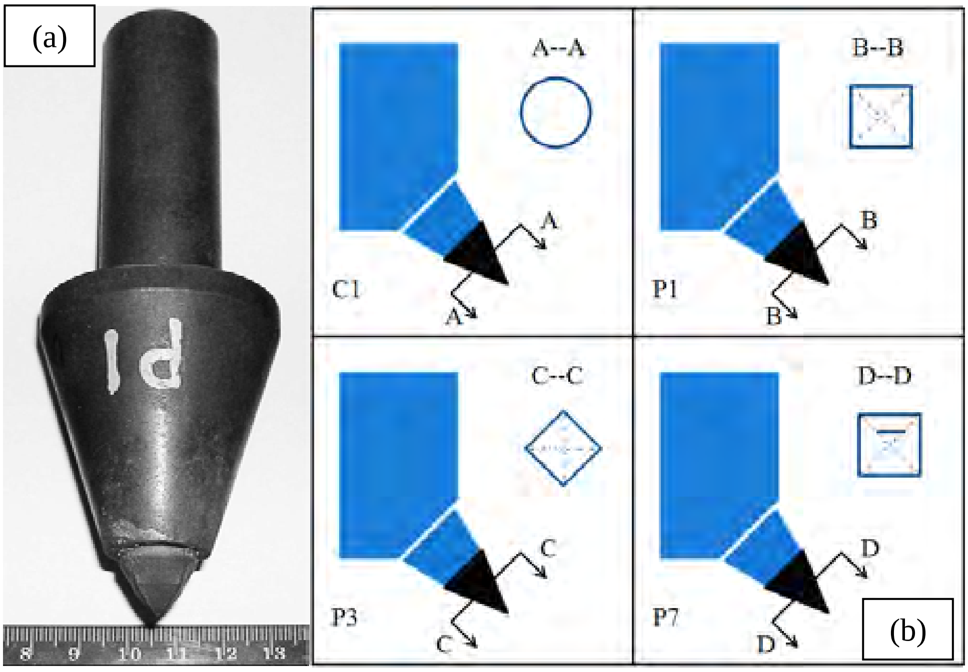

Fig. 5.3 A pick with PCD pyramidal bit (a) and mountings of different bit shapes (b)

Table 5.1 Properties of the Helidon sandstone

Bulk density (t/m^3)	Apparent porosity by volume	Compressive Strength (MPa) (Dry/Wet)	Modulus rupture (MPa) (Dry/Wet)
2.26-2.3	9-11%	44-50/26-35	13.5-15.0/8.5-10

Table 5.2 Properties of granite

Shear Modulus GPa	Bulk Density t/m^3	Compressive strength MPa	Tensile strength MPa	Young's modulus GPa	Poisson ratio
22.9	2.9	167-180	9	55	0.2

5.4 Results and Analyses

5.4.1 Chipping process

Fig. 5.4 schematically illustrates the cutting process, where ψ_0 is the half included angle of a bit, α is the angle of attack, β_c is the clearance angle and h is the depth of cut. Before chip formation, denoted by '1', the bit consumes some energy to crush the material in front of the bit. This process repeats as cutting proceeds. For instance, Zone 3 is a new crushed zone in which the material becomes small particles before chip '2' is formed. The major cracks in generating chips '1' and '2' can be assumed to be penny-shaped [217].

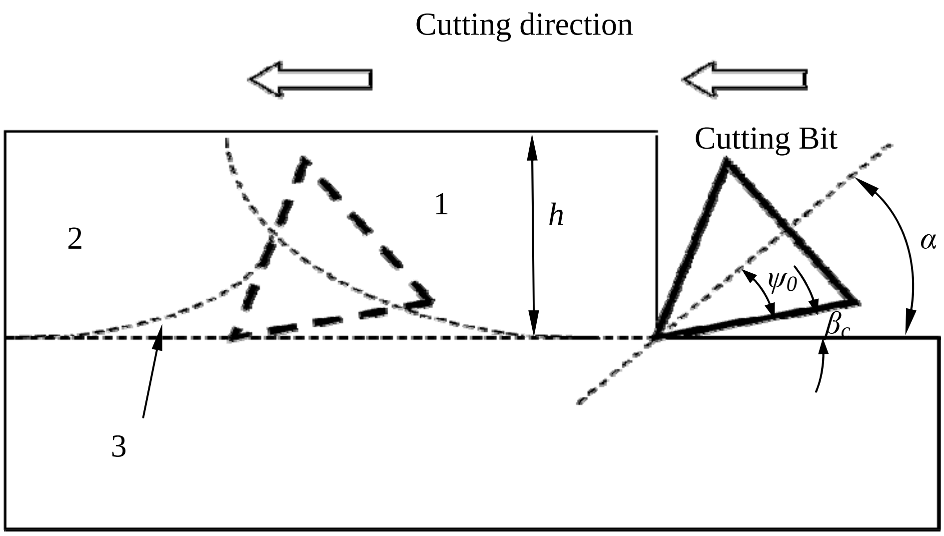

Fig. 5.4 Structure of linear cutting

Fig. 5.5 shows the snapshots in the cutting process with C1 under the conditions of depth of cut = 10mm, speed of cut = 0.015m/s and angle of attack = 45°. The figure demonstrates the chipping mechanism described above. Fig. 5.5(a) shows the bit starts to move before contacting the rock surface. Fig. 5.5(b) demonstrates the moment that major cracking took place associated with crashing to form dust particles.

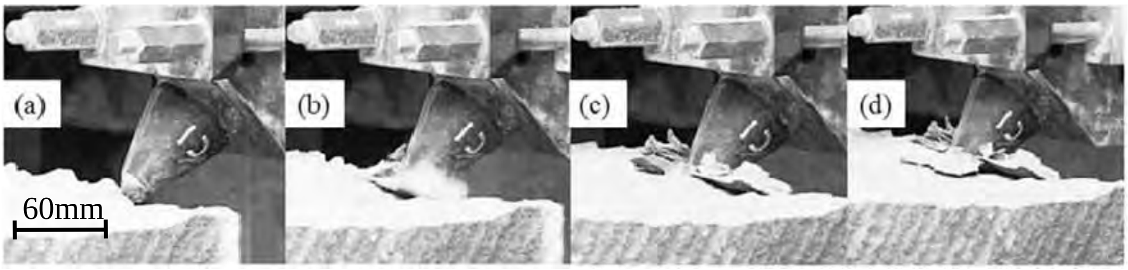

Fig. 5.5 Snapshots of the chipping process with C1. (a) The bit starts its contact with the sample; (b) Crashing takes place and dust participles are generated; and (c) and (d) Chipping occurs.

When using the pyramidal bit under the P1 condition, the bit’s vertexes generate higher stress concentration, leading to an increase of the number of major chips as shown in Fig. 5.6. It should be noted that compared with cutting using the conical bit under the same cutting conditions, dust generation in the present case is significantly reduced and much larger fragments are produced.

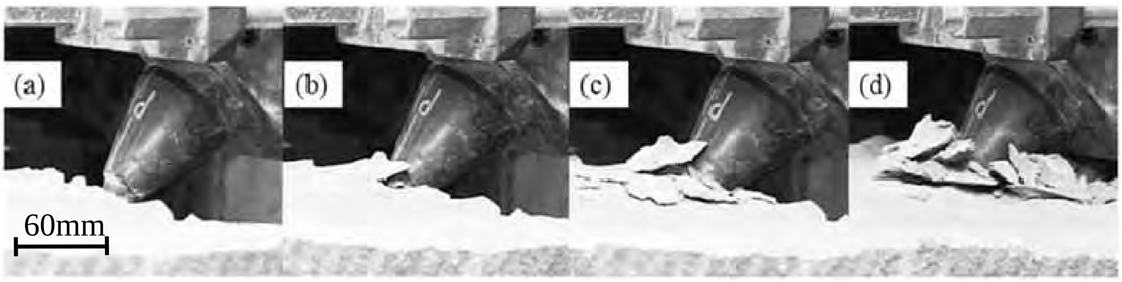

Fig. 5.6 Snapshots of the chipping process with P1. (a) The bit starts its contact with the sample; (b) Crashing and chipping take place; and (c) and (d) Major chipping occurs.

The cutting with P3 shows similar characteristics to that of P1. However, since in the present case all the four pyramid ridges interacted with the material more directly due to the orientation of the pyramid, the details of the chipping are different, as demonstrated in Fig. 5.7. Because of the leading pyramid ridge, the front chips are often broken into smaller pieces.

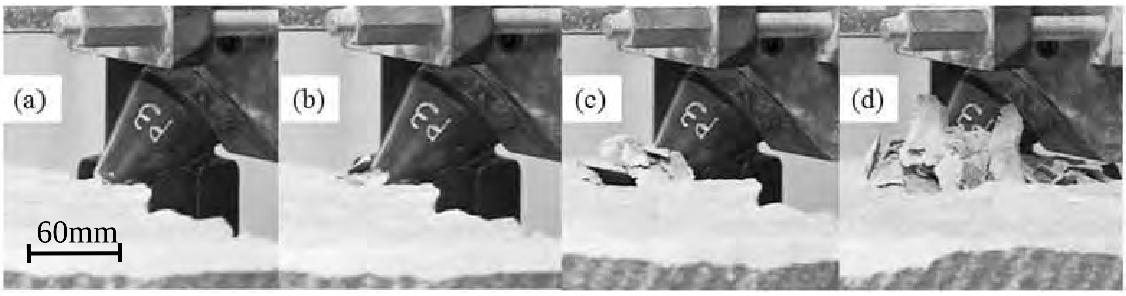

Fig. 5.7 Snapshots of the chipping process with P3. (a) The bit starts its contact with the sample; (b) Crashing and chipping take place; and (c) and (d) Major chipping occurs.

Compared with cuttings by P1 and P3, the cutting with P7 avoided the effects from the leading edge of the pyramid on forming the broken chips, which is close to that of P1 as shown in Fig. 5.8(b), but the major chips emanated from the cutting seem to be more as shown in Fig. 5.8(c) which may infer that the smaller bit angle lead to the large crack.

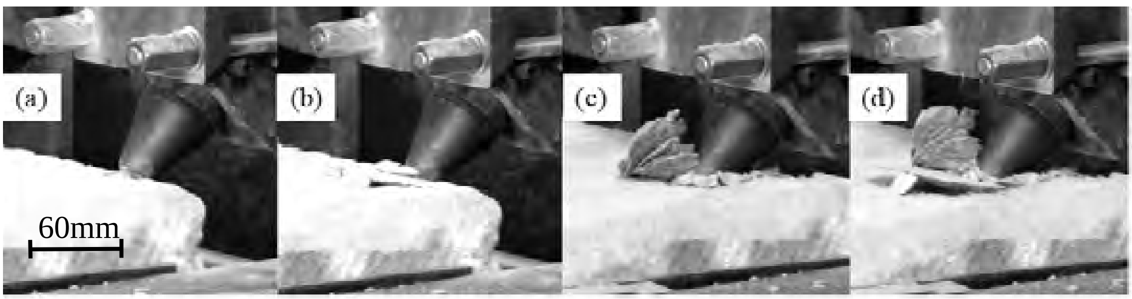

Fig. 5.8 Snapshots of the chipping process with P7. (a) The bit starts its contact with the sample; (b) Crashing and chipping take place; and (c) and (d) Major chipping occurs.

5.4.2 Excavated rock fragments

5.4.2.1 *Chip morphology and crush zone*

The chip in linear cutting, as shown in Fig. 5.9 (b) and (c), is still shell-shaped, which implies that the median crack type [117] should be also predominant and similar to that in edge chipping. It is also worth noting that different bit configurations induce various crush zone size (as shown in Fig. 5.9 (b)), which reflects the distinct energy consumption in producing one chip. More energy is needed to form a larger crush zone. It was also noted that the crush zone size of the chip in edge chipping (Fig. 5.9 (d)) is smaller than that in linear cutting at the same depth of cut, which indicates that larger energy consumption for creating a chip in linear cutting is needed. Fig. 5.10 shows four sets of chips generated by different bit configurations. Chip size variation in each set is due to the different cutting conditions in the continuous cutting process. Energy consumption under P7 could be the least, due to the smallest crush zone size.

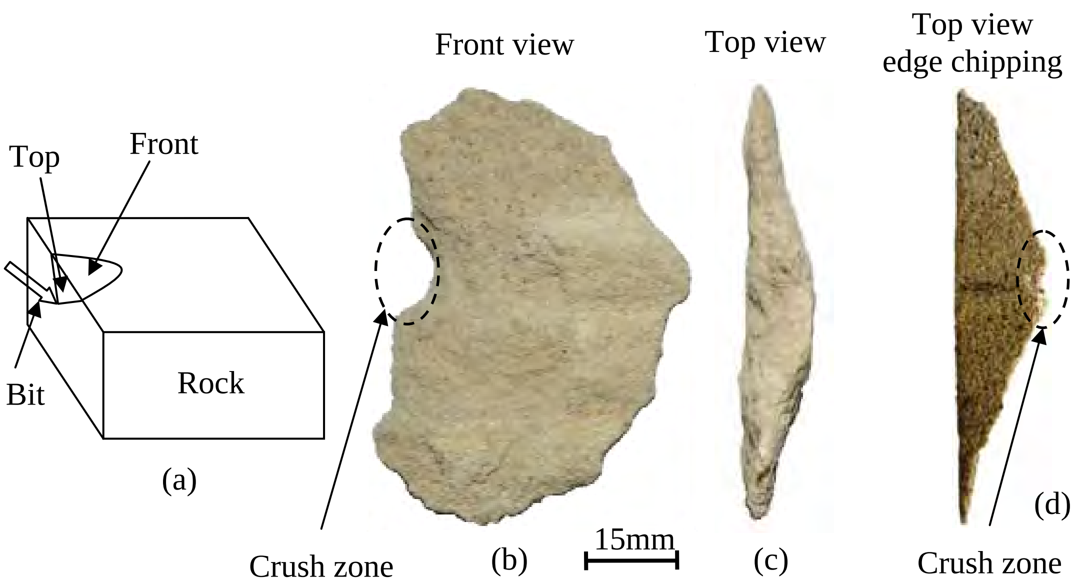

Fig. 5.9 Schematic of chip formation (a); Front and top views of a chip formed by the bit with P7 at DOC = 15mm, SOC = 0.5m/s and AOA = 45° (b-c); Top view of a chip at DOC = 15mm in perpendicular edge chipping (d)

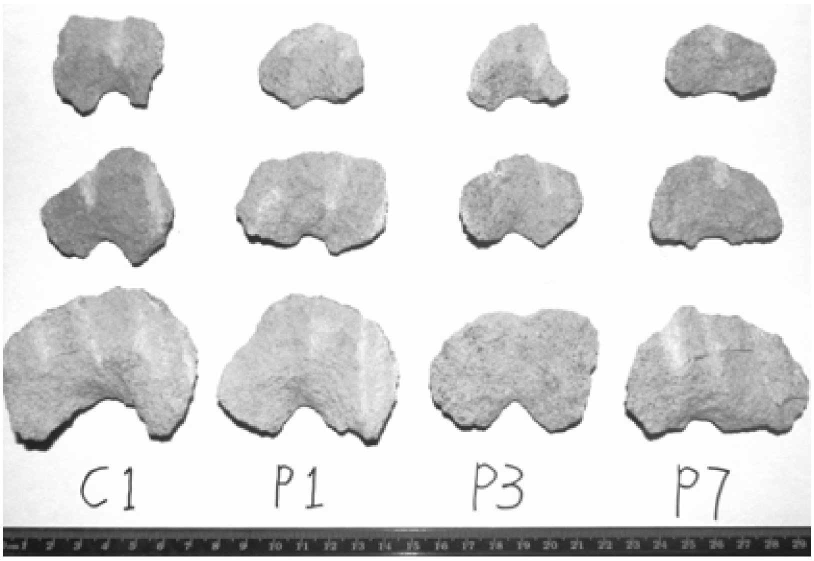

Fig. 5.10 Different groups of chips created by C1, P1, P3 and P7 at DOC = 15mm, SOC = 0.5m/s and AOA = 45°

5.4.2.2 *Fragment distribution*

Chips in the continuous cutting process can be arranged into different groups of different ranges of size. Fig. 5.11 (a) and (b) shows the results of the chip size distribution when cutting at 5mm and 10mm depths of cut, 0.5m/s cutting speed and 45° degree attack angle. The scale of the horizontal axis refers to the size of the apertures and the columns demonstrate the fragment size. For each aperture, the length of the bar represents different chip masses. Statistical calculations show that at 5mm depth of cut (see Fig. 5.11(a)), bit P7 tends to generate more large chips than other bits. For the chips over 4mm P7 generates about 74% of the total chip mass, C1 63%, P1 63% and P3 54%. At 10mm depth of cut, the major chips (over 16mm) generated by P7 constitute 62%, still more than C1 50%, P1 61% and P3 51%. Since bit P7 is the most effective in producing large chips and reducing energy consumption, its efficiency should be much higher than the other bits. In addition, the increase of the depth of cut reduces the fraction of the relative fine grains. The fine grain fractions which pertain to C1, P1, P3 and P7 are respectively 29%, 26%, 33% and 16% at 5mm depth of cut and 19%, 14%, 18%, 10% at 10mm depth cut. The smallest amount of fine grains produced by bit P7 may partly be ascribed to the smallest size of the crush zone.

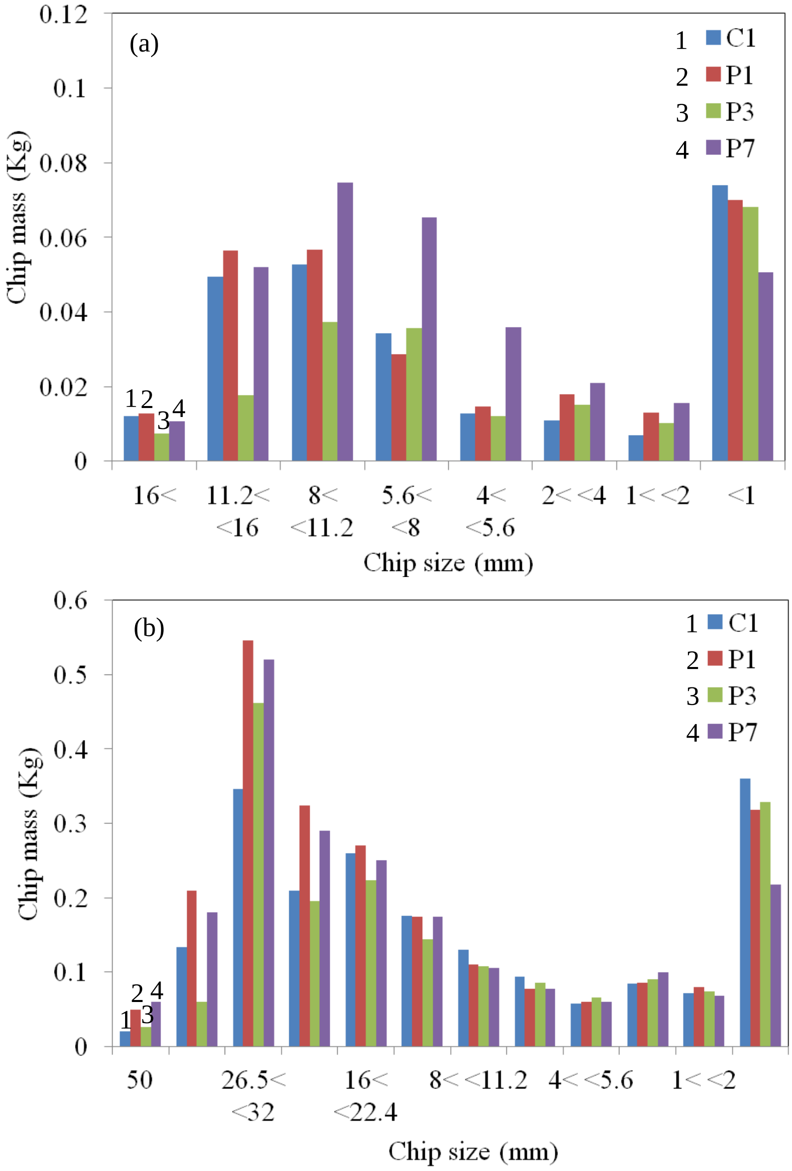

Fig. 5.11 Size distribution of the chips at DOC = 5mm (a) and DOC=10mm (b), SOC = 0.5m/s and AOA = 45°

5.4.3 Cutting grooves and excavated rock mass

Fig. 5.12 shows the groove cross-sections generated by the above three bits, and the geometry of each groove is schematically demonstrated for each case, where $\phi_{C1} = 73^{\circ}$, $\phi_{P1} = 76^{\circ}$, $\phi_{P3} = 79^{\circ}$ and $\phi_{P7} = 75^{\circ}$ are the corresponding breaking angles measured after the linear cutting tests. It can be observed that although the ‘v’ shapes generated by C1, P1, P3 and P7 are similar to each other, their cross section areas are different. If we use this area as a measurement, at the same depth of cut, bits P1 and P7 can excavate more volume of rock. This is consistent with the measurements of the rock mass excavated by the bits, as shown in Fig. 5.13.

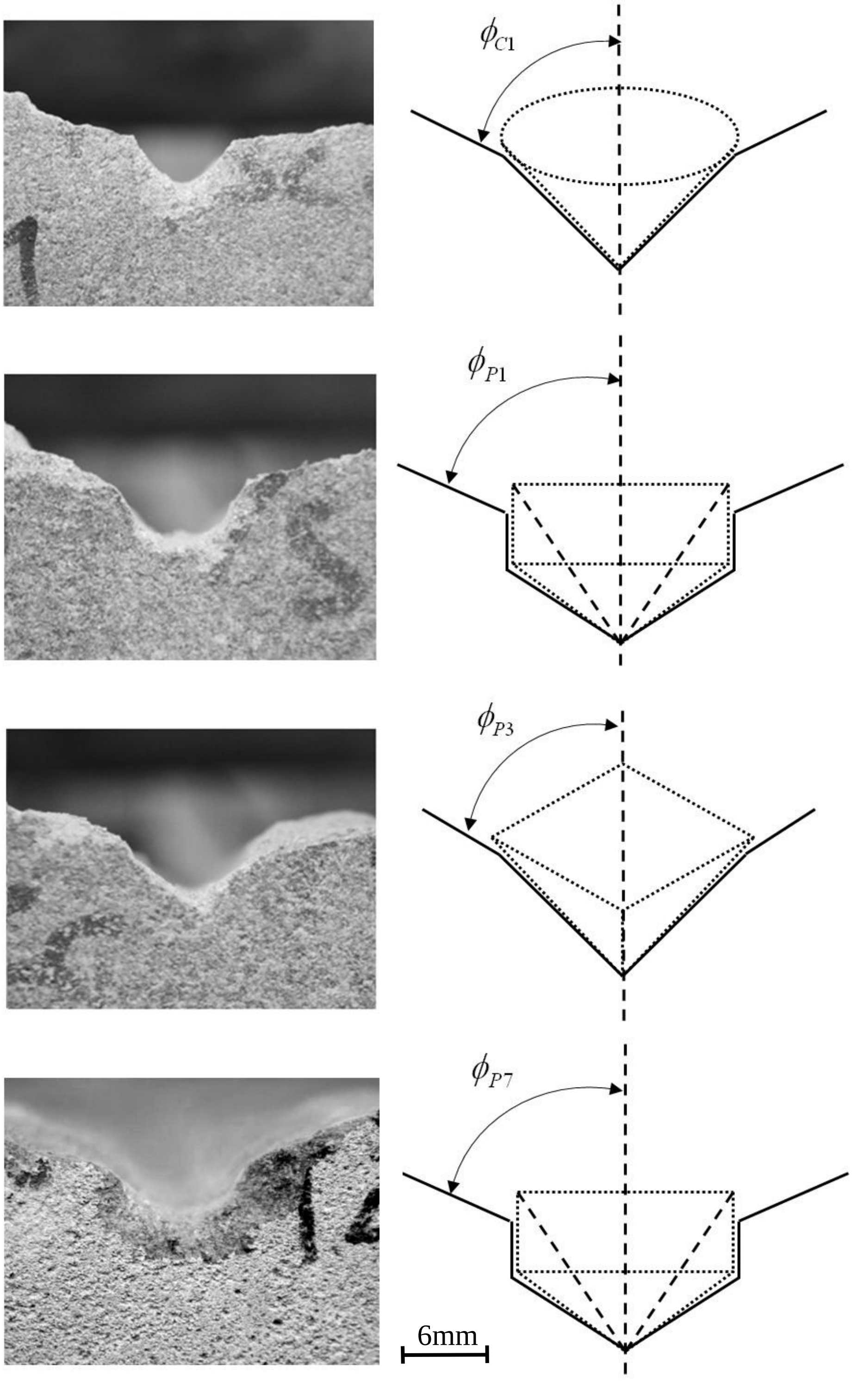

Fig. 5.12 Grooves generated by Bits C1, P1, P3 and P7 at DOC = 10mm, SOC = 0.5m/s and AOA = 45°

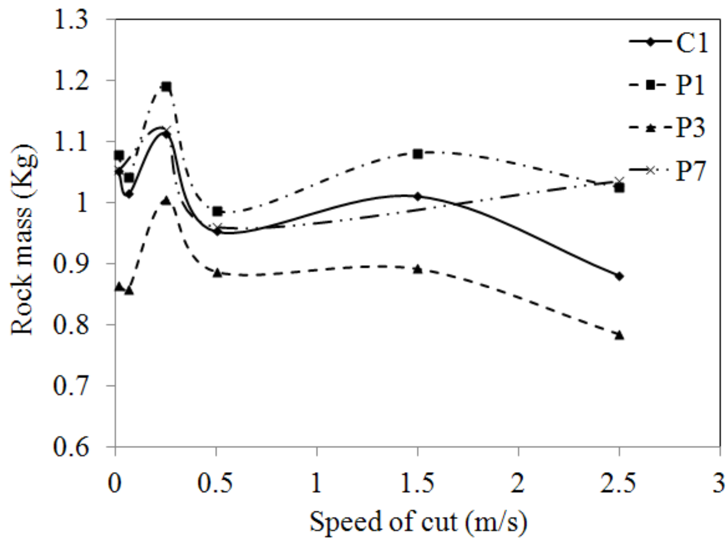

Fig. 5.13 Rock mass excavated at different speeds of cut (depth of cut = 10mm; angle of attack = 45^o)

Fig. 5.13 plots the results from a number of cuttings, which were repeated at least three times with each bit. The data points shown in the figure are the average of repeated experiments. Bits C1, P1 and P7 produced similar rock mass while the bit P3 produced 5~10% less. It is interesting to notice the embossment in each curve is between 0.25m/s to 0.5m/s with about 15% deviation from its neighbouring points. It infers the existence of an optimum cutting speed.

5.4.4 Forces and specific energy

Normal and cutting forces are important for assessing the cutability of bits and selecting suitable machines. Shown in Figs. 5.14 and 5.15 are the normal and cutting forces versus time under the conditions of 5mm depth of cut, 0.5m/s speed of cut and 45° angle of attack.

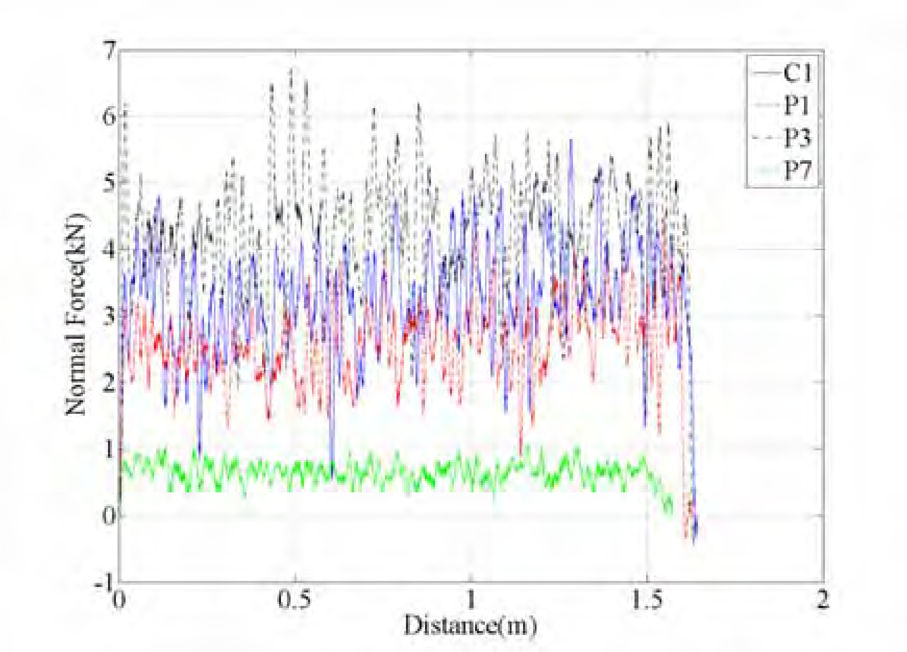

Fig. 5.14 Normal force *vs* distance (DOC = 5mm, SOC = 0.5m/s; AOA = 45^o)

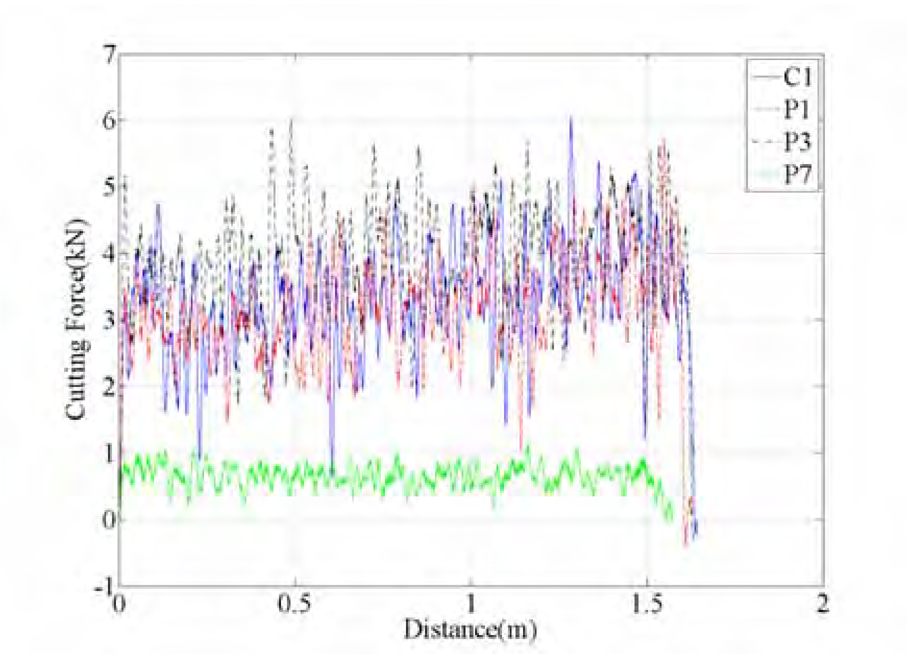

Fig. 5.15 Cutting force *vs* cutting distance (DOC = 5mm, SOC = 0.5m/s; AOA = 45^o)

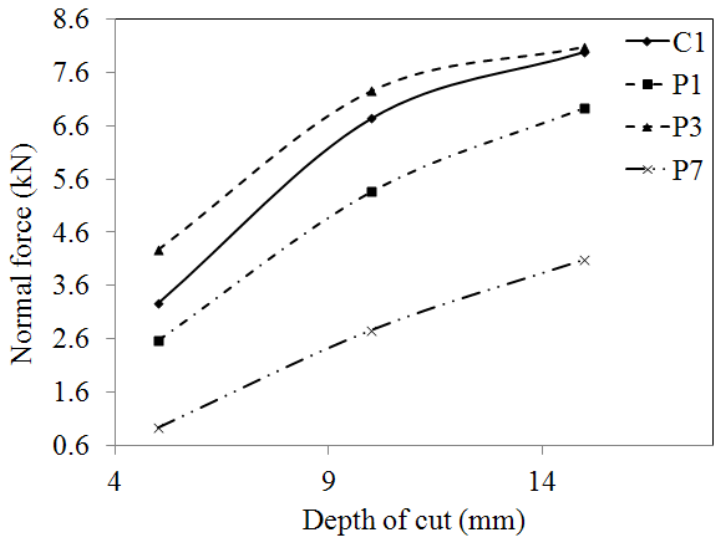

Fig. 5.16 Normal force vs. depth of cut (speed of cut = 0.5m/s; angle of attack = 45^{o})

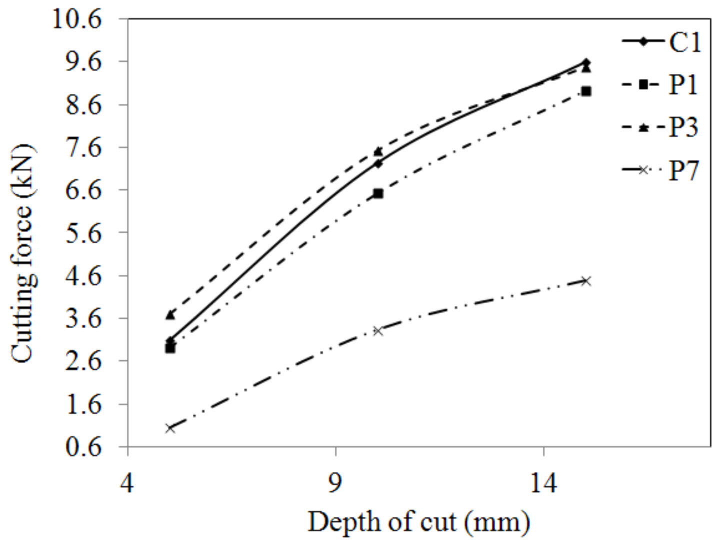

Fig. 5.17 Cutting force vs. depth of cut (speed of cut = 0.5m/s; angle of attack = 45^{o})

Figs. 5.16 and 5.17 show the normal and cutting forces versus depth of cut, in which each data point represents the average force of at least three repeated tests. Both forces increase non-linearly with depth of cut. It is also noticed that P7 always gives rise to the least normal and cutting forces, which elucidates the superior configuration of P7.

Figs. 5.18 and 5.19 plot the average normal and cutting forces corresponding to the speed of cut with fixed depth of cut, 10mm and angle of attack, 45^o. Corresponding to the embossment in the mass curve, there are depressions between 0.065m/s and 0.25m/s in all force curves, indicating the optimum speed in this range. Nevertheless the depression is negligible for bit P7. It should be pointed out that bit P7 still performs superiorly over the other three in terms of minimum dependence on the cutting speed, which can significantly improve the cutting efficiency since high-speed cutting can be applied. Another point which can be noteworthy is the speed range from 0.065m/s to 0.25m/s, in which the cutting forces (in Fig. 5.19) drop to the minimum. An optimum cutting speed falls in this range which infers the speed should affect the cutting mechanics. Although Nishimatsu [81] and Roxborough [218-219] reported that the cutting speed does not affect the process and mechanics of rock cutting, the minimum cutting speed that they employed was at 0.41m/s, at which the force increases to the similar value to those at higher speeds.

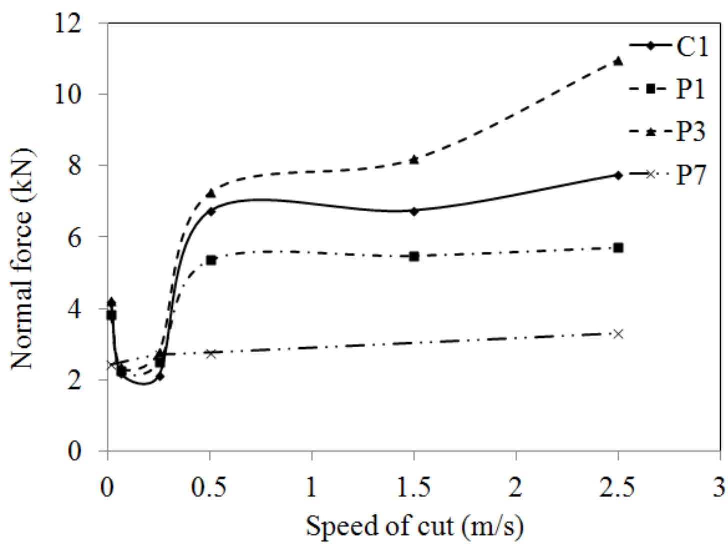

Fig. 5.18 Normal force vs. speed of cut (depth of cut = 10mm; angle of attack = 45^o)

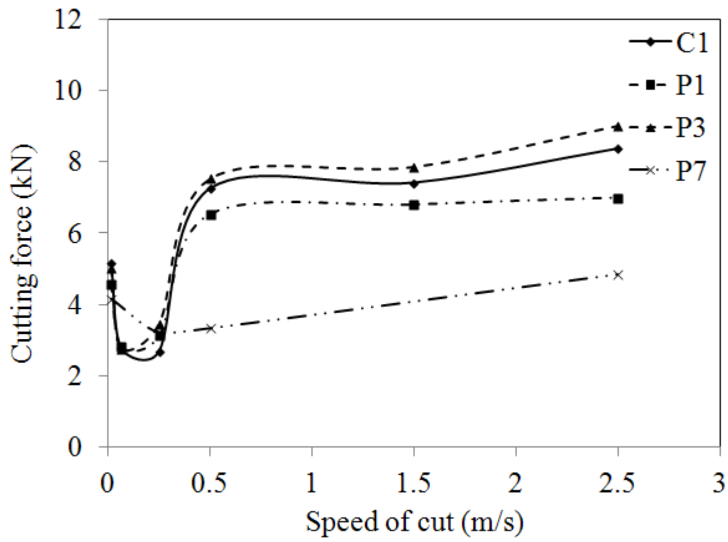

Fig. 5.19 Cutting force vs. speed of cut (depth of cut = 10mm; angle of attack = 45^{o})

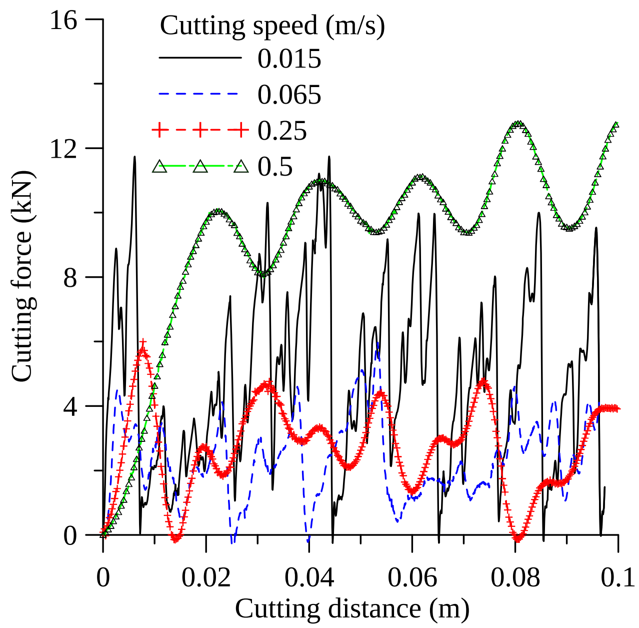

Fig. 5.20 Comparison of raw cutting force curves (depth of cut = 10mm; angle of attack = 45^{o})

To explain the occurrence of minimum average cutting force at the speed between 0.065 and 0.25 m/s, we plot the cutting force versus cutting distance in Fig. 5.20 for different speeds. It is noteworthy that the forces pertaining to the cutting speeds 0.015m/s and 0.065m/s drop to zero periodically, which demonstrates that the cutting process at a sufficient low speed is a series of discrete chipping processes. For each chipping process, the contact between the bit and the rock causes a local crushing before chipping as illustrated in Fig. 3.10 in Chapter 3. The lower cutting speed leads to the smaller crushing zone, resulted in steeper rise of the contact force due to less energy dissipation in local crushing. As shown Fig. 5.20, with the increase of cutting speed, the cutting force rises at the reducing rate. When cutting speed is higher than 0.25m/s, the cutting process becomes continuous manifested by the nonzero cutting force for a long cutting distance. Higher cutting speed also leads to less fluctuation of forces, indicating that the interval of two discrete chipping becomes smaller. The critical speed is between 0.065m/s and 0.25m/s in this test, which also corresponds to the minimum average cutting force shown in Fig. 5.19. The increase of cutting force with cutting speed is attributed to the positive strain rate effect of materials [220]. This is a common phenomenon found in rocks and many other materials. However, in the discrete chipping process, the decrease of the cutting force with the increase of the cutting speed remains unanswered.

The schematics shown in Fig. 5.21 may be a qualitative answer of the above question. In the chipping process, the increase of penetration depth leads to larger normal force. At a large penetration depth (in Fig. 5.21), the chipping is due to not only the horizontal penetration but also the normal expansion. This normal force makes the chipping easier, leading to the reduction of the cutting force. With the reduction of the cutting speed, the local crushing zone size and the penetration depth decrease, resulting in the increase of cutting force. We are now clear about the physical picture of the minimum cutting force occurring at a critical cutting speed. This is due to two competing mechanisms: (1) the increase of cutting speed leads to the increase of the force due to the strain rate effect and (2) the increase of normal force induced by the increase of the penetration depth leads to the reduction of the cutting force. At low speed, the strain rate effect is not significant and the cutting force reduces due to the second mechanism. With the speed increases, the first mechanism dominates. The minimum cutting force occurs at the transition point, at which the cutting mechanism transits from the slow to the fast discrete chipping processes. In the above discussions, two assumptions have been adopted: (i) The local crushing zone size and the penetration depth increase with speed; and (ii) a larger penetration reduces the cutting force. For the first assumption, experimental evidence can be found from the edge chipping tests. Figs. 5.22 and 5.23 show that the larger cutting speed leads to the smaller cutting force and larger crush zone. The second assumption is based on the fact that rock fractures much more easily under a tensile stress. The quantitative modelling of the effects of penetration depth is not presented here. It will be a subject of my further research.

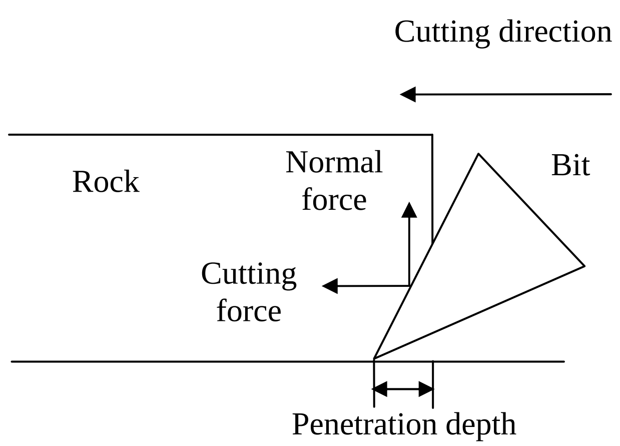

Fig. 5.21 Schematics of cutting

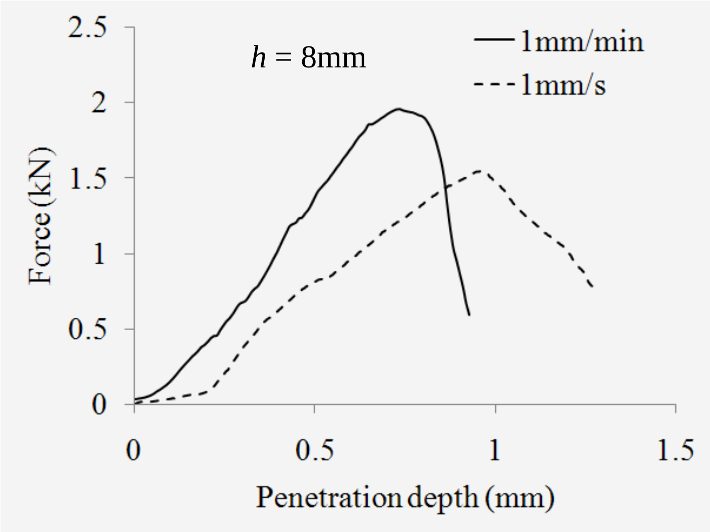

Fig. 5.22 Force comparison in edge chipping tests at 1mm/min and 1mm/s

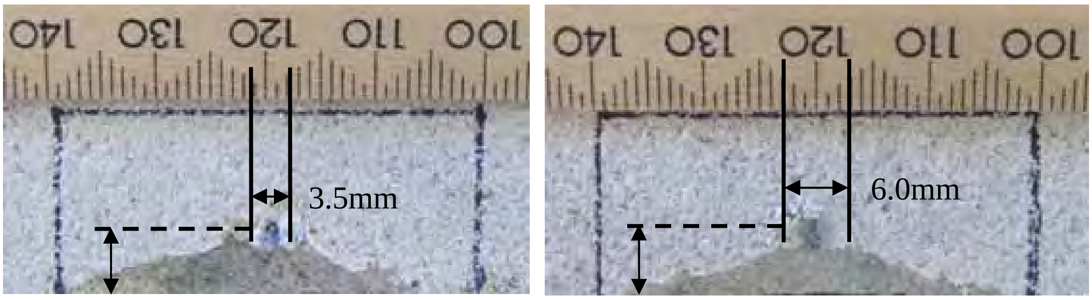

Fig. 5.23 Comparison of crush zone size at 1mm/min and 1mm/s

Specific energy, defined as the amount of work required to excavate a unit volume of rock, is one of the important parameters to measure cutting efficiency. In a linear cutting test, the total external work can be obtained through integration of the cutting force with respect to the cutting distance. Fig. 5.24 shows the variation of specific energy with a change of the depth of cut when the speed of cut was 0.5m/s and angle of attack was 45^o. It can be seen that bit P7 always renders the smallest specific energy among all bit configurations, which further elucidates that pyramidal bottom flat is the most efficient orientation for excavation. With increasing the depth of cut, the magnitudes of specific energy decrease, and their difference becomes less, indicating that the effect of bit profile and orientation on energy consumption becomes less significant.

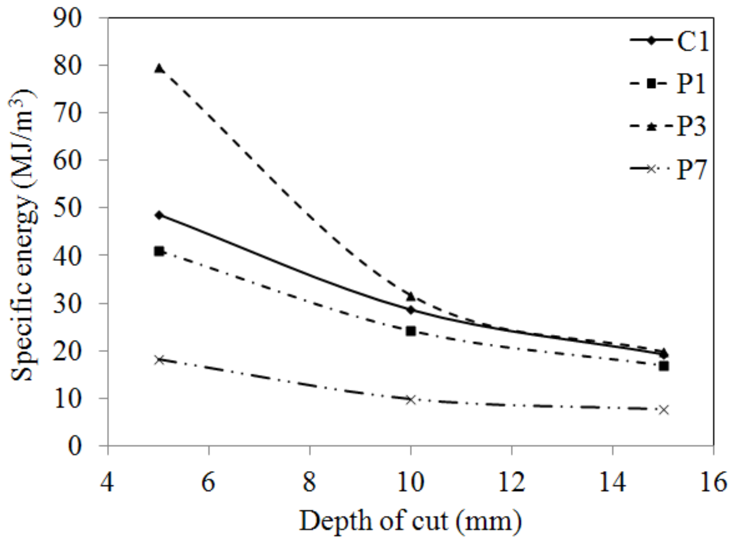

Fig. 5.24 Specific energy vs. depth of cut (speed of cut = 0.5m/s; angle of attack = 45°)

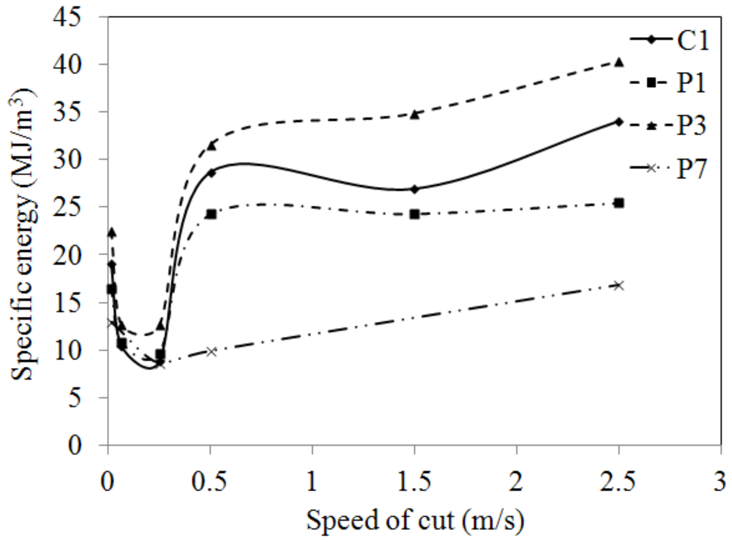

Fig. 5.25 Specific energy vs. speed of cut (depth of cut = 10mm; angle of attack = 45°)

The effect of the cutting speed on the specific energy was also examined in Fig. 5.25, in which the depth of cut is 10mm and the angle of attack is 45°. It can be seen that there is a critical speed of cut, at around 0.2 m/s, under which the external energy required to excavate the unit volume of rock is minimal. It can also be seen that the specific energy is sensitive to the speed of cut when it is around the above critical speed, but its variation levels off when the speed of cut is beyond 0.5 m/s. In the neighbourhood of the critical speed, the effect of bit geometry and orientation is small. Beyond 0.5 m/s, P7 always gives the lowest specific energy, demonstrating the merit of the P7 configuration.

Moreover, Fig. 5.26 shows the specific energy versus the angle of attack. It is noted that the angle 55° is the most appropriate in terms of specific cutting energy. It is also noticed that the bit under P7 led to the least specific energy at all three attack angles, which is due to the much smaller total energy consumption and equivalent excavated rock mass. As a whole, the P7 configuration is the optimum as the bit always generates the least specific energy and highest cutting efficiency under all conditions.

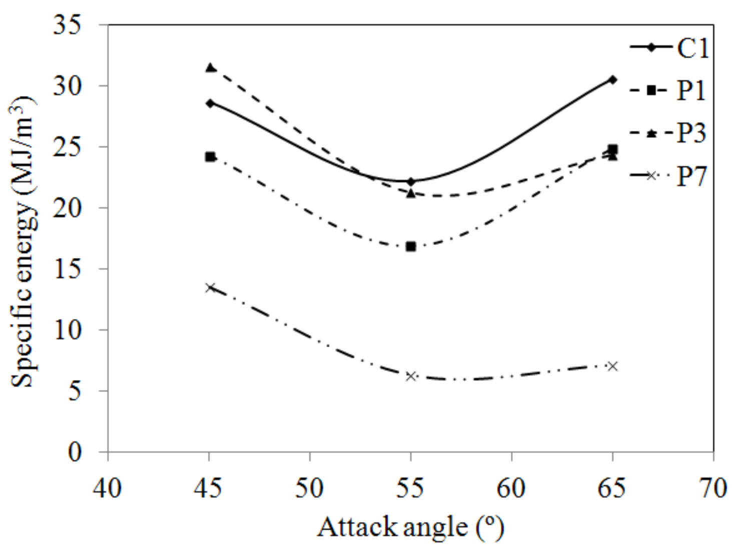

Fig. 5.26 Specific energy vs. angle of attack at 10mm depth of cut and 0.5m/s

5.4.5 Bit wear

Wear tests were first conducted with the pyramidal bits in order to investigate the endurance of the pyramidal ridges. Fig. 5.27 shows the microscope images of the bit profiles before and after cutting. It demonstrates that the PCD material has excellent wear resistance. No wear can be detected even on the pyramid ridges after a cut of 500m. Figs. 5.28 and 5.29 show a series of comparable microscope images for PCD and WC conical bit profiles. For PCD bit shown in Fig. 5.28, after 43 cuts, which is about 73.1m at various speeds ranging from 0.3m/s to 2.5m/s, the bit shape is still in good condition except for some small local chippings.

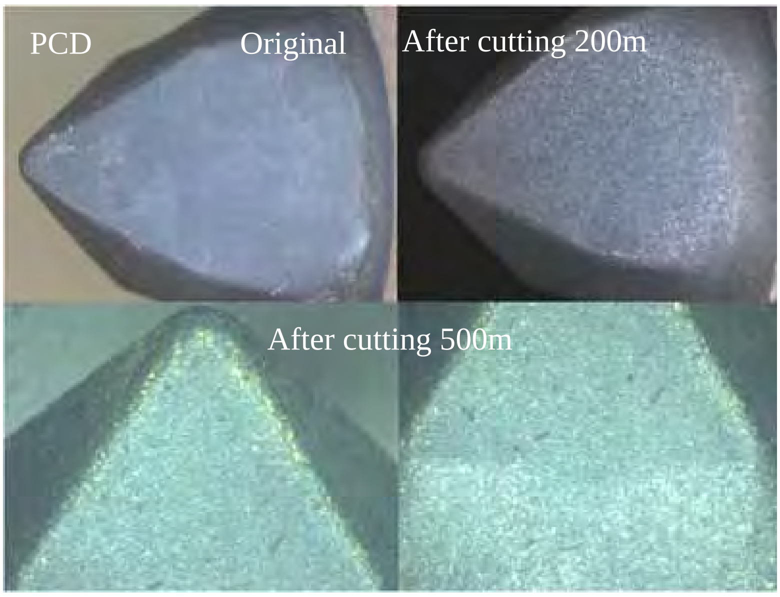

Fig. 5.27 Wear resistance on cutting sandstone with pyramidal PCD bit

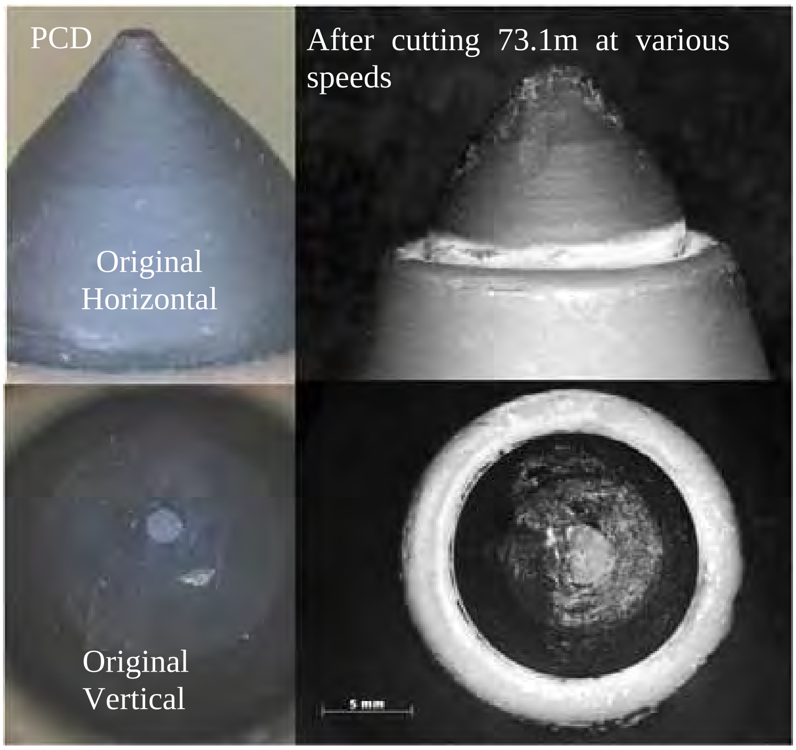

Fig. 5.28 Wear images of PCD conical bit on cutting granite

In comparison, for WC bits in Fig. 5.29, after cutting only 1.7m at 2.5m/s, the bit tip was seriously damaged and could not be further utilized. Even when speed was reduced to 0.3m/s, still after cutting 1.7m, the shape was also ruined, followed by a big chip on the cutting surface.

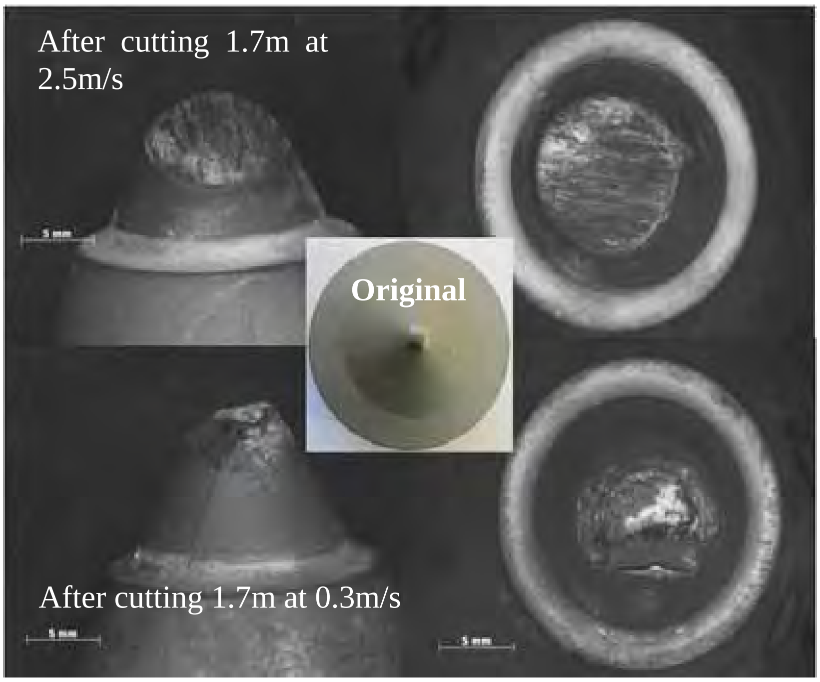

Fig. 5.29 Wear images of WC conical bit on cutting granite

PCD bits are therefore more effective in resisting wear and can cut much longer distance than WC ones, which is also confirmed in [161].

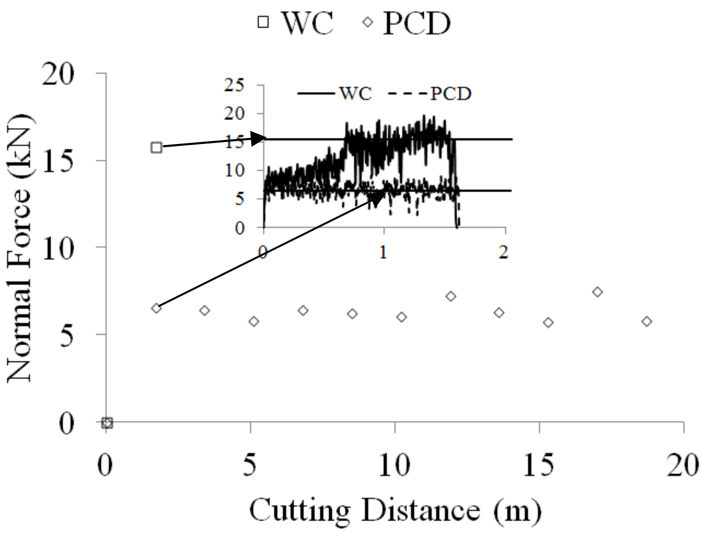

Fig. 5.30 Normal forces for PCD and WC vs cutting distance at 0.3m/s

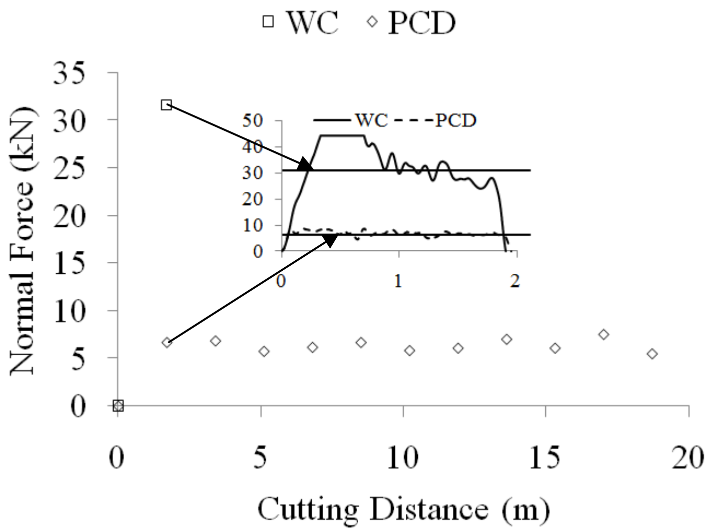

Fig. 5.31 Normal forces for PCD and WC vs cutting distance at 2.5m/s on cutting granite

Normal force is related to the average sliding friction force. In order to quantitatively demonstrate the comparative wear variations of both PCD and WC bits, the relationship between normal force and cutting distance was plotted at the speed of 0.3m/s and 2.5m/s respectively, shown in Fig. 5.30 and Fig 5.31. Each point in both figures represents the average normal force in a 1.7m cut. The WC bits induce sharp increase of the normal force at a short distance due to the quick enlargement of the wear flat (see Fig. 5.29). PCD bits possess a much higher wear resistance, which is manifested by the flat curve after cutting over 15 times longer distance than the maximum cutting distance by WC bits. Fig. 5.30 and 5.31 infer that WC bits are almost not applicable to cutting of hard granite due to the quick wear of the bit at very short cutting distances. It was also found that a large number of quartz crystals (shown in Fig 5.32) exist in the granite structure, which impacts and abrades the contact areas of the PCD bit for local surface chippings. This phenomenon was also reported in other references: Sneddon demonstrated that the damage of PCD materials is mainly due to the local failure of structure, caused by mechanical behaviours [115]; Dunn and Lee [221] found that the fracture mode of the PCD part of the diamond composite tool under cyclic loading is brittle shear fracture, which belongs to the mechanical fatigue mechanism. Pin et al. [222], further confirmed that mechanical micro-chipping of the PCD layer is one of the four principal fracture modes.

Fig. 5.32 Texture of Harcourt granite

The wear of the improved bit made from PCD is also minor when cut on sandstone over 238m, at different speeds, different depths of cut and different angles of attack, as shown in Fig.5.33. It shows the cutting surface before (left) and after (right) cutting. The wear happens at the edge of the surfaces. The shape of the bit is almost intact. Even when it was applied for cutting granite, the shape of the bit was not changed seriously, as shown in Fig. 5.34.

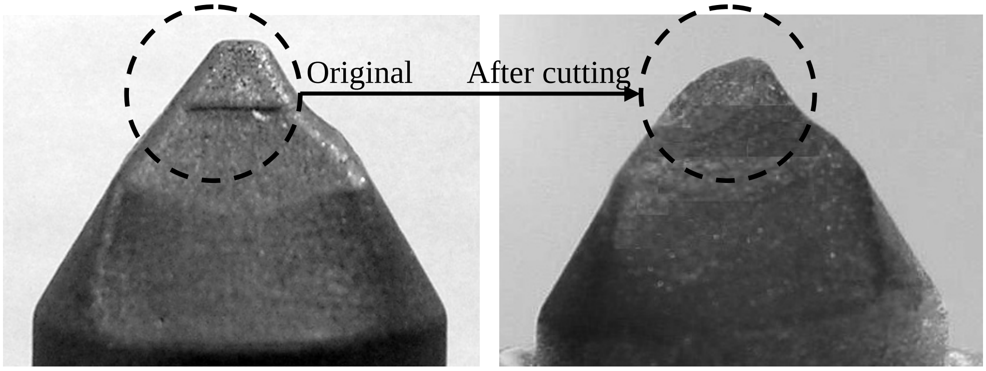

Fig. 5.33 Wear of improved bit after cutting 238m on sandstone

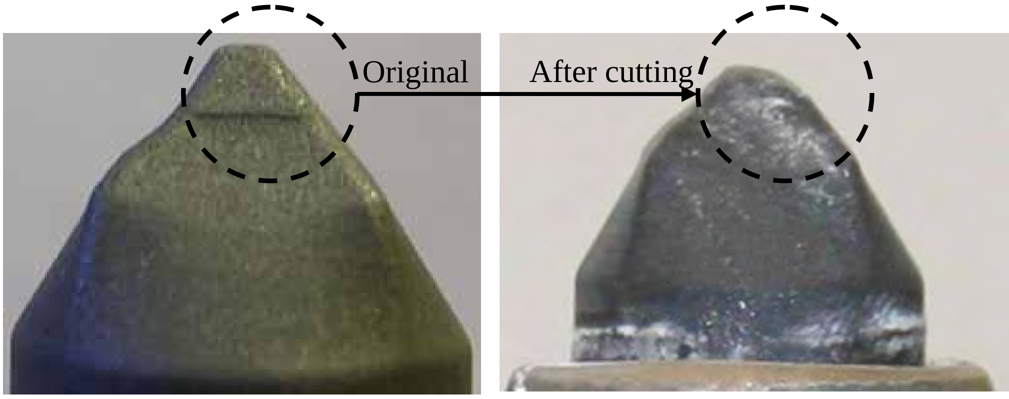

Fig. 5.34 Wear of improved bit after cutting 20.4m on granite

As a summary, wear performance of PCD bits is superior to that of WC, except for the local chippings, which may be attributed to its high temperature endurance resistant to deform and wear.

5.5 Discussions

5.5.1 Application of cutting force model

As mentioned in Chapter.2, edge chipping is similar to rock cutting and the first peak of the cutting force in linear cutting at a low speed of 0.015m/s resembles the maximum chipping force at edge chipping. Therefore, we may exploit the formulation in Chapter 4 to investigate the linear cutting force.

Curves of the first loop in a complete cutting force curve under C1, P1, P3 and P7 conditions are shown in Fig. 5.35. It is interesting to note the curves are similar to those in edge chipping. Therefore, we may employ the previous regression result (the exponent 1.33) to investigate whether the power relationship between the first peak force and the depth of cut still exists.

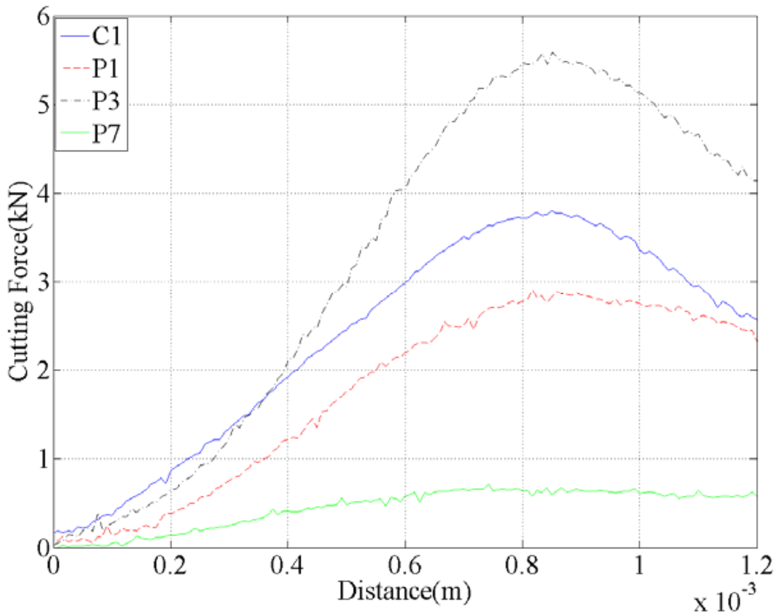

Fig. 5.35 The first loop of cutting force history by C1, P1, P3 and P7 (at depth of cut = 5mm, speed of cut = 0.015m/s; angle of attack = 45^o)

Fig. 5.36(a)-(c) shows the power relations between the first peak cutting force, maximum cutting force, mean cutting force and depth of cut respectively. The cutting force data can be well fitted by the derived power relation in edge chipping, which validates the feasibility of exploiting the formulation in edge chipping to assess the cutting forces in linear cutting. Thus, the mean cutting force can be expressed as:

$$F_{mc} = \kappa' h^{4/3} \tag{5.1}$$

where κ' is a coefficient related to the material properties in dynamic mode. Total cutting energy consumption E_t could be represented as:

$$E_t = F_{mc} L_D \tag{5.2}$$

where L_D is the cutting distance. The volume of the excavated rock mass can be simply represented as:

$$V = S_c L_D = \kappa'' h^2 L_D \tag{5.3}$$

where S_c is the cross sectional area of the groove. If the cross sectional area can be approximated as a triangle, $S_c \propto h^2$, it could be further expressed as $S_c = \kappa'' h^2$. Then Eqs. 5.1-5.3 lead to the specific energy:

$$SE = \frac{F_{mc} L_D}{V} = \kappa^* h^{-2/3} \tag{5.4}$$

where κ^* is another coefficient related to the rock properties. The power relation between specific energy and depth of cut ($SE \propto h^{-2/3}$) is close to the trend in the experimental results shown in Fig. 5.24.

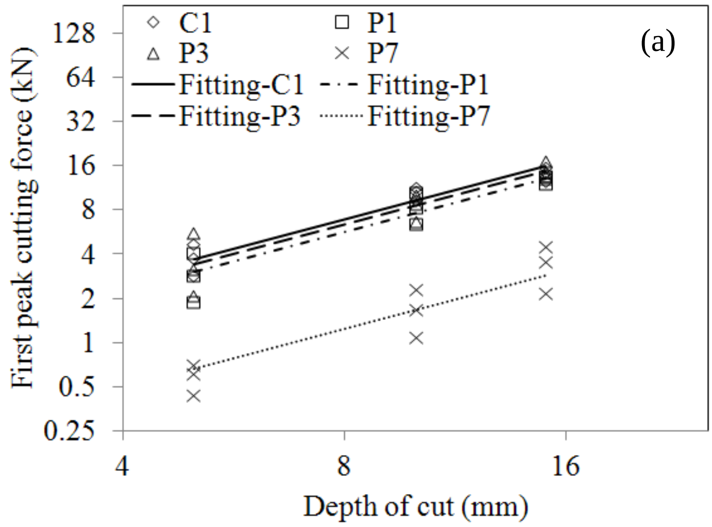

C1
P1
P3
P7
Fitting-C1
Fitting-P1
Fitting-P3
Fitting-P7
(a)
First peak cutting force (kN)
128
64
32
16
8
4
2
1
0.5
0.25
4
8
16
Depth of cut (mm)

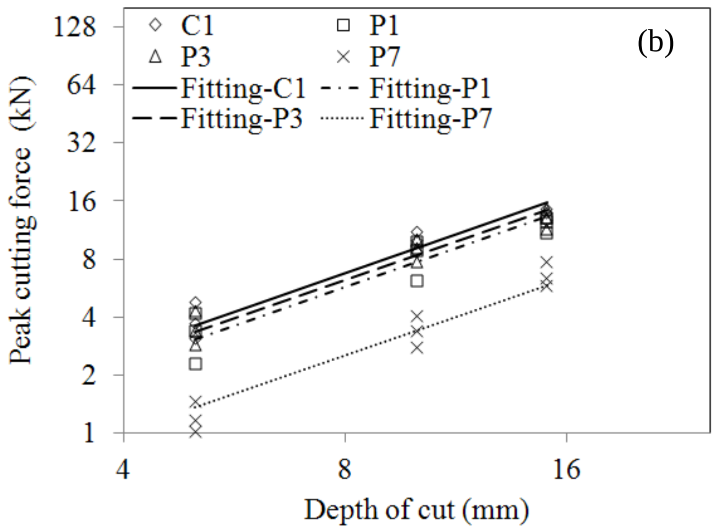

C1
P1
P3
P7
Fitting-C1
Fitting-P1
Fitting-P3
Fitting-P7
(b)
Peak cutting force (kN)
128
64
32
16
8
4
2
1
4
8
16
Depth of cut (mm)

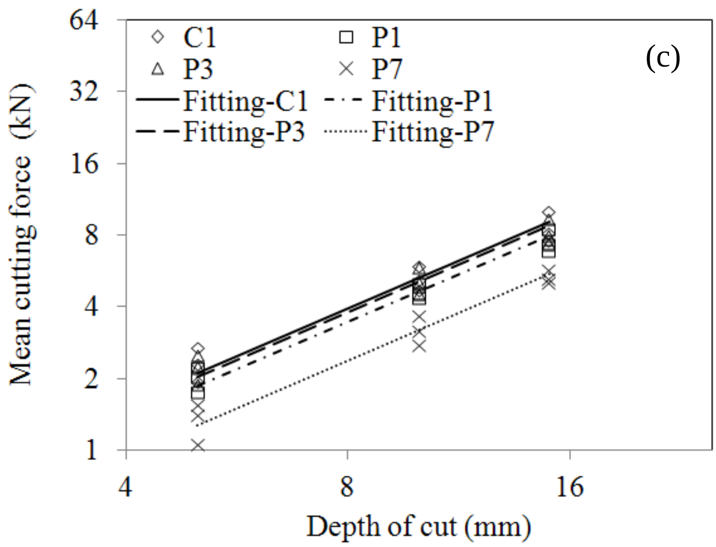

Fig. 5.36 The first peak cutting force (a), peak cutting force (b) and mean cutting force (c) by C1, P1, P3 and P7

Furthermore, it is found that the amplitude of the peak cutting force in linear cutting is larger than the maximum chipping force in edge chipping, which may be due to the dynamic effects. There are many other experimental investigations on the dynamic effect of the rock properties, demonstrating the increase of rock strength under dynamic loading, such as the dynamic Young's modulus [223-226] and toughness [227-229]. Moreover, since the total energy consumption is directly related to the mean cutting force, the smallest amplitude of the mean cutting force induced by P7 may refer to the size of the crush zone, as the average radius of chips formed by P7 in the same group is the smallest (averagely, 3 times for C1, 1.6 times for P1, 2.7 times for P3).

5.5.2 Fractal analyses: the bit cutting efficiency

Previous investigations on bit cutting efficiency concentrated on the qualitative description of specific energy. However, profound quantitative analysis is also essential as it can provide a specific quantity for straightforwardly evaluating cutting efficiency. In the literature, cutting efficiency can be quantitatively evaluated by the ratio between fracture surface energy and total external mechanical energy [194-195]. In this research, the external mechanical energy consumption in relation to the mean cutting force of different bits has been directly obtained from experimental results. Therefore, the exploration of cutting efficiency is then transited to focus on the fracture surface energy, which can be assessed by the product of the energy release rate and the fracture surface area of the chips. Thus, to obtain the total fracture surface area of all fragments in one cutting process becomes a necessity. Fragmentation analysis can be used to acquire the fracture surface area of the total fragments [230], depending on the mass and size distribution of the fragments directly obtained from a sieve or screen analysis. As the size distribution of the fragments in linear cutting has been obtained in Section 5.4.2, the fragmentation analysis can conveniently be employed to set up a link between the chip sizes and the fragment surface area. Therefore, the fractal law is applied to specifically calculate the fracture surface areas for comparing the cutting efficiency of all cutting configurations.

In terms of Eq. 4.4, fracture surface energy can be denoted as the doubled product of the material specific fracture energy γ and surface area S. And the total surface area S of all fragments in linear cutting can be expressed as the following equation [230]:

$$S = \chi^* \int_{r_{d\min}}^{r_{d\max}} r_d^2 dN \tag{5.6}$$

where χ^* is a geometrical factor in relation to the shape of the chip. r_d is the dimension of the specific aperture of a sieve. N is the number of chips sized larger than r_d. From fractal law, N is related to r_d by:

$$N = Cr_d^{-D} \tag{5.7}$$

where D is the fractal exponent and C is the fitting coefficient. Then, derivate the power law to obtain:

$$dN = Cr_d^{-D-1}dr_d \tag{5.8}$$

Put Eq. 5.8 into Eq.5.6, which gives rise to:

$$S = \frac{C\chi^*}{D-2}\left(\frac{1}{r_{d\,\min}^{D-2}} - \frac{1}{r_{d\,\max}^{D-2}}\right) \tag{5.9}$$

Figs 5.37-5.38 show the fractal fitting curves for all cutting configurations at 5mm and 10mm depths of cut respectively. The power law was still found to exist with exponents in the range from 2 to 3 (as shown in Table 5.3 and 5.4), which can be confirmed by previous experimental studies: Engleman et al. [231] determined the fractal exponent D of a value of about 2.5 for all cutting configurations when testing sandstone. Turcotte [230] listed the D values from previous experimental studies on fragment size distribution of high velocity impacts, explosion, volcanic ejecta and even nuclear explosion, for example 2.56 for basalt fragments from projectile impacting, 2.5 for broken granites due to nuclear detonation and 2.82 for terrace sand and gravels. Thus, if we assert that the conchoidal shape of the fragments is predominant under all cutting configurations, the total fracture surface area can be evaluated by the product of $C/(D-2)$ and $1/r_{\min}^{D-2} - 1/r_{\max}^{D-2}$, with determining the fractal exponent D and factor C.

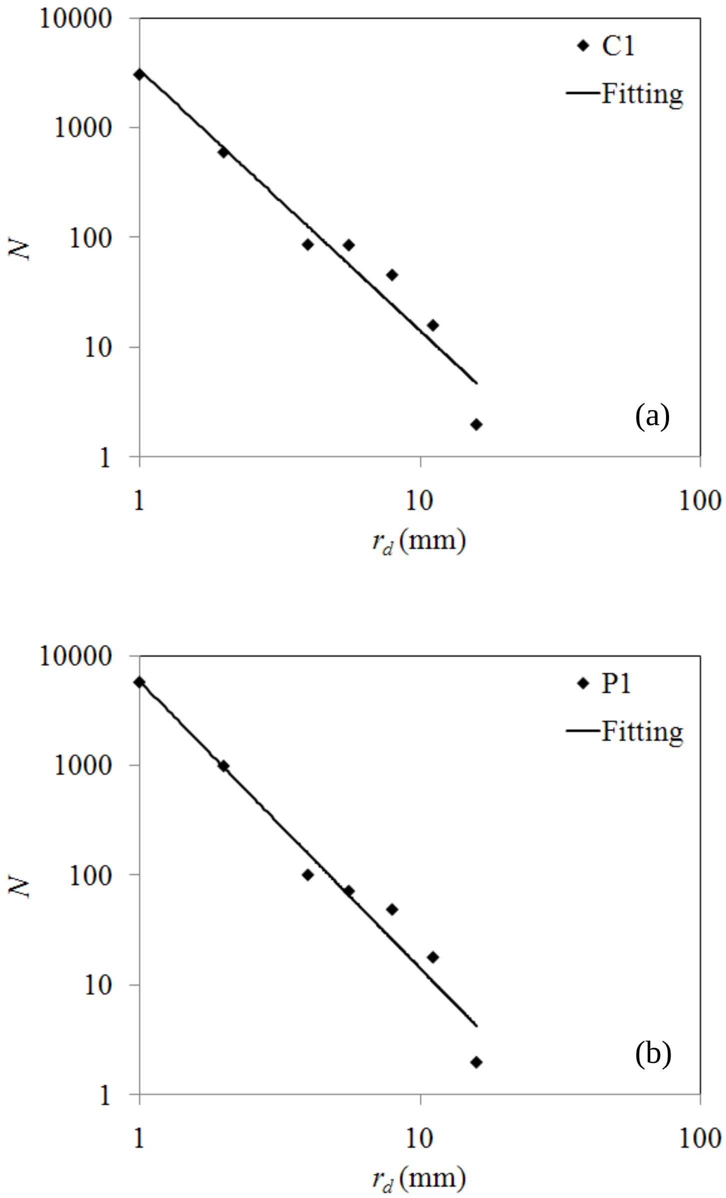

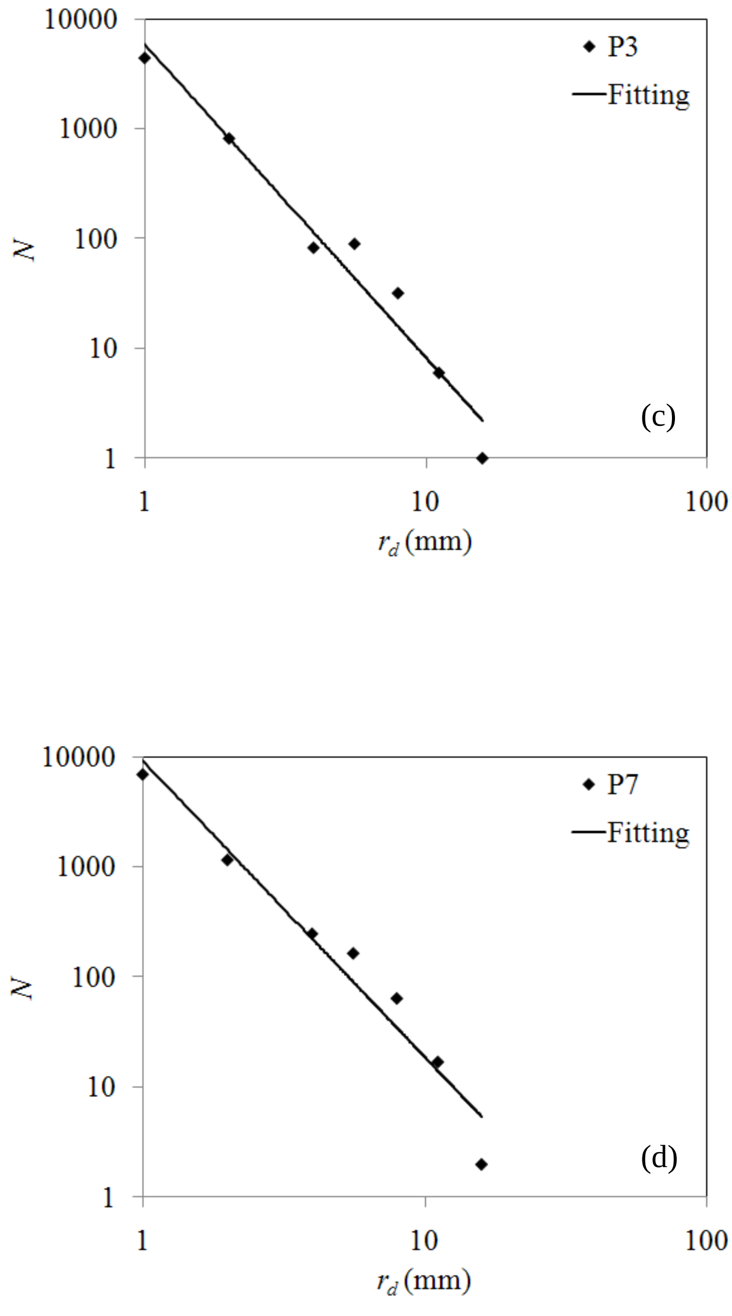

Fig. 5.37 Power fitting between N and linear dimension r_d at 5mm depth of cut with C1, P1, P3 and P7

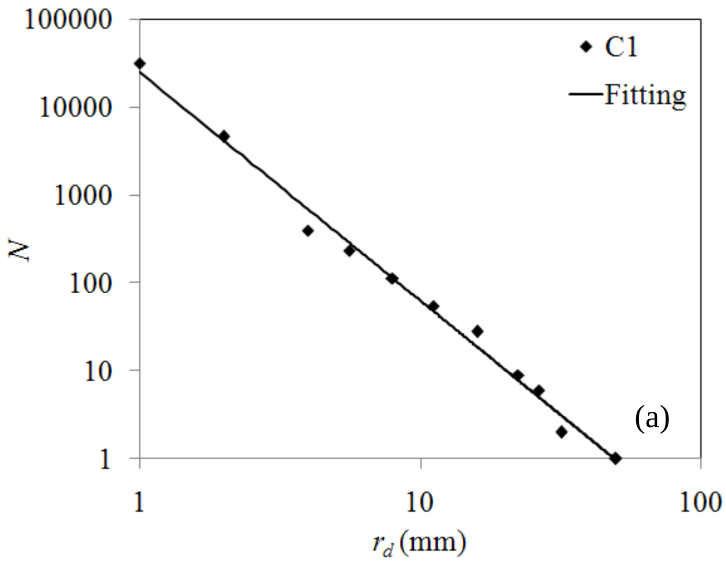

100000
10000
1000
100
10
1
N
C1
Fitting
(a)
1
10
100
r_d (mm)

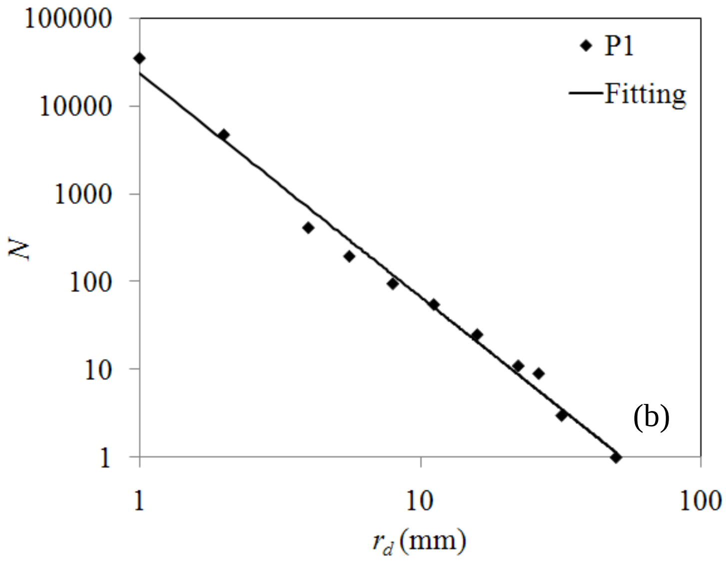

100000
10000
1000
100
10
1
N
P1
Fitting
(b)
1
10
100
r_d (mm)

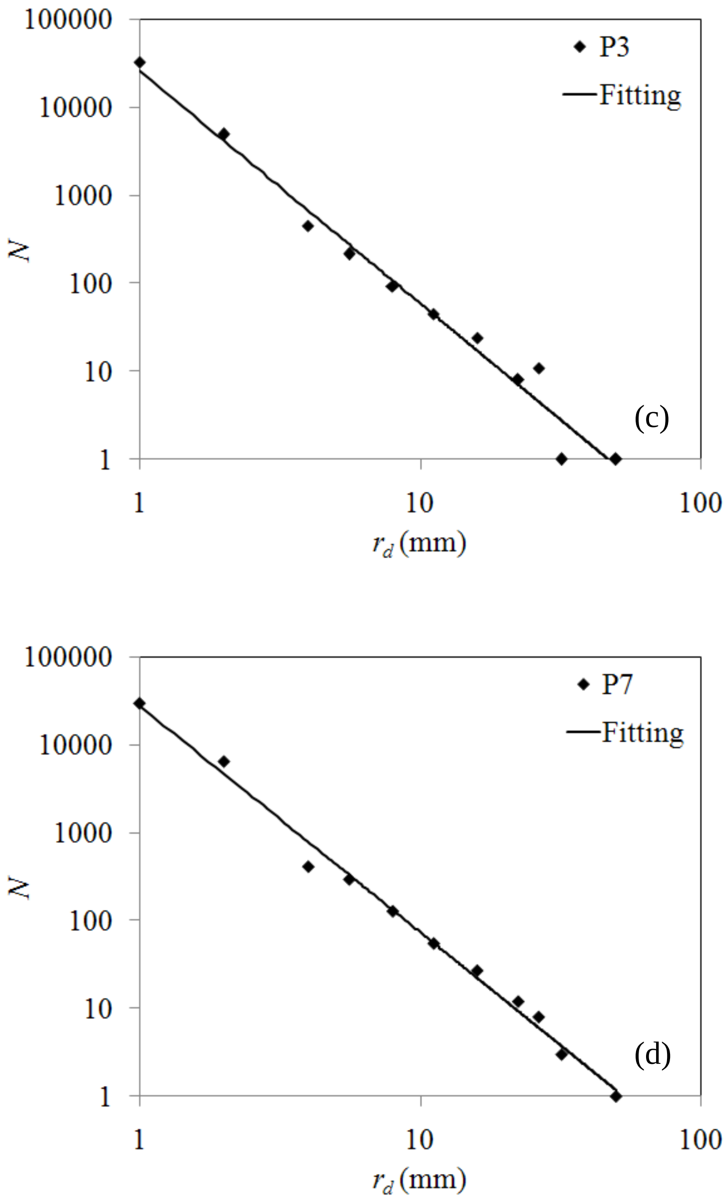

Fig. 5.38 Power fitting between N and linear dimension r_d at 10mm depth of cut with C1, P1, P3 and P7

Calculations in Tables 5.3 and 5.4 show that Bit P7 induces the biggest fracture surface area at both depths of cut with regard to the biggest values of $\frac{C}{D-2}(\frac{1}{r_{\min}^{D-2}}-\frac{1}{r_{\max}^{D-2}})$. Moreover, the smallest total mechanical energy consumption further demonstrates Bit P7 possesses the largest ratio of fracture surface energy and total mechanical energy, which elucidates P7 configuration possesses the highest cutting efficiency.

Table 5.3 Statistical information of fragmentation at 5mm depth of cut

5mm	C1	P1	P3	P7
C	3425	5947	5921	9200
D	2.378	2.613	2.847	2.684
$\frac{C}{D-2}(\frac{1}{r_{\min}^{D-2}}-\frac{1}{r_{\max}^{D-2}})$	6995.784	8819.245	6735.64	12524.9

Table 5.4 Statistical information of fragmentation at 10mm depth of cut

10mm	C1	P1	P3	P7
C	25399	23849	26455	27589
D	2.601	2.544	2.643	2.572
$\frac{C}{D-2}(\frac{1}{r_{\min}^{D-2}}-\frac{1}{r_{\max}^{D-2}})$	38235.14	38620.48	37817.49	43086.25

5.5.3 Summary of effect of speed, angle and depth on cutting force

In previous experimental analyses, the mean cutting force in relation to cutting efficiency was only evaluated against a single parameter, such as mean cutting force vs depth of cut and mean cutting force vs speed of cut. Multi-factor analysis assists in investigating the cutting efficiency comprehensively, as cutting performance is often affected by several principal parameters [40, 99]. Therefore, the relationship between the mean cutting force and two of the operating parameters is established in order to further investigate and compare the cutting performances by different cutting configurations.

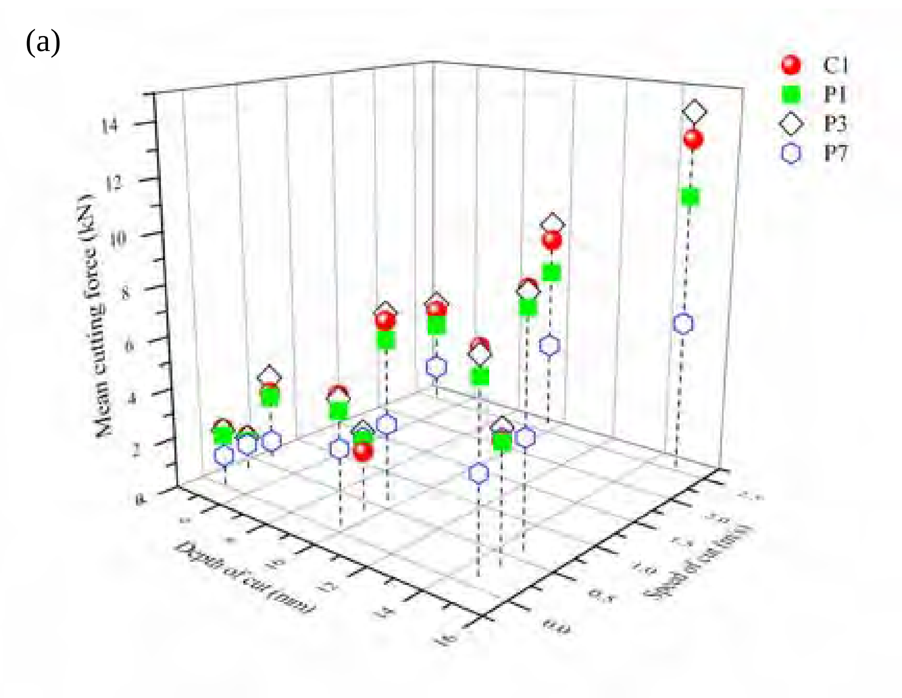

(b)

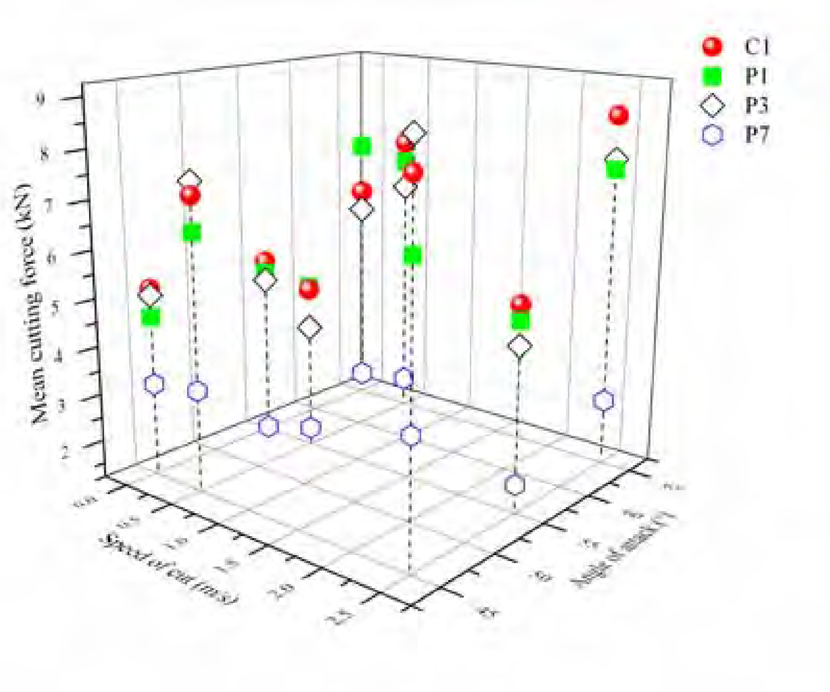

Fig. 5.39 3D scatter plots: (a) Mean cutting force against depth of cut and speed of cut at AOA = 45°; (b) Mean cutting force against speed of cut and angle of attack at DOC = 10mm

3D statistical scatter plots are then employed for validating the effectiveness of the P7 configuration. As the angle of attack does not vary in a cutting process, we firstly fix the attack angle at 45° to check the effects by changing the depth of cut and speed of cut (shown in Fig. 5.39 (a)). The distribution and location of the points show that the force increase follows the increment of the depth of cut and the P7 configuration gives rise to the lowest force values. Another 3D plot describing the force change in relation to the angle of attack and speed of cut at 10mm depth of cut is shown in Fig. 5.39(b). Bit P7 still induces the lowest mean cutting forces at all chosen speeds, 0.015m/s, 0.5m/s and 2.5m/s and angles, at 45°, 55°, and 65°, which further elucidates the availability of the P7 configuration.

In summary, the 3D multi-variate analyses comprehensively investigate the cutting performances of Bits C1, P1, P3 and P7 with regard to depth of cut, speed of cut and angle of attack. Results still reflect that the P7 configuration is the most effective.

5.6 Conclusions

The bit profile and the orientation of the pyramidal bit affect the size of fragments and cutting efficiency. Compared with C1 and P3, the P1 configuration led to less specific energy and more quantity of fragments, which also demonstrates the availability of the bottom-flat orientation. The P7 profile was found to induce the least mean cutting force and a similar quantity of fragments to P1, which led to the least specific energy of all cutting configurations. The higher cutting efficiency of Bit P7 was validated by fragmentation analysis in relation to the fracture surface energy and 3D multi-variate analysis with regard to the comprehensive factor effect. The formulation by fractal law demonstrates that the larger fracture surface area depends on the bigger product of $C/(D-2)$ and $1/r_{\min}^{D-2} - 1/r_{\max}^{D-2}$. Subsequent calculations in Tables 5.3 and 5.4 strongly verify that the P7 configuration induces the largest fracture surface area, which further elucidates that the P7 configuration gives rise to higher cutting efficiency. Moreover, 3D multi-variate analysis also indicates that for a comprehensive factor effect on cutting efficiency, the P7 configuration is still the most effective.

Experimental results also demonstrate that bits from PCD material invoked less average friction force during cutting due to its super hardness and strong wear resistance, even when cutting on hard granite. Cutting speed also influences the wear rate: higher speed arouses faster temperature increase and bigger wear flat shown in Fig. 5.29. Cutting on the relatively uniform sandstone causes little wear even for the pyramidal bit. Quartz crystals embedded in the Harcourt granite texture results in serious impact and abrasion on the PCD surface, which brings about local chipping, due to the super hardness and brittleness of PCD material. Nevertheless, the PCD bit exhibits much better wear resistance on rock cutting and it is potentially a promising material which could be applied in the future to mining sites.

Furthermore, an increase of the depth of cut results in the increase of both normal and cutting forces and the decrease of specific energy. It was also noted that the deviation of different specific energy induced by four bits becomes less significant with the increment of the depth of cut. The critical speed of cut was found to be at about 0.25 m/s, regardless of the bit geometry and orientation. Above this speed, increasing the speed of cut increases the effect of bit profile and orientation. This critical cutting speed may provide a reference for the efficient linear cutting speed of the roadheaders and longwall shearers in the real mining sites.

Moreover, the power relationship between the peak chipping force and depth of cut derived in edge chipping tests can also be applied in assessing the correlations between linear cutting forces (mean, peak and first peak) and depth of cut, due to the match of the experimental data. The dynamic effect of material properties is properly a reason for the deviation of the force amplitudes in edge chipping and linear cutting, which can be investigated in the further research. Nevertheless, this force-depth relation unveils an implicit relevance existing in the force formulation of rock cutting, which further assisted examination of the power correlation between specific energy and depth of cut. The trend of the experimental data curves confirms to this power law.

Chapter 6

Conclusions

6.1 Summary of major contributions

In this thesis, research focused on the validation and improvement of the pyramidal bit for the improvement of cutting efficiency in a mining site. Then, two stages of experimental work, namely edge chipping and linear cutting experiments, were conducted to determine a suitable bit profile for improving cutting efficiency.

In edge chipping tests, the crack mechanisms and geometrical similarity of chips were firstly investigated. Results demonstrated that the stress concentration of the pyramidal bit ridges induces quick generation of radial and median cracks in rocks and less abrasion of the contact surface, which leads to symmetrical fracture surfaces and fewer fine grains. This phenomenon suggests the possibility of using a pyramid bit rather than a conical bit in rock cutting. The chips formed at different depths of cut possess geometrical similarity in terms of the constant ratio between chip length and chip width, which brings about significant convenience in analysing the critical chipping force and fracture energy.

Moreover, the 2D crack trajectory during chipping at the side view of the chip is found to be close to a straight line, angled with the axis of external force. Specifically, the 2D crack trajectory was well predicted by the direction of maximum shear stress in the Boussinesq stress field, which also elucidates that the energy dissipation should be along the shortest crack path. Moreover, the deviated angle between the crack trajectory and force axis is found to be approximately linearly correlated with the attack angle. This angle was also validated by the stress calculations from the prediction of the crack trajectory.

Several assumptions were made for investigating the relation among the peak chipping force, depth of cut and the inclination angle, based on such experimental observations: geometrical similarity of chip dimensions, force relation between chipping and indentation, linear relation between crack deviated angle and attack angle, and ratio between fracture surface energy and total external mechanical work. Good agreement between the theoretical and experimental results validates the availability of the derivation and assumptions. Specifically, the force-angle relation therefore inspires further research on a cutting force prediction for the mining pick with consideration of the attack angle, while the force-depth relation for the perpendicular peak force theoretically elucidates the best-fit power relationship between peak perpendicular force and depth of cut ($F_{pp} \propto h^{1.3}$) in Quinn's experimental findings [129]. Further exploration leads to the derivation of fracture toughness as a function of the peak chipping force and the depth of cut. To acquire the toughness of brittle and opaque rock, one only needs to fabricate a block sample with polished surface and then conduct several chipping tests at different prescribed distances. It was also found that the magnitude of β can be verified by assuming flat fracture surfaces, which shows that the energy dissipation plane is close to being planar.

In linear cutting tests, the improvement of the original pyramidal bit was mainly based on the reduced top cutting angle, curved lateral surface for reducing friction and optimum cutting orientation (bottom flat P1). Then cutting performances of all four kinds of bit configurations were compared: the conical bit (C1), the pyramidal bit with bottom flat (P1), the pyramidal bit with bottom edged (P3) and the newly modified pyramidal bit (P7). Results demonstrated that the P7 configuration is the most efficient as it leads to much lower mean cutting force, more big fragments and bigger cross section area of the cutting grooves. Fractal and 3D multi-variate analyses were employed to validate the cutting efficiency of P7. The formulation in fractal analysis demonstrates the bigger ratio between C and $D-2$ together with bigger fractal exponent D (as the value of $1/r_{\min}^{D-2} - 1/r_{\max}^{D-2}$ is not fluctuating dramatically with all cutting configurations), resulting in a larger fracture surface area in the fragments. The statistical calculations strongly demonstrate the P7 configuration will induce bigger fracture surface and higher cutting efficiency in relation to the ratio between the fracture surface energy and total energy consumption reflected by the mean cutting force. 3D multi-variate analysis further demonstrates that the P7 configuration is still the superior even for comprehensive factors effect on cutting performances.

In addition, the application of PCD material significantly improves the wear resistance. The improved bit design was based on the optimum cutting orientation with the intention to reduce serious friction of the side surface. The modifications were to reduce the top cutting angle (for minimising the cutting force), to increase the bottom cutting angle (for strengthening the bit damage-resistance) and to introduce a curved side surface (for reducing the friction and the consequent fine grain (dust) generation). Experimental results demonstrate that specific energy and cutting force reduce to 1/3 of the previous results. Besides, the wearability of polycrystalline diamond (PCD) bits and tungsten carbide (WC) bits was also compared. The wear of the WC bit is mainly in the format of flat abrasion because of the removal of the binder Co together with the WC grains, while, the wear of the PCD bit is mainly due to local chipping. It is then concluded that the PCD bit has much higher wear resistance since it possesses much higher stiffness to avoid deformation and also withstand higher temperatures.

It is also found that the relation between the excavated rock mass and the depth of cut is quadric, which is mainly due to the different geometries of the cross sectional area of the cutting groove. Especially, when the speed of cut varies between 0.25m/s and 0.5m/s, an embossment exists in each data curve with the relative height about 15%, which indicates that there could be an optimum speed range, which leads to the formation of sufficiently large chips. With our tools, the optimum cutting speed should be around 0.25m/s. The excavated rock mass also varies with cutting tools. If the cutting speed is fixed at say 0.5m/s, the optimum attack angle was found to be 55° which is due to the lowest specific energy. Specific energy under the conditions of conical (C1), pyramidal bottom flat (P1), pyramidal bottom edged (P3) and modified pyramid (P7) decreases with the increase of the depth of cut.

Specifically, with recalling the power relationship between the peak chipping force and depth of cut in edge chipping tests, the exponent in edge chipping was exploited to assess the cutting forces in linear cutting. It was found that for the best fit of first peak force (F_{1pc}), peak cutting force (F_{pc}) and mean cutting force (F_{mc}), the power relation still remains within the range from 1.19 to 1.49, with an average of 1.39, which is close to the theoretical result. It further derives the power relation between specific energy and depth of cut ($SE \propto h^{-2/3}$), which explains the trend of the experimental results.

6.2 Future research

Future research will focus on the formulation or coefficient determination of the bit shape effects on the peak force, as the current derivation cannot explain the deviation of the peak force induced by different bit profiles. Also, the dynamic effect of the rock properties should be investigated in rock cutting tests in order to correlate the formulation in edge chipping with the mean cutting force in linear cutting due to the existence of the power relation and the close exponent value to the analytical result. Next, as crush zone size is related to the bit shape, it is necessary to find a way of calculating the crush zone so as to predict the amount of fine grains and also the total energy consumption. For wear, the formulation of the material removal is helpful to predict the bit life and deep exploration of the wear mechanism of the PCD material is also useful in guiding the future application in rock cutting with a point attack bit.

Furthermore, in some of the linear cutting tests on granite, fracture of the bit occurred. It was noted that the bonding of the PCD material to the metal shank was not strong enough, especially under serious impacting by hard crystals, which then brings about the further investigations: adding new chemical additives into the brazing solder or employing a convenient mechanical clamper to hold the PCD bit. The wear of the shoulder of the shank will lead to the falling off of the bit, which refers to a demand for the partial hardening of the shank body.

References

[1] Inyang H.I., *Developments in Drag Bit Cutting of Rocks for Energy Infrastructure.* International Journal of Surface Mining, Reclamation and Environment, 2002. **16**(4): p. 248-260.

[2] Bilgin N., Demircin M.A., Copur H., Balci C., Tuncdemir H., and Akcin N., *Dominant rock properties affecting the performance of conical picks and the comparison of some experimental and theoretical results.* International Journal of Rock Mechanics and Mining Sciences, 2006. **43**(1): p. 139-156.

[3] Bilgin N., Yazici S., and Eskikaya S., *A model to predict the performance of roadheaders and impact hammers in tunnel drivages.* Int. Eurock, 1996. **96**: p. 2-5.

[4] Mishnaevsky Jr L., *Rock fragmentation and optimization of drilling tools.* Fracture of Rock, 1998: p. 167-203.

[5] Hood M. and Alehossein H., *A development in rock cutting technology.* International Journal of Rock Mechanics and Mining Sciences, 2000. **37**(1-2): p. 297-305.

[6] Hurt K. and Evans I., *Point attack tools: an evaluation of function and use for rock cutting.* Mining Engineer, 1981. **140**: p. 673-5.

[7] Evans I., *A theory of the cutting force for point-attack picks.* Geotechnical and Geological Engineering, 1984. **2**(1): p. 63-71.

[8] Fowell R. and Ochei N., *A comparison of dust make and energy requirements for rock cutting tools.* Geotechnical and Geological Engineering, 1984. **2**(1): p. 73-83.

[9] Hurt K.G. and McAndrew K.M., *Cutting efficiency and life of rock-cutting picks.* Mining Science and Technology, 1985. **2**: p. 139-151.

[10] Ranman K.E., *A model describing rock cutting with conical picks.* Rock mechanics and rock engineering, 1985. **18**(2): p. 131-140.

[11] Guo H., Aziz N.I., and Schmidt L.C., *Rock cutting study using linear elastic fracture mechanics.* Engineering fracture mechanics, 1992. **41**(5): p. 771-778.

[12] Goktan R. *Prediction of drag bit cutting force in hard rocks*. in *Proc. of the 3rd Int.Symp. on Mine Mechanization and Automation.* 1995. Golden, Colorado.

[13] Mishnaevsky L., *Physical mechanisms of hard rock fragmentation under mechanical loading: a review.* International Journal of Rock Mechanics and Mining Sciences, 1995. **32**(8): p. 763-766.

[14] Roxborough F.F. and Liu Z.C. *Theoretical considerations on pick shape in rock and coal cutting*. in *Proceedings of the sixth underground operator's conference*. 1995. Kalgoorlie, WA, Australia.

[15] Khair A.W., *The effects of bit geometry on rock cutting efficiency*. Applied Occupational and Environmental Hygiene, 1996. **11**(7): p. 695-700.

[16] Goktan R. *A suggested improvement on Evans' cutting theory for conical bits*. in *Proceedings of the fourth international symposium on mine mechanization and automation*. 1997. Brisbane, Queensland.

[17] Goktan R.M. and Gunes N., *A semi-empirical approach to cutting force prediction for point-attack picks.* J South Afr Inst Min Metall, 2005. **105**: p. 257-63.

[18] Balci C. and Bilgin N., *Correlative study of linear small and full-scale rock cutting tests to select mechanized excavation machines.* International Journal of Rock Mechanics and Mining Sciences, 2007. **44**(3): p. 468-476.

[19] Gunes Yilmaz N., Yurdakul M., and Goktan R., *Prediction of radial bit cutting force in high-strength rocks using multiple linear regression analysis.* International Journal of Rock Mechanics and Mining Sciences, 2007. **44**(6): p. 962-970.

[20] Tiryaki B., *In situ studies on service life and pick consumption characteristics of shearer drums.* JOURNAL-SOUTH AFRICAN INSTITUTE OF MINING AND METALLURGY, 2004. **104**(2): p. 107-122.

[21] Powell F., *Design guidelines for picks[to prevent underground gas ignitions]*. Colliery Guardian, 1991. **239**: p. 139-41.

[22] Hurt K. and Laidlaw D., *Laboratory comparison of three rock cutting tools.* Tunnels and Tunnelling, 1979. **11**(4): p. 13-16.

[23] Cashdollar K.L., *Coal dust explosibility*. Journal of Loss Prevention in the process industries, 1996. **9**(1): p. 65-76.

[24] Cashdollar K.L., Sapko M.J., Weiss E.S., and Hertzberg M. *Laboratory and mine dust explosion research at the Bureau of Mines*. 1987: American Society for Testing and Materials.

[25] Bartknecht W. and Zwahlen G., *Dust explosions: course, prevention, protection*. 1989: Not Avail.

[26] Fayed M.E. and Otten L., *Handbook of powder science and technology*. Van Nostrand Reinhold Co., 1984, 1984: p. 850.

[27] Nagy J. and Verakis H.C., *Development and control of dust explosions*. 1983: CRC.

[28] Eckhoff R.K., *Dust explosions in the process industries*. 2003: Gulf professional publishing.

[29] Hood M., *Cutting strong rock with a drag bit assisted by high-pressure water jets.* Journal of the South African Institute of Mining and Metallurgy, 1976. **77**(4): p. 79-90.

[30] Leach S., Walker G., Smith A., Farmer I., and Taylor G., *Some Aspects of Rock Cutting by High Speed Water Jets [and Discussion]*. Philosophical Transactions for the Royal Society of London. Series A, Mathematical and Physical Sciences, 1966. **260**(1110): p. 295-310.

[31] Rehbinder G., *A theory about cutting rock with a water jet.* Rock Mechanics and Rock Engineering, 1980. **12**(3): p. 247-257.

[32] Borm P.J.A., *Toxicity and occupational health hazards of coal fly ash (CFA). A review of data and comparison to coal mine dust.* Annals of Occupational Hygiene, 1997. **41**(6): p. 659.

[33] MacGregor I., Baker R., and Luyckx S., *A comparison between the wear of continuous miner button picks and the wear of pointed picks used in South African collieries.* Mining Science and Technology, 1990. **11**(2): p. 213-222.

[34] Bailey S. and Perrott C., *Wear processes exhibited by WC-Co rotary cutters in mining.* Wear, 1974. **29**(1): p. 117-128.

[35] Rogers S. and Roberts B., *Wear mechanisms associated with rock excavation using attack picks.* Mining Science and Technology, 1991. **12**(3): p. 317-323.

[36] Osburn H., *Wear of rock-cutting tools.* POWDER MET, 1969, 12, 471-502, 1969.

[37] Verhoef P.N.W., *Wear of rock cutting tools: implications for the site investigation of rock dredging projects.* 1997.

[38] Hurt K. and McStravick F., *High performance shearer drum design.* Colliery Guardian, 1988. **236**: p. 428-9.

[39] Achanti V. and Khair A., *Cutting Efficiency Through Optimized Bit Configuration–An Experimental Study Using A Simulated Continuous Miner.* Mineral Resources Engineering, 2001. **10**(4): p. 427-434.

[40] Hurt K. and MacAndrew K., *Cutting efficiency and life of rock-cutting picks.* Mining Science and Technology, 1985. **2**(2): p. 139-151.

[41] Achanti V.B. and Khair A.W., *Bit geometry effects on failure characteristics of rock.* Mining Engineering, 2000. **52**(Compendex): p. 101-107.

[42] Addala S., *Relationship between cutting parameters and bit geometry in rotary cutting*. 2000, West Virginia University.

[43] Khair A.W., *The Effect of Bit Geometry on Rock Cutting Efficiency.* Applied occupational and environmental hygiene, 1996. **11**(7): p. 695-700.

[44] Qayyum R.A., *Effects of bit geometry in multiple bit-rock interaction*. 2003, West Virginia University.

[45] Wahab Khair A., Reddy N., and Quinn M., *Mechanisms of Coal fragmentation by a continuous miner.* Mining Science and Technology, 1989. **8**(2): p. 189-214.

[46] Rabinowicz E., *Friction and wear of materials*. 1965: Wiley New York.

[47] Kenny P. and Johnson S., *The Effect of Wear on the Performance of Mineral Cutting Tools.* Colliery Guardian, 1976. **224**(6): p. 246–251.

[48] Kenny P. and Johnson S., *An investigation of the abrasive wear of mineral-cutting tools.* Wear, 1976. **36**(3): p. 337-361.

[49] Mehrotra P., *A model for wear of conical coal mining bits.* Wear of Materials 1985, 1985: p. 491-500.

[50] Kenny P. and Johnson S., *Non-Blunting Tool for Cutting Coal and Rock.* Colliery Guardian, 1977. **225**(10): p. 760-763.

[51] Mishnaevsky L. *A brief review of Soviet theoretical approaches to dynamic rock failure*. 1993.

[52] Lindqvist P.A., *Rock fragmentation by indentation and disc cutting some theoretical and experimental studies.* 1982.

[53] Mishnaevsky L. *Physical mechanisms of hard rock fragmentation under mechanical loading: a review*. 1996: Elsevier.

[54] Fedorov V.S., *Scientific Foundations of Drilling Regimes.* Gostoptekhizdat Moscow, 1951.

[55] Moscalev A.N., *Increase in Intensity of Rock Fragmentation.* Nedra, Moscow, 1972.

[56] Australian T.S., *CURRENT & EMERGING ROCK CUTTING TECHNOLOGY.* 2007.

[57] Zeuch D., Holcomb D., and Lauson H., *Analysis of consolidation of granulated rocksalt using a plastic flow model of isostatic hot-pressing*. 1985, Sandia National Labs., Albuquerque, NM (USA).

[58] Lindqvist P., *The potential of ISEE in different plasma environments.* ESA Spacecraft/Plasma Interactions and their Influence on Field and Particle Meas. p 25-33(SEE N 84-17253 08-18), 1983.

[59] Blokhin V.S., *Improvement of Drilling Tool Efficiency.* Teknika, Kiev, 1982.

[60] Nikiforovsky V.S. and Shemyakin Y.l., *Impact Fracture of Solids.* Nauka, Novosibirsk, 1979.

[61] Zipf R., *A fundamental study of respirable dust generation in coal.* Mining Science and Technology, 1989. **9**(1): p. 87-99.

[62] Evans I., Pomeroy C., and Establishment M.R., *The Strength, Fracture, Ad Workability of Coal*. 1966: Pergamon Press.

[63] Howarth D. and Bridge E. *Microfracture beneath blunt disc cutters in rock.* 1988: Elsevier.

[64] Zipf R. and Bieniawski Z., *Estimating the crush zone size under a cutting tool in coal.* Geotechnical and Geological Engineering, 1988. **6**(4): p. 279-295.

[65] Evans I., *Theoretical aspects of coal ploughing.* Mechanical Properties of Non-Metallic Brittle Materials: p. 451.

[66] GRAY K., Armstrong F., and Gatlin C., *Two-Dimensional Study of Rock Breakage in Drag-Bit Drilling at Atmospheric Pressure.* Journal of Petroleum Technology, 1962. **14**(1): p. 93-98.

[67] Wang J.K. and Lehnhoff T. *Bit penetration into rock--A finite element study*. 1976: Elsevier.

[68] Zeuch D., Swenson D., and Finger J. *Subsurface Damage Development In Rock During Drag-Bit Cutting: Observationsa Nd Modelp Redictions*. 1983.

[69] Korinets A., Chen L., Alehossein H., and Lim W., *DIANA modeling of a rolling disc cutter and rock indentation.* Second NARMS, rock mechanics tools and techniques. Montreal: Balkema, 1996: p. 647–54.

[70] Tang C., *Numerical simulation of progressive rock failure and associated seismicity.* International Journal of Rock Mechanics and Mining Sciences, 1997. **34**(2): p. 249-261.

[71] Kou S., Lindqvist P.A., Tang C., and Xu X., *Numerical simulation of the cutting of inhomogeneous rocks.* International Journal of Rock Mechanics and Mining Sciences, 1999. **36**(5): p. 711-717.

[72] Guo H., Aziz N., and Schmidt L., *Rock cutting study using linear elastic fracture mechanics.* Engineering Fracture Mechanics, 1992. **41**(5): p. 771-778.

[73] Saouma V.E. and Kleinosky M.J. *Finite element simulation of rock cutting: a fracture mechanics approach*. 1984.

[74] Liu H., *Numerical modelling of the rock fracture process under mechanical loading.* 2002.

[75] Hoek E. and Bieniawski Z., *Brittle fracture propagation in rock under compression.* International Journal of Fracture, 1965. **1**(3): p. 137-155.

[76] Lindqvist P.A., *Stress fields and subsurface crack propagation of single and multiple rock indentation and disc cutting.* Rock Mechanics and Rock Engineering, 1984. **17**(2): p. 97-112.

[77] Wei X., Wang C.Y., Yuan H.L., and Xie Z., *Study of Fracture Mechanism of Rock Cutting.* Key Engineering Materials, 2003. **250**: p. 200-208.

[78] Evans I. *A theory of the basic mechanics of coal ploughing*. 1962.

[79] Finnie I., Streit R., and Foote L., *Relationship of coal properties and machine parameters to continuous mining machine cutting rates. Open file report (final) 15 Oct 76--15 Apr 77*. 1977, MB Associates, San Ramon, CA (USA).

[80] Roxborough F.F., *Cutting Rocks with Picks.* The mining engineer, 1973: p. 445-452.

[81] Nishimatsu Y. *The mechanics of rock cutting*. 1972: Elsevier.

[82] Rånman K.E., *A model describing rock cutting with conical picks.* Rock Mechanics and Rock Engineering, 1985. **18**(2): p. 131-140.

[83] Cigla M. and Ozdemir L. *Computer modeling for improved production of mechanical excavators*. 2000.

[84] Hurt K. and MacAndrew K., *Designing roadheader cutting heads.* Mining Engineer, 1981. **141**: p. 167-70.

[85] Hurt K., Morris C., and MacAndrew K. *The design and operation of boom tunnelling machine cutting heads*. 1982.

[86] Hurt K.G. and MacAndrew K.M., *Cutting efficiency and life of rock-cutting picks.* Mining Science and Technology, 1985. **2**(2): p. 139-151.

[87] Hurt K., MacAndrew K., and Morris C. *Boom roadheader cutting vibration: Measurement and prediction*. 1988.

[88] Hurt K., *Rock cutting experiments with point attack tools.* Colliery Guardian Coal International, 1980. **4**: p. 25-32.

[89] Hurt K. and EVANS I. *A Laboratory Study of rock cutting using point attack tools*. 1980.

[90] Hurt K., *Roadheader cutting heads and picks.* Colliery Guardian, 1988. **236**: p. 332.

[91] H.P. S., *Prediction of the performance of disc cutters in anisotropic rock* International Journal of rock Mechanics and Mining Sciences Geomechanics Abstract, 1985. **22**(3): p. 153-161.

[92] Barker J. *A laboratory investigation of rock cutting using large picks*. 1964: Elsevier.

[93] Evans I., *Basic mechanics of the point-attack pick.* Colliery Guardian, 1984. **232**: p. 189.

[94] Goktan R. and Gunes N., *A semi-empirical approach to cutting force prediction for point-attack picks.* J South Afr Inst Min Metall, 2005. **105**: p. 257–263.

[95] LIU S., DU C., and CUI X., *Research on the cutting force of a pick.* Mining Science and Technology (China), 2009. **19**(4): p. 514-517.

[96] Johnson K.L., *Contact Mechanics*. 1987: Cambridge University Press.

[97] Hughes H. *Some aspects of rock machining*. 1972: Elsevier.

[98] Mellor M. *Normalization of specific energy values*. 1972: Elsevier.

[99] Bilgin N., Demircin M., Copur H., Balci C., Tuncdemir H., and Akcin N., *Dominant rock properties affecting the performance of conical picks and the comparison of some experimental and theoretical results.* International Journal of Rock Mechanics and Mining Sciences, 2006. **43**(1): p. 139-156.

[100] Roxborough F. and Liu Z. *Theoretical considerations on pick shape in rock and coal cutting*. 1995.

[101] Goktan R.M., *A theoretical comparison of the performance of drag picks in relation to coal-strength parameters.* J. S. Atr. Inst. Min. Metal., 1992. **92**(4): p. 85-87.

[102] Goktan R.M., *Prediction of drag bit cutting force in hard rocks.* Proceedings of the third international symposium on mine mechanization and automation, 1995: p. 1031-1039.

[103] Roxborough F. and Rispin A., *The mechanical cutting characteristics of the lower chalk.* Tunnels and Tunnelling, 1973. **5**(1): p. 45–67.

[104] SELLIN R.H.J., *A laboratory investigation into the interaction between the flow in the channel of a river and that over its flood plain.* La Houille Blanche, 1964(7): p. 793-802.

[105] Roxborough F.F. *Research in mechanical rock excavation: progress and prospects*. 1975.

[106] Roxborough F.F. and Phillips H.R. *Rock excavation by disc cutter*. 1975: Elsevier.

[107] Khair A., Xu D., and Ahmad M., *Principles of bit wear and dust generation.* Proceedings of new Technology in Mine Health and Safety, SME, Littleton, CO, Febrauary, 1992: p. 175-183.

[108] Roepke W. and Hanson B., *Effect of asymmetric wear of point attack bits on coal-cutting parameters and primary dust generation.* NTIS, SPRINGFIELD, VA(USA). 1983., 1983.

[109] Ersoy A. and Waller M., *Wear characteristics of PDC pin and hybrid core bits in rock drilling.* Wear, 1995. **188**(1-2): p. 150-165.

[110] Li X.B., Summers D., Rupert G., and Santi P., *Experimental investigation on the breakage of hard rock by the PDC cutters with combined action modes.* Tunnelling and Underground Space Technology, 2001. **16**(2): p. 107-114.

[111] Glowka D. and Stone C., *Effects of thermal and mechanical loading on PDC bit life.* SPE Drilling Engineering, 1986. **1**(3): p. 201-214.

[112] Kuru E. and Wojtanowicz A. *An experimental study of sliding friction between PDC drill cutters and rocks*. 1995: Elsevier.

[113] Jurewicz S.R., Jensen K.M., and Tibbitts G.A., *Superabrasive cutting element with enhanced durability and increased wear life, and apparatus so equipped*. 1998, Google Patents.

[114] Glowka D. and Stone C., *Thermal response of polycrystalline diamond compact cutters under simulated downhole conditions.* Old SPE Journal, 1985. **25**(2): p. 143-156.

[115] Sneddon M. and Hall D., *Polycrystalline diamond: manufacture, wear mechanisms, and implications for bit design.* Journal of Petroleum Technology, 1988. **40**(12): p. 1593-1601.

[116] Morrell R. and Gant A.J., *Edge chipping of hard materials.* International Journal of Refractory Metals and Hard Materials. **19**(4-6): p. 293-301.

[117] Chai H. and Lawn B.R., *A universal relation for edge chipping from sharp contacts in brittle materials: A simple means of toughness evaluation.* Acta Materialia, 2007. **55**(7): p. 2555-2561.

[118] Petit F., Vandeneede V., and Cambier F., *Ceramic toughness assessment through edge chipping measurements--Influence of interfacial friction.* Journal of the European Ceramic Society, 2009. **29**(11): p. 2135-2141.

[119] Cao Y., *Failure analysis of exit edges in ceramic machining using finite element analysis.* Engineering Failure Analysis, 2001. **8**(4): p. 325-338.

[120] Xu C., Ai X., and Huang C., *Fabrication and performance of an advanced ceramic tool material.* Wear, 2001. **249**(5-6): p. 503-508.

[121] Symonds B.L., Cook R.F., and Lawn B.R., *Dynamic fatigue of brittle materials containing indentation line flaws.* Journal of Materials Science, 1983. **18**(5): p. 1306-1314.

[122] Quinn J.B. and Quinn G.D., *Material properties and fractography of an indirect dental resin composite.* Dental Materials, 2010. **26**(6): p. 589-599.

[123] Ustundag C., Tur Y., and Capoglu A., *Mechanical behaviour of a low-clay translucent whiteware.* Journal of the European Ceramic Society, 2006. **26**(1-2): p. 169-177.

[124] Chiu W., Thouless M.D., and Endres W., *An analysis of chipping in brittle materials.* International Journal of Fracture, 1998. **90**(4): p. 287-298.

[125] McCormick N., *Edge flaking of brittle materials.* Advanced Engineering with Ceramics London, 14-15 December 1989, 1990: p. 307-318.

[126] McCormick N., *Edge flaking as a measure of material performance.* Met. Mater., 1992. **8**(3): p. 154-156.

[127] Morrell R., *Edge flaking-similarity between quasistatic indentation and impact mechanisms for brittle materials.* Key Engineering Materials, 2005. **290**: p. 14-22.

[128] Morrell R. and Gant A., *Edge chipping of hard materials.* International Journal of Refractory Metals and Hard Materials, 2001. **19**(4-6): p. 293-301.

[129] Quinn J., Su L., Flanders L., and Lloyd I., *"EDGE TOUGHNESS" AND MATERIAL PROPERTIES RELATED TO THE MACHINING OF DENTAL CERAMICS.* Machining Science and Technology, 2000. **4**(2): p. 291-304.

[130] Thouless M.D., Evans A.G., Ashby M.F., and Hutchinson J.W., *The Edge Cracking and Spalling of Brittle Plates.* Acta Metallurgica, 1987. **35**(6): p. 1333-1341.

[131] Zaayman E., Morrison G., and Field J.E., *Edge flaking in diamond.* International Journal of Refractory Metals & Hard Materials, 2009. **27**(2): p. 409-416.

[132] Liu H. and Luleå S., *Numerical modelling of the rock fragmentation process by mechanical tools.* Luleå University of Technology, Luleå, Sweden, 2004.

[133] Cotterell B., Kamminga J., and Dickson F.P., *The Essential Mechanics of Conchoidal Flaking.* International Journal of Fracture, 1985. **29**(4): p. 205-221.

[134] Liu H., Kou S., Lindqvist P.A., and Tang C., *Numerical simulation of the rock fragmentation process induced by indenters.* International Journal of Rock Mechanics and Mining Sciences, 2002. **39**(4): p. 491-505.

[135] Richard R., *Neanderthals and the Garden of Eden*: RW Richard.

[136] Almond E.A. and Mccormick N.J., *Constant-Geometry Edge-Flaking of Brittle Materials.* Nature, 1986. **321**(6065): p. 53-55.

[137] Thouless M., Evans A., Ashby M., and Hutchinson J., *The edge cracking and spalling of brittle plates.* Acta Metallurgica, 1987. **35**(6): p. 1333-1341.

[138] Danzer R. and Paar R., *Edge strength of brittle materials.* Fortschrittberichte Der Dsch Keram Gese, 1994. **10**(3): p. 77-84.

[139] Gogotsi G., Galenko V., Mudrik S., Ozersky B., Khvorostyany V., and Khristevich T., *Fracture resistance estimation of elastic ceramics in edge flaking: EF baseline.* Journal of the European Ceramic Society, 2010. **30**(6): p. 1223-1228.

[140] Gogotsi G. and Mudrik S., *Fracture resistance of technical and optical glasses: edge flaking of specimens.* Strength of materials, 2010: p. 1-7.

[141] Gogotsi G.A., *Fracture behaviour of Mg-PSZ ceramics: Comparative estimates.* Ceramics international, 2009. **35**(7): p. 2735-2740.

[142] Gogotsi G.A., *Mechanical behaviour of a silicon nitride particulate ceramic composite.* Ceramics international, 2009. **35**(3): p. 1109-1114.

[143] Gogotsi G.A. and Mudrik S.P., *Fracture barrier estimation by the edge fracture test method.* Ceramics international, 2009. **35**(5): p. 1871-1875.

[144] Gogotsi G., Mudrik S., and Galenko V., *Evaluation of fracture resistance of ceramics: Edge fracture tests.* Ceramics international, 2007. **33**(3): p. 315-320.

[145] Gogotsi G.A., Lomonova E.E., and Pejchev V.G., *Strength and fracture toughness of zirconia crystals.* Journal of the European Ceramic Society, 1993. **11**(2): p. 123-132.

[146] Gogotsi G.A. and Ostrovoy D.Y., *Mechanical behaviour of partially stabilized zirconia crystals with terbia and ceria additives.* Journal of the European Ceramic Society, 1995. **15**(12): p. 1177-1184.

[147] Lawn B., *Fracture of Brittle Solids-Second Edition.* 1993. **Chp.2**: p. 20.

[148] Griffith A.A., *The phenomenon of rupture and flow in solids.* Trans. Royal Soc. of London, 1920. **221**: p. 163.

[149] Atkinson B.K. and Avdis V., *Fracture-Mechanics Parameters of Some Rock-Forming Minerals Determined Using an Indentation Technique.* International Journal of Rock Mechanics and Mining Sciences, 1980. **17**(6): p. 383-386.

[150] Swain M. and Atkinson B., *Fracture surface energy of olivine.* Pure and Applied Geophysics, 1978. **116**(4): p. 866-872.

[151] Swain M. and Lawn B. *Indentation fracture in brittle rocks and glasses*. 1976: Elsevier.

[152] Tada H., Paris P.C., Irwin G.R., and Books24x7 I., *The stress analysis of cracks handbook*. Vol. 130. 2000: ASME press New York.

[153] Lawn B.R. and Fuller E., *Equilibrium penny-like cracks in indentation fracture.* Journal of Materials Science, 1975. **10**(12): p. 2016-2024.

[154] Herzberg R.W., *Deformation and fracture mechanics of engineering materials.* New York, 1976.

[155] Quinn G., Salem J., Bar On I., and Jenkins M., *The New Astm Fracture Toughness of Advanced Ceramics Standard: PS 070 97.* 1998.

[156] Quinn J.B. and Lloyd I.K., *Comparison of Methods to Determine the Fracture Toughness of Three Glass Ceramics at Elevated Temperatures.* Journal of the American Ceramic Society, 2000. **83**(12): p. 3070-3076.

[157] Guo H., Aziz N.I., and Schmidt L.C., *Rock Fracture-Toughness Determination by the Brazilian Test.* Engineering Geology, 1993. **33**(3): p. 177-188.

[158] Nelson P.P., Ingraffea A.R., and Orourke T.D., *Tbm Performance Prediction Using Rock Fracture Parameters.* International Journal of Rock Mechanics and Mining Sciences, 1985. **22**(3): p. 189-192.

[159] Sanio H.P., *Prediction of the performance of disc cutters in anisotropic rock* international Journal of rock Mechanics and Mining Sciences Geomechanics Abstract, 1985. **22**(3): p. 153-161.

[160] Tiryaki B., Gipps I.D., and Li X.S., *Rapid Estimation of Rock Cuttability using Fracture Toughness and Rock Strength.* Advances in Abrasive Technology Xii, 2009. **76-78**: p. 591-596.

[161] Li X. and Boland J., *The wear characteristics of superhard composite materials in abrasive cutting operations.* Wear, 2005. **259**(7-12): p. 1128-1136.

[162] Laugier M.T., *Toughness Determination of Some Ceramic Tool Materials Using the Method of Hertzian Indentation Fracture.* Journal of Materials Science Letters, 1985. **4**(12): p. 1542-1544.

[163] Beste U. and Jacobson S., *A new view of the deterioration and wear of WC/Co cemented carbide rock drill buttons.* Wear, 2008. **264**(11-12): p. 1129-1141.

[164] Brown G.J. and Reddish D.J., *Experimental relations between rock fracture toughness and density.* International Journal of Rock Mechanics and Mining Sciences, 1997. **34**(1): p. 153-155.

[165] Kahraman S. and Altindag R., *A brittleness index to estimate fracture toughness.* International Journal of Rock Mechanics and Mining Sciences, 2004. **41**(2): p. 343-348.

[166] Zhang Z.X., *An empirical relation between mode I fracture toughness and the tensile strength of rock.* International Journal of Rock Mechanics and Mining Sciences, 2002. **39**(3): p. 401-406.

[167] Chiu W.C., Thouless M.D., and Endres W.J., *An analysis of chipping in brittle materials.* International Journal of Fracture, 1998. **90**(4): p. 287-298.

[168] Scieszka S.F., *Edge failure as a means of concurrently estimating the abrasion and edge fracture resistance of hard-metals.* Tribology International, 2005. **38**(9): p. 834-842.

[169] Quinn J.B., Sundar V., Parry E.E., and Quinn G.D., *Comparison of edge chipping resistance of PFM and veneered zirconia specimens.* Dental Materials, 2010. **26**(1): p. 13-20.

[170] Wyeth D. and Atkins A., *Mixed mode fracture toughness as a separation parameter when cutting polymers.* Engineering Fracture Mechanics, 2009. **76**(18): p. 2690-2697.

[171] Gogotsi G.A. and Mudrik S.P., *Glasses: New approach to fracture behavior analysis.* Journal of Non-Crystalline Solids, 2010. **356**(20-22): p. 1021-1026.

[172] Quinn J. and Mohan R. *Geometry of edge chips formed at different angles*. in *the 29th International Conference on Advanced Ceramics and Composites*. 2005. Hobken, NJ, USA: Wiley Online Library.

[173] Chai H. and Lawn B.R., *Edge chipping of brittle materials: effect of side-wall inclination and loading angle.* International Journal of Fracture, 2007. **145**(2): p. 159-165.

[174] Lardner T., Ritter J., Shiao M., and Lin M., *Behavior of indentation cracks near free surfaces and interfaces.* International Journal of Fracture, 1990. **44**(2): p. 133-143.

[175] Roepke W. and Hanson B., *Coal cutting forces on primary dust control during cutting.* Min Eng, 1984. **36**: p. 636–643.

[176] Roxborough F. and Rispin A., *A laboratory investigation into the application of picks for mechanized tunnel boring in the lower chalk.* The mining engineer, 1973. **133**: p. 1-13.

[177] Fowell R., *The mechanics of rock cutting.* Compressive rock engineering, 1993: p. 155-176.

[178] Zhang L. and Arsecularatne J., *Cutting tip and tool.* PCT/AU2008/000969 2008.

[179] Arsecularatne J.A. and Zhang L.C., *Novel coal cutting picks* Industrial Presentation File, 2005.

[180] Fischer-Cripps A.C., *Introduction to contact mechanics*. 2000: Springer Verlag.

[181] Lawn B. and Evans A., *A model for crack initiation in elastic/plastic indentation fields.* Journal of Materials Science, 1977. **12**(11): p. 2195-2199.

[182] Ishikawa H. and Shinkai N., *Critical load for median crack initiation in Vickers indentation of glasses.* Journal of the American Ceramic Society, 1982. **65**(8): p. c124-c127.

[183] Sollami P.A. and Sollami J.L., *Conical bit*. 1987, Google Patents.

[184] Erdogan F. and Sih G., *On the crack extension in plates under plane loading and transverse shear(Crack extension in a large plate under plane loading and transverse shear, studied in terms of local stress and strain concentrations).* ASME, TRANSACTIONS, SERIES D- JOURNAL OF BASIC ENGINEERING, 1962.

[185] Ruan H., Chen A., and Lu J., *Characterization of plastically graded nanostructured material: Part I. The theories and the inverse algorithm of nanoindentation.* Mechanics of Materials, 2010. **42**(5): p. 559-569.

[186] Carroll M.M., *Mechanics of Geological Materials.* Applied Mechanics Reviews, 1985. **38**(10): p. 1256-1261.

[187] Lawn B.R., *Fracture of brittle solids*. 1993: Cambridge Univ Pr.

[188] Goktan R. *A suggested improvement on Evans' cutting theory for conical bits*. 1997.

[189] Tiryaki B., Boland J., and Li X., *Empirical models to predict mean cutting forces on point-attack pick cutters.* International Journal of Rock Mechanics and Mining Sciences, 2010. **47**(5): p. 858-864.

[190] Su O. and Ali Akcin N., *Numerical simulation of rock cutting using the discrete element method.* International Journal of Rock Mechanics and Mining Sciences, 2010.

[191] Kim E., Rostami J., and Swope C. *Measurement of Conical Bit Rotation*. 2009.

[192] Gogotsi G.A., *Crack resistance of modern ceramics and ceramic composites. II. EF method.* Powder Metallurgy and Metal Ceramics, 2006. **45**(7-8): p. 328-336.

[193] Chai H. and Ravichandran G., *On the mechanics of surface and side-wall chipping from line-wedge indentation.* International Journal of Fracture, 2007. **148**(3): p. 221-231.

[194] Carroll M., *Mechanics of Geological Materials.* Applied Mechanics Reviews, 1985. **38**: p. 1256.

[195] Tutluoglu L., Hood M., and Barton C. *An Investigation of the Mechanisms of Water Jet Assistance on the Rock Cutting Process*. 1983.

[196] Lam L. and Teng J., *Design-oriented stress-strain model for FRP-confined concrete.* Construction and Building Materials, 2003. **17**(6-7): p. 471-489.

[197] Ochiai S. and Murakami Y., *Tensile strength of composites with brittle reaction zones at interfaces.* Journal of Materials Science, 1979. **14**(4): p. 831-840.

[198] Matthewson M. and Field J., *An improved strength-measurement technique for brittle materials.* Journal of Physics E: Scientific Instruments, 1980. **13**: p. 355.

[199] Qasim T., Bush M.B., Hu X., and Lawn B.R., *Contact damage in brittle coating layers: influence of surface curvature.* Journal of Biomedical Materials Research Part B: Applied Biomaterials, 2005. **73**(1): p. 179-185.

[200] Sedlacek R. and Halden F.A., *Method for tensile testing of brittle materials.* Review of Scientific Instruments, 1962. **33**(3): p. 298-300.

[201] Lawn B., *Partial cone crack formation in a brittle material loaded with a sliding spherical indenter.* Proceedings of the Royal Society of London. Series A. Mathematical and Physical Sciences, 1967. **299**(1458): p. 307.

[202] Suresh S., Shih C., Morrone A., and O'Dowd N., *Mixed Mode Fracture Toughness of Ceramic Materials.* Journal of the American Ceramic Society, 1990. **73**(5): p. 1257-1267.

[203] Lubarda V., Krajcinovic D., and Mastilovic S., *Damage model for brittle elastic solids with unequal tensile and compressive strengths.* Engineering Fracture Mechanics, 1994. **49**(5): p. 681-697.

[204] Hardy H. and Jayaraman N., *An investigation of methods for the determination of the tensile strength of rock*. 1970.

[205] Teufel L. and Clark J., *Hydraulic fracture propagation in layered rock: Experimental studies of fracture containment.* Old SPE Journal, 1984. **24**(1): p. 19-32.

[206] Steif P.S., *Crack extension under compressive loading.* Engineering Fracture Mechanics, 1984. **20**(3): p. 463-473.

[207] Ahrens T.J. and Rubin A.M., *Impact-induced tensional failure in rock.* Journal of geophysical research, 1993. **98**(E1): p. 1.

[208] Xu S., De Freitas M., and Clarke B.A. *The measurement of tensile strength of rock*. 1988.

[209] Sih G.C., Fracture L.U.I.o., and Mechanics S., *Handbook of stress-intensity factors*. 1973: Institute of Fracture and Solid Mechanics, Lehigh University.

[210] Hsieh C.C. and Su C.S., *Management inputs and mechanical harvesting of vegetable soybean in Taiwan.* Vegetable Soybean: p. 61.

[211] Chang S.H., Choi S.W., Bae G.J., and Jeon S., *Performance prediction of TBM disc cutting on granitic rock by the linear cutting test.* Tunnelling and Underground Space Technology, 2006. **21**(3-4): p. 271.

[212] Tiryaki B. and Dikmen A.C., *Effects of rock properties on specific cutting energy in linear cutting of sandstones by picks.* Rock Mechanics and Rock Engineering, 2006. **39**(2): p. 89-120.

[213] Tuncdemir H., Bilgin N., Copur H., and Balci C., *Control of rock cutting efficiency by muck size.* International Journal of Rock Mechanics and Mining Sciences, 2008. **45**(2): p. 278-288.

[214] Fowell R.J. and Ochei N.N., *A Comparison of Dust Make and Energy-Requirements for Rock Cutting Tools.* International Journal of Mining Engineering, 1984. **2**(1): p. 73-83.

[215] Achanti V.B. and Khair A.W., *Bit geometry effects on failure characteristics of rock.* Mining Engineering, 2000. **52**(6): p. 101-107.

[216] Perott C.M., *the influence of temperature on performance of hard metal rock bit.* Metaux Corros. Ind., 1980. **55**(653): p. 16-23.

[217] Mishnaevsky L.L., *Investigation of the Cutting of Brittle Materials.* International Journal of Machine Tools & Manufacture, 1994. **34**(4): p. 499-505.

[218] Roxborough F., King P., and Pedroncelli E., *Tests on the cutting performance of continuous miner.* system, 1981. **5**: p. 6.

[219] Roxborough F. and Pedroncelli E., *Practical evaluation of some coal-cutting theories using a continuous miner.* Mining Engineer, 1982. **142**: p. 145-56.

[220] Grady D. *Shock-wave properties of brittle solids*. 1996.

[221] Dunn K. and Lee M., *The fracture and fatigue of sintered diamond compact.* Journal of Materials Science, 1979. **14**(4): p. 882-890.

[222] Tze-Pin L., Hood M., Cooper G.A., and Xiaohong L., *Wear and failure mechanisms of polycrystalline diamond compact bits.* Wear, 1992. **156**(1): p. 133-150.

[223] Guyer R., McCall K., Boitnott G., Hilbert Jr L., and Plona T., *Quantitative implementation of Preisach-Mayergoyz space to find static and dynamic elastic moduli in rock.* J. Geophys. Res, 1997. **102**(B3): p. 5.

[224] King M. *Static and dynamic elastic moduli of rocks under pressure*. 1969.

[225] Ide J.M., *Comparison of statically and dynamically determined Young's modulus of rocks.* Proceedings of the National Academy of Sciences of the United States of America, 1936. **22**(2): p. 81.

[226] Cheng C. and Johnston D.H., *Dynamic and static moduli.* Geophysical Research Letters, 1981. **8**(1): p. 39-42.

[227] Zhang Z., Kou S., Yu J., Yu Y., Jiang L., and Lindqvist P.A., *Effects of loading rate on rock fracture.* International Journal of Rock Mechanics and Mining Sciences, 1999. **36**(5): p. 597-611.

[228] Costin L. *Static and dynamic fracture behavior of oil shale*. 1981: ASTM International.

[229] Tang C. and Xu X., *A new method for measuring dynamic fracture toughness of rock.* Engineering Fracture Mechanics, 1990. **35**(4-5): p. 783-791.

[230] Turcotte D.L., *Fractals and chaos in geology and geophysics*. 1997: Cambridge Univ Pr.

[231] Englmana R., Rivier N., and Jaeger Z., *Size distribution in sudden breakage by the use of entropy maximization.* Journal of Applied Physics, 1988. **63**(9): p. 4766-4768.

Appendix

List of publications

Yao Q., Zhang, L., Bao, R., Lunn, J., Melmeth, C., *Edge Chipping of Rock: An Experimental Study*. Key Engineering Materials, 2010. **443**: p. 456-461.

Bao R., Zhang L., *Yao Q.*, and Lunn J., *Estimating the Peak Indentation Force of the Edge Chipping of Rocks Using Single Point-Attack Pick.* Rock Mechanics and Rock Engineering: p. 1-9.

Qingyu Yao, Seyed Saleh Mostafavi, Ronghao Bao, L.C. Zhang, Jason Lunn, Craig Melmeth, *PICK PROFILE EFFECT ON THE LINEAR CUTTING OF SANDSTONE*, published in the proceedings of 45th ARMA Symposium, San Francisco, US, 2011

Q.Y. Yao, L.C. Zhang, R.H. Bao, S.S. Mostafavi, J. Lunn, C. Melmeth, *Wear Performance of PCD and WC Mining Picks*, published in the proceeding of AES-ATEMA'2011 International Conference Milan, ITALY

Seyed Saleh Mostafavi, *Qingyu Yao*, L.C. Zhang, Jason Lunn, Craig Melmeth, *The Effect of Pick Orientation on Rock fragmentation by Mechanical Tools*, published in the proceedings of 12th ISRM Congress Beijing 2011

Qingyu Yao, Ronghao Bao, L.C. Zhang, Seyed Saleh Mostafavi, Jason Lunn, Craig Melmeth, *Edge Chipping of Rock: a New Measurement of Rock Toughness*, t*o be submitted to International Journal of Rock Mechanics and Mining Sciences*

Qingyu Yao, Seyed Saleh Mostafavi, L.C. Zhang, Jason Lunn, Craig Melmeth, *Analyses on Mechanism of Inclined Rock Chipping*, to be submitted to Rock Mechanics and Rock Engineering

S.S. Mostafavi, *Q.Y. Yao*, L.C. Zhang, J. Lunn, C. Melmeth, *Modelling the Geometrical Similarity in Edge Chipping*, to be submitted to Rock Mechanics and Rock Engineering